Design and development of cellulose based composites for the built environment

by

Melvin Glenn Veigas

A thesis submitted to the graduate faculty

in partial fulfillment of the requirements for the degree of

MASTER OF SCIENCE

Major: Architecture

Program of Study Committee:
Ulrike Passe, Co-major Professor
Behrouz Shafei, Co-major Professor
Firat Erdim, Committee Member

The student author, whose presentation of the scholarship herein was approved by the program of study committee, is solely responsible for the content of this thesis. The Graduate College will ensure this thesis is globally accessible and will not permit alterations after a degree is conferred.

Iowa State University

Ames, Iowa

2019

DEDICATION

This thesis is dedicated to Neil, my family, and my mentors.

TABLE OF CONTENTS

Page

LIST OF FIGURES

Page

LIST OF TABLES

Page

NOMENCLATURE

YA	Young's Modulus
CLT	Cross Laminated Timber
MDL	Mobile Diagnostics Lab
ECC	Engineered Cement Composite
CNC	Cellulose Nanocrystals
PVA	Polyvinyl Alcohol
ASTM	American Society for Testing and Materials
UTM	Universal Testing Machine

DEFINITIONS

Non -Renewable Materials - materials that are manufactured or created from raw materials that cannot be replenished in a period that is sustainable.

Compressive Strength - the capacity of a material or structure to withstand loads tending to reduce size.

Tensile Strength - the capacity of a material or structure to withstand loads tending to elongate size.

Toughness - the ability of a material to absorb energy and plastically deform without fracturing.

ACKNOWLEDGMENTS

I would like to thank my committee chairs, Ulrike Passe for believing in me and giving me the opportunity to succeed, Dr. Behrouz Shafei for being open to the possibilities and trusting in me, and my committee member Firat Erdim for his valuable input throughout this endeavor. I would also like to thank Dr. Meysam Najimi for his time and expertise on material formulation, fabrication, and his critical eye. The PCC lab, Jeremy McIntyre and Doug Wood in helping me with the experimentation process.

In addition, I would also like to thank my family for supporting me through this creative process. My friends in the United States, Canada, Qatar, India, and ETF who believed in me, kept me focused and motivated. My colleagues who pushed me to think critically. The department faculty and staff for guiding me towards future endeavors.

ABSTRACT

Cellulose is a versatile material with numerous contemporary applications in textiles, food, and biomaterials. Contemporary research is focused on modifying the structural and thermal properties of cellulose to create novel composites with cellulose nano-crystals, lignocellulosic pulp, and foamed cellulose to name a few. Significant advances have been made in improving the properties of cellulose. Adding aligned cellulose nano-fibers to concrete to improve its mechanical properties or combining with polymers for better durability can lead to new applications specifically in design and construction. These new forms of cellulose through optimization and combination with other materials provide opportunities for reducing material usage, as the life-cycle cost involved in the transformation of traditional materials such as brick, concrete, and steel in construction is significant. Therefore, this thesis reviewed cellulose research pertinent to the field of building construction and explored three cellulose based applications at two different scales.

The three investigations explored utilizing cellulose, in two forms, as an alternative to non-renewable materials that constitute the standardized wall assembly. Focusing on a widely available, renewable, and bio-degradable material such as cellulose would provide an alternative to the energy intensive materials that make up the standardized wall assembly. Therefore, the primary goals were:

1. Reducing the percentage of non-renewable materials utilized in the contemporary wall assembly.

2. Utilizing a widely available, biodegradable, and renewable material like cellulose as an alternative to traditional building materials.

3. Transforming cellulose, manifesting as various fibers, into a structural or thermal component based on location, availability, and programmatic requirements.

For the first study, the mobile diagnostics lab was utilized to generate Data from custom concrete panels inserted into the removable wall assembly creating a baseline to compare future cellulose concrete panels. The fiber composite study primarily optimized fiber proportion for effective mechanical properties. Therefore, additional work needs to be carried out into fiber and mix proportion optimization to create a thermally efficient composite panel.

For the second investigation, cellulose based thin shell structures were cast as a framework for future applications utilizing cellulose available in various forms around the world (Table 5-1). The shells were envisioned as enclosures for community gathering spaces in rural regions. Additionally, they could serve as a blueprint for crafting spaces in regions facing humanitarian crises and shortage of traditional building materials such as lumber, glass, steel, and brick.

The third study investigated the interfacial bond between the fiber and cement matrix in concrete by coating the fiber surface in polyester resin and shellac prior to dispersion in the composite mix. The coated sisal fiber embedded composites exhibited improved toughness, ductility, and flexural capacity, compared with unreinforced ECC composites.

CHAPTER 1. INTRODUCTION

This research project began with the question: can advances in contemporary cellulose processing improve the customary wall assembly rooted in economic principles towards sustainable processes, and lead to the integration of novel technologies? The investigation started with an examination of the contemporary architype of a wall assembly. A wall assembly as the term implies is an assemblage of diverse materials fulfilling specific functions such as structural integrity, weatherproofing, and environmental mediation. The contemporary wall assembly is the result of the necessity to control and optimize interior space for thermal comfort, privacy, community on one hand, and material optimization guided by building standards, fire and safety codes, as well as economic goals on the other. In the construction industry these economic goals are prioritized during assembly design over other factors leading to reduced resilience, higher life cycle, and cheaper material components of the wall assembly. Material selection for the contemporary wall assembly is narrowly defined by functions they are required to fulfil. This selection is bound by their function with respect to cost. As a result, building assemblies, regardless of region, favor a standardized material palette optimized for function and cost, overlooking other factors such as vernacular traditions, cultural norms, recyclability, and micro-climate, among others.

This approach towards building assemblies and standardization has created a ubiquitous architectural language across varied environmental, cultural, and geographic conditions. Therefore another question can be asked: can a novel material be utilized in a manner that accounts for a holistic set of parameters such as micro-climate, vernacular, culture, and technology to fulfil the multifarious needs that are expected from a contemporary building assembly?

This reliance on standardized building assemblies has favored specific building materials. Some of the standard building materials, used commonly, are lumber, concrete, steel, and plastic composites. From (Figure 1-1) and (Table 1-1) the percentage of non-renewable materials utilized in building construction has significantly risen, with implications for resource depletion, energy use, and emissions. The consumption of non-renewable materials, with high embodied energy, consisting of lumber, concrete, steel, and plastic composites, is significant (Figure 1-2). Therefore, there is a tremendous opportunity and need to reduce material consumption with high embodied energy as they contribute significantly to energy use and carbon emissions.

This concern prompted a re-examination of the various renewable materials available in the construction industry both from natural sources such as biomass as well as waste products originating from agricultural, and manufacturing processes.

Cellulose derived from biomass, from both natural, and waste sources, fit this condition. The natural sources of cellulose are from plants, and trees. It is one of the integral structural components of plants and is at the center of this investigation. Crop residue from farming constitutes a secondary source of natural fiber. Cellulose from paper-based waste products such as cardboard boxes from manufacturing industry constitute a tertiary source of cellulose.

Therefore, rather than evaluate the wall assembly through the lens of standardized products that are common in the building industry, this multifaceted investigation looks at the novel techniques and processes reframing the properties of cellulose for design and construction.

This thesis studies the new processes in biochemistry and renewables, which lead to new forms of cellulose, that show potential in various building materials and wall assemblies. These cellulose based materials could be an alternative to the material consumption and high embodied energy associated with traditional materials in the contemporary wall assembly.

The Contemporary Architectural Wall Assembly and Material Consumption

Beginning in late 1900s Modernism emerged from a desire to break with architectural traditions and cultural norms characterized by breakthroughs in engineering and building technology. In "Towards a new architecture" Le Corbusier states "It is necessary to press on toward the establishment of *standards* in order to face the problem of perfection" (Le 1970). Advances in manufacturing technology after World War II facilitated the standardization and mass production of building materials to create a building typology(Jencks 2016) that allowed buildings to be built faster and cheaper, creating a standardized architectural language (Mitchell 2004).

The contemporary wall assembly, a collection of building products, is the continuation of a standardized ethos which has continued since the advent of modernism. The reproduction of standardized building forms, itself a collection of products, relies on finite traditional materials with high embodied energy and has strained our natural resources (Fuchs 2008). This paradigm of standardization and non-renewable material production having high embodied energy is unsustainable.

As a result, researchers are developing novel materials, with specific performance goals at multiple scales, leading to improvements in building technology and construction. Strengthened cellulose fibers, spider silk fibers and structural fungal bricks are few of the new materials being developed (Sauer 2010). The production of these new materials is rapidly being

defined and developed by advances made in chemistry, construction technology, and robotics (Mori 2002). In the process of developing these new materials the role of the architect is significant. It affords a critical look at how materials and processes can play a key role in defining a high-performance building envelope and spatial conditions, while holistically considering factors such as, vernacular, material locality, material sourcing, logistics, waste (agricultural and manufactured), and global material flows.

Global material flows and consumption in construction

Buildings, their materials, and their components over their lifetime, consume approximately 40% of raw materials entering the global economy (Gillian, Mohamad Monkiz, and Phillip 2009). Construction materials account for 40-50% of global Green House Gas (GHG) emissions (Board 2000, California et al. 2000).

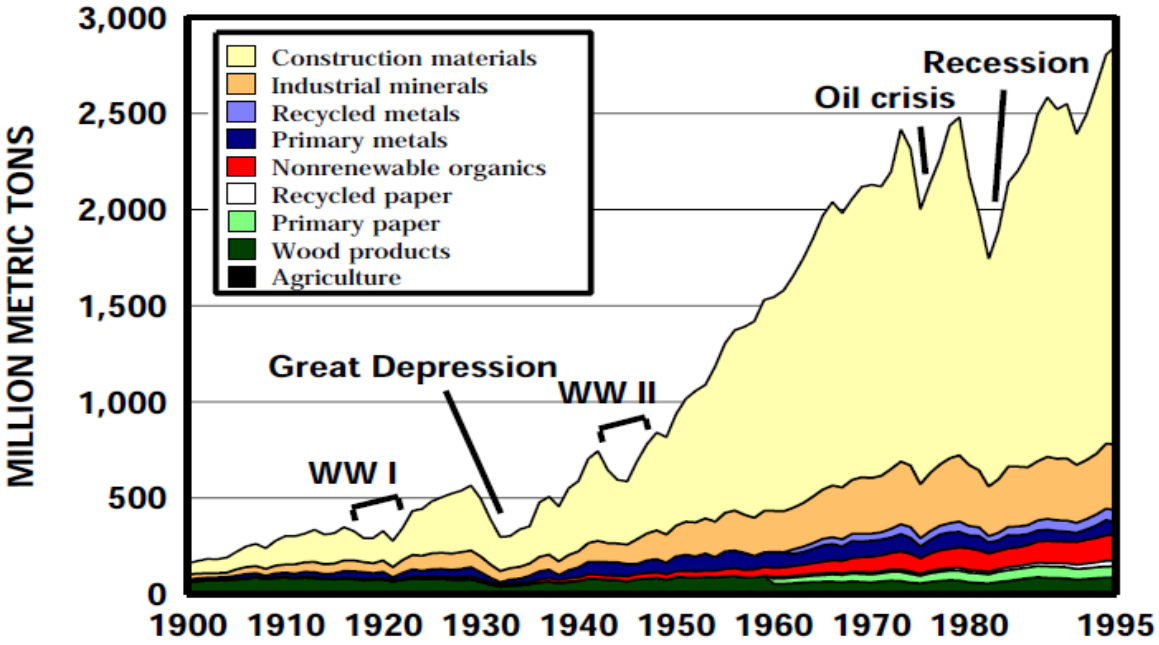

Figure 1-1 Total volume of raw materials consumed in the United States1900-1995. Reprinted with permission from (Matos and Wagner 1998) Annual Review of Energy and the Environment

In the United States the construction industry is the largest consumer of materials, with non-renewable materials representing over 75% of total volume by weight with significant energy expended in transforming them into construction products and contributing to CO_2 emissions (Matos and Wagner 1998, Zabalza Bribián, Valero Capilla, and Aranda Usón 2011).

(Figure 1-1 & Figure 1-2) illustrate the consumption of raw materials in the United States with significant increase in the quantity of materials consumed in the construction sector. (Figure 1-2)indicates that from 1950 onwards non-renewable materials (non-renewable organic, primary metals, industrial minerals, and construction materials) account for 90% by mass in comparison to renewable materials (agriculture, wood products and primary paper), which make up the remaining 10%.

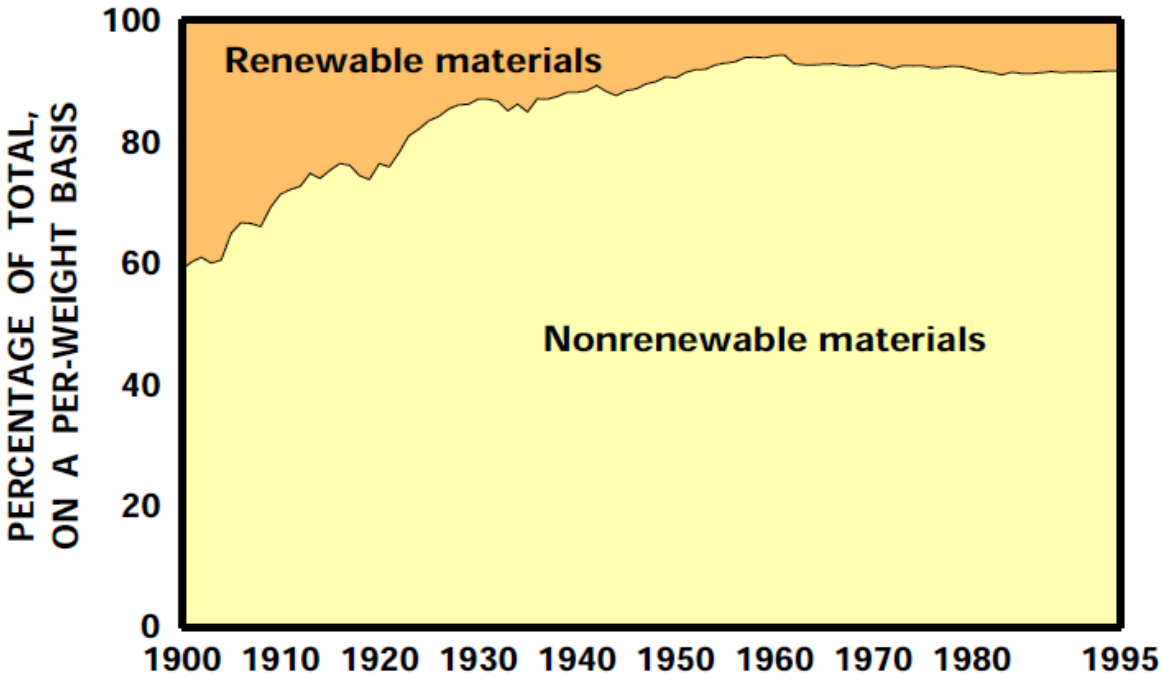

Figure 1-2 -Percentage of total volume of raw materials consumed in the United States 1900-1995, divided by renewable and non-renewable materials. Reprinted with permission from (Matos and Wagner 1998) Annual Review of Energy and the Environment

Table 1-1 and Table 1-2 highlight the embodied energy of building materials specifically lumber, concrete, and steel, and their share of fossil fuels consumed during their extraction, refinement and production.

Table 1-1 Embodied energy of materials for conventional input-output method, and hybrid input-output based method. Reprinted with permission from (Dixit, Culp, and Fernandez-Solis 2015) Copyright (2015) American Chemical Society.

	conventional IO-based method	IO-based hybrid method
Material	embodied energy (A) (kBtu/lb)	embodied energy (B) (kBtu/lb)
carpet (3/8 in. thick), level loop	235.25	228.21
wood lumber	2.19	2.42
hardwood plywood & veneer	11.54	13.95
softwood plywood & veneer	3.01	3.64
paints & coatings	28.99	22.82
adhesives	56.16	21.64
plastic pipes &fittings	42.23	46.86
polystyrene foam insulation	104.84	104.7
bricks	2.07	1.57
clay wall & floor tiles (1/4 in. thick)	18.99	14.38
vitrified clay sewer pipes	8.39	6.36
flat glass	10.6	10.29
cement	1.91	3.13
concrete	0.46	0.54
gypsum, bldg. products	9.05	10.12
lime	1.67	1.87
stone	1.31	1.22
mineral wool insulation	11.83	11.9
virgin steel	10.41	10.11
primary aluminum	29.19	79.3
copper	18.76	24.67

We see that they require 40-60% of non-renewable resources (Coal, Petroleum, Natural-gas) in transforming them from a raw material to a finished product (Zabalza Bribián, Valero Capilla, and Aranda Usón 2011, Dixit, Culp, and Fernandez-Solis 2015).

An opportunity exists for the development of building materials for contemporary assemblies with low embodied energy, and material consumption which will lead to greater material efficiency, and an optimized building assembly as an alternative to the traditional makeup of the contemporary assembly

Therefore, this thesis investigates applications of cellulose at the nano-scale as cellulose nano-crystals, and at the micro scale as ¼'' sisal fibers. The first intervention uses cellulose nano-crystals to create concrete panels, as a way of creating thinner panels with effective thermal resistance. The second intervention involves embedding ¼'' sisal in a cementitious matrix as a reinforcement replacement. The third explores the application of cellulose nano crystals in creating shells for rural communities and disaster hit regions.

Concrete consumption

Typically, concrete consists of 12% cement and 80% aggregate by mass. According to the United States Geological Survey (USGS), domestic production of concrete for the year 2015 required 80.4million tons of Portland cement, and 2.4 million tons of masonry cement, with the peak of concrete production reaching 99 million tons in 2005 (Ober 2016).The global production of cement at 1.6 billion tons accounts for 7% of total GHG emissions (Kumar 2001). In addition, the manufacturing of concrete requires 10-11 billion tons of sand, gravel, and crushed rock, and approximately 1 trillion litres of fresh water for mixing (Kumar 2001). Cellulose based composites can provide alternatives to concrete ultimately reducing material consumption.

Table 1-2 The percentage of total embodied energy for a collection of construction materials. Reprinted with permission from (Dixit, Culp, and Fernandez-Solis 2015) Copyright (2015) American Chemical Society.

	% of various energy sources in total embodied energy				
Material	Oil and Gas	Coal	Electricity	Natural gas	Petroleum
carpet (3/8 in. thick), level loop	1.6	4.21	36.35	23.11	29
wood lumber	1.35	0.81	27.33	10.46	49.76
hardwood plywood & veneer	1.2	1.12	32.94	14.01	42.58
softwood plywood & veneer	1.2	1.12	32.94	14.01	42.58
paints & coatings	2.76	4.45	23.87	21.67	41.88
adhesives	2.53	4.66	26.02	21.49	39.37
plastic pipes & fittings	3.27	2.12	23.26	20.15	47.34
polystyrene foam insulation	2.56	3.07	24.34	24.61	40.48
bricks	0.31	2.14	23.2	51.91	17.02
clay wall & floor tiles (1/4 in. thick)	0.31	2.14	23.2	51.91	17.02
vitrified clay sewer pipes	0.31	2.14	23.2	51.91	17.02
glass	0.28	1.18	28.36	55.97	11.1
cement	0.22	38.3	28.16	6.03	24.37
concrete	0.41	21.05	24.28	14.61	32.98
gypsum, bldg. products	0.3	22.49	18.5	26.56	29.65
lime	0.3	22.49	18.5	26.56	29.65
stone	0.72	3.76	33.64	17.11	30.27
mineral wool insulation	0.52	3.82	39.01	35.55	15.54
virgin steel	0.18	26.43	38.07	24.7	7.91
primary aluminum	3.54	0.48	64.69	9.17	21.04
copper	0.13	6.29	51.09	26.96	11.24

Cellulose

Cellulose, the structural component of plants and trees, is a renewable material as it is found in abundance in nature (Klemm et al. 2005). It is biodegradable and versatile as it is an integral component in construction specifically, Structural lumber, sheathing, wall cladding, and thermal insulation. It is a major structural component of lumber, from wall framing, automobile door frames to bio-degradable films and food packaging. Additionally, it can be recycled and efficiently returned to the environment as bio-degradable material.

In plants, cellulose forms the skeletal structure and is organized in a cellular hierarchy. Cellulose in combination with hemicellulose and lignin form the basic structure and gives native materials, such as wood, cotton, flax, and hemp, their properties. The cellulose molecules arranged in the cell walls of plants have characteristic orientations based on cell wall function and plant type. The changes in fiber orientation determine modulus of elasticity and mechanical strength, so adapting the parameters of cellulosic manmade fibers to custom

requirements by targeting orientation can enable us to create technical fibers with high orientation and high modulus of elasticity (Gibson 2012).

The cell wall of plants is made up of four basic building blocks, cellulose, hemicellulose, lignin and pectin. Cellulose displays remarkable mechanical properties, and with a young's modulus of approximately 130 GPa, and tensile strength close to 1 GPa (Gibson 2012). Similarly, lignin has a modulus of approximately 3 GPa and a strength of about 50 MPa. The cell wall of plants is formed by cellulose fibers reinforcing a matrix of hemicellulose and either lignin or pectin in one or more layers, with volume fraction and orientation of cellulose fibers varying in each layer (Gibson 2012).

Cellulose is versatile and has been chemically produced as a raw material for 150 years. It has numerous applications in fields such as textiles, which began using synthetic fibers from wood cellulose rather than natively occurring cellulose (Klemm et al. 2005). Cellulose is the most common organic polymer representing 1.5×10^{12} tons of total biomass production and is a nearly inexhaustible source of raw materials (Kaplan 1998). It is increasingly being used to develop products that fit the growing need for sustainable products, which have low embodied energy and life cycle associated with it (Klemm et al. 2005).

Scales of cellulose, and applications as a building material

Today wood and its major structural component cellulose are widely utilized at multiple scales and for various situations. Due to its versatility cellulose is utilized in various ways in traditional construction. A few being, structural wall framing utilizing repeating elements of treated lumber, thermal elements such as blown in cellulose to regulate the thermal environment, sheathing elements such as shingles, siding and sheathing boards which protect the structural and thermal elements of the building. Additionally, contemporary mechanical

and chemical techniques are opening possibilities of utilizing cellulose as a building material in a high-performance assembly, especially at the Nanoscale.

The orientation of the cellulose fibers gives the plant cell wall its mechanical strength and allows it to be a self-supporting structure. The changes in fiber orientation determine modulus of elasticity and mechanical strength. Therefore by controlling and modulating the parameters of cellulosic manmade fibers to custom requirements by targeting fiber orientation can enable us to create technical fibers with high orientation and high modulus of elasticity (Gibson 2012). By controlling fiber orientation, we could potentially obtain the desired mechanical strength for a given spatial condition.

Cellulose is an important skeletal component of plants and is formed by repeated chains of D-glucose building blocks and is characterized by "hydrophilicity, chirality, biodegradability, broad chemical modifying capacity, and its formation of versatile semi crystalline fiber morphologies that has seen numerous applications as coatings, films, membranes, pharmaceuticals and food" (Klemm et al. 2005).

Recent advances in the field of chemistry and bio-renewables have led to improvements in the properties of cellulose, with the creation of cellulose nanofibers possessing improved mechanical properties. They are obtained from natural (wood and plant fibers) and regenerated sources (recycled fibers) with potential applications in the field of construction. Additionally, new techniques have been developed greatly improving the mechanical properties of cellulose from traditional sources (discarded wood pulp, agricultural waste) by spinning or chemically treating them to achieve fiber alignment resulting in stronger tensile strength, which allows new applications (Håkansson et al. 2014, Hospodarova, Stevulova, and Sicakova 2015).

CHAPTER 2. LITERATURE REVIEW

This section details how cellulose fibers have been utilized and modified at various scales by various researchers and architects. They include mechanically aligning cellulose fibers to make them stronger, using cellulose fibers in the form of paper tubes, to embedding cellulose fibers in concrete to make it stronger. In the next section I outline three possibilities which provide avenues for research and application.

Cellulose at the Nanoscale

Stronger cellulose filaments through hydrodynamic alignment of cellulose nanofibrils (CNF).

Cellulose fibers obtained from trees have immense potential in bio-based building materials. The main constituent of cellulose fibers are nanoscale fibrils which have potential as a bio based building material (Siró and Plackett 2010). Fibrils in cellulose fibers are organized in a nanoscale lamellar structure (Håkansson et al. 2014). They have highly ordered spiralling orientation along the fiber axis (Eichhorn et al. 2001), with the fibers demonstrating high ultimate strength and stiffness varying widely depending on mean fibril orientation (El-Hosseing and Page 1975, Siró and Plackett 2010, Gibson 2012, Reiterer et al. 1999, Burgert et al. 2002, Eder et al. 2013). Manufactured properties of CNF are different from those of the individual cellulose fibers derived from wood highlighting the importance of alignment of fibrils and their assembling in a controlled manner to achieve strong and stiff filaments (Eichhorn et al. 2001, Burgert et al. 2002).

To achieve desired mechanical strength (Håkansson et al. 2014) utilized a process that combined hydrodynamic alignment with a dispersion-gel transition producing homogenous and smooth filaments from a low-concentration dispersion of cellulose nanofibrils, obtaining specific ultimate strength higher than previously obtained filaments of cellulose nanofibrils. The filaments were prepared using a surface controlled gel transition (Fall et al. 2011, Fall et al. 2013, Jeffery 1922) in combination with hydrodynamically inducing fibril alignment. (Håkansson et al. 2014) describes an idealized version of the process. In a liquid dispersion, the fibrils are free to rotate due to strong electrostatic repulsion. Flow acceleration results in the alignment of the fibrils in the direction of the flow (Jeffery 1922, Köster et al. 2008, Trebbin et al. 2013). To prevent loss of alignment due to Brownian diffusion, an electrolyte was diffused into the suspension reducing the electrostatic repulsion between the particles and freezing the aligned structure into a gel.

Hydrodynamical alignment can be achieved in two ways, first by increasing or decreasing the cross-section of the flow channel, accelerating or decelerating flow, resulting in fibril orientation perpendicular (decelerating flow) or parallel (acceleration) to the flow direction (Trebbin et al. 2013, Jeffery 1922, Köster et al. 2008). Second, through wet spinning, where a fibril dispersion is injected into the outer co-flowing liquid, or sheath flow. The sheath flow has a higher or lower speed than the core flow, inducing shear that accelerates or decelerates the stream with the fibrils and affects alignment (Kiriya et al. 2012). (Håkansson et al. 2014) highlight the improvements in mechanical strength through the alignment of cellulose pulp fibers with the fibrils having a specific ultimate strength comparable to glass fibers and specific stiffness comparable to Kevlar®.

Structural and mechanical properties of wet-spun fibers made from natural cellulose nanofibers.

(Iwamoto, Isogai, and Iwata 2011) investigated spinning natural cellulose with two objectives. The first was to fabricate a new type of cellulose fiber using natural cellulose nano-fibers. Natural fibers found in wood pulp, cotton and ramie fibers are an alignment of cellulose microfibrils limited in their flexibility due to their individual cell wall shapes. In contrast regenerated cellulose fibers are made by dissolution and reconstruction of cellulose molecules, allowing infinitely long and desirable fiber shapes to be obtained (Iwamoto, Isogai, and Iwata 2011).

The difference between natural and regenerated cellulose is in their crystalline structure, with natural cellulose being classified as cellulose I and regenerated cellulose as cellulose II (Iwamoto, Isogai, and Iwata 2011). Due to the higher elastic modulus of cellulose I when compared to cellulose II (Nishino, Takano, and Nakamae 1995), natural cellulose fibers have potentially higher stiffness and strength compared to regenerated fibers, with spinning maintaining the cellulose I structure, allowing flexible material design and retaining the physical properties of cellulose (Iwamoto, Isogai, and Iwata 2011) The second objective for spinning the cellulose was to control the alignment of the cellulose nano-fibers thereby controlling ultimate strength.

(Iwamoto, Isogai, and Iwata 2011) utilized cellulose nano-fibers prepared from wood pulp and tunicate cellulose by 2,2,6,6-tetra-methylpiperidinyl-1-oxyl (TEMPO)-mediated oxidation, and, was wet spun to produce cellulose-I fibers. They studied the nano-fibers using an atomic force microscopy (AFM), scanning electron microscope (SEM) and wide-angle diffractions.

They present the various samples of fibers spun from wood, tunicate fibers and natural cellulose fibers, cotton (Gassan and Bledzki 1999), and regenerated cellulose fibers lyocell (Johnson et al. 2008). The mechanical properties of the tunicate fibers were not influenced by the spinning rate. The Young's modulus and tensile strength of the wood-spun fibers increased with a faster spinning rate due to an increase in orientation index. Apart from the wood-spun fibers, all the spun fibers displayed higher young's moduli and lower strengths compared with lyocell (Johnson et al. 2008).

Cellulose as ¼'' Fibers as in a Cementitious Composite.

Cement composites utilizing cellulosic fibers in pulp form from wastepaper.

In addition to natural and manufactured sources of cellulose, cellulose fibers can be obtained from copious quantities of lignocellulosic waste, such as vegetable fibers, wood pulp, and pulp from waste paper. (Hospodarova, Stevulova, and Sicakova 2015) utilized this cellulosic pulp, partially substituting the filler in a cement mixture. Varying densities and compressive strength of the two types of cellulosic fibers (bleached wood pulp and recycled paper) and three mixes each, were made and observed.

(Hospodarova, Stevulova, and Sicakova 2015) cast fiber-reinforced cement composites in two stages. They mixed the with 50 %wt. of water, cement, sand and, remaining water added and mixed to obtain a uniform fiber dispersion. The mixture was poured into 40 mm × 40 mm × 160 mm at +18 °C and cured for two days and unmoulded. After letting set for an 28 days the composites were weighed and tested for their density and compressive strength (Hospodarova, Stevulova, and Sicakova 2015).

Out of the two sets of composites, the first set created from waste paper show higher values for strength (16.28-21.85MPa) when compared to the compressive strength of the second set from wood pulp (13.84-18.72MPa). For each of the two sets there was an increase in compressive strength with increasing fiber content in each of the amount of cellulose in the mix up to 5%wt. (Hospodarova, Stevulova, and Sicakova 2015).

Cement composites utilizing coated cellulosic fibers from fibrous Plants

Limited research is being carried out in using cellulose fibers as reinforcement in cement-based composites. The following is a summary of a few studies conducted on embedding natural fibers in concrete.

Fan and Ahmed (Ahmad and Fan 2018) investigated imbedding sisal fiber, in the form of 3mm diameter string, coated with epoxy, polyurethane, vinylester, and polyester in a cementitious matrix. They focused on the interface between fiber reinforcement and cementitious matrix highlighting the inability of uncoated fiber in developing into compact interface. This was due to the absorption/desorption during the curing process, leading to low mechanical properties of the composite.

They highlight the strength and stiffness of sisal fiber ranging from 550MPa to 750MPa when compared to jute ranging from 300MPa to 800 MPA, highlighting its use as plaster reinforcement in the building industry, and its potential to reinforce composites for use in low-cost housing applications.

The authors used natural sisal fiber rope composed of 3-ply twined yarns to make up 3mm diameter string. The four resins, known for their slow cure time, were epoxy, polyurethane, vinylester and polyester. They speculate that, due to the abundance of hydroxyl in the sisal, the glucose chains are held together using hydrogen bonds between hydroxyl

groups to form microfibrils, and these OH bonds are the primary reason for a strong interface bonding between the fiber and the matrix.(Ahmad and Fan 2018)

The two issues in using natural fiber is their ability to absorb moisture altering the strength and durability, and moisture-induced swelling/shrinkage resulting in early cracking of concrete prior to loading. The authors discuss the effects of the coating on the natural fiber, with significant reduction in the intensity of OH resulting in reduced water absorption.(Ahmad and Fan 2018)

Additionally, the resin coating reduces open porosity between fiber and cement matrix, decreasing permeability to water intake. This leads to reduced fiber swelling when mixed in the cementitious matrix, resulting in a compact interface due to the reduction in formation of voids between various components. The compactness of the interfacial region depends on the type of resin coating used with Epoxy more compact than the polyurethane coated sisal, which is more compact than vinylester and polyester coated natural fiber composites. The fiber reinforced composites displayed high toughness and a degree of flexibility and plasticity in the composite (Ahmad and Fan 2018).

Filho et al. (Silva, Mobasher, and Filho 2009) analysed the strain hardening properties of cementitious composites utilizing sisal with a strength of 400MPa, by analysing cracking mechanism in a multilayer sisal fiber reinforced composite (SFRC). They attribute the enhanced strength and ductility of the composite to the ability of fibers to bridge matrix cracks and transfer loads, resulting in a distributed microcrack system.

The authors attribute the aging process of fibers in the matrix to mineralization resulting in decreased tensile strength and decreased fiber pull-out ligament after fracture. The authors used a cementitious matrix consisting of 50% Portland cement, 30% metakaolin (MK), and

20% calcined waste crushed clay brick, reducing calcium hydroxide production, showing no reduction in strength and toughness from accelerated aging tests (Silva, Mobasher, and Filho 2009).

Due to the low volume of fibers, the stiffness of the composite is dominated by matrix properties. After initiation of cracks in the matrix, they are bridged by the longitudinal fibers. Following initial cracks, other matrix cracks are initiated through the specimen at regular intervals and propagate across the width. The stiffness of the composite with reinforced sisal fiber keeps newly formed cracks from widening, promoting multiple cracking behaviour. The stiffness affects the rate of reduction of crack spacing. It reaches a steady state, and is defined as saturation crack spacing, beyond which no reduction in crack spacing is observed as no new cracks form (Toledo Filho et al. 2009).

The authors report average ultimate tensile strength of 12 MPa and initial modulus of 34.17GPa indicative of high mechanical performance from the sisal fibers indicating suitability for structural applications. Additionally, they note the elevated toughness value of 45.95 and 22.13 KJ/m_2 in tension and bending respectively demonstrating high ductility of the sisal composite (Toledo Filho et al. 2009).

Filho et al (Filho, Silva, and Filho 2013) continued their work investigating the durability of sisal fibers in cement composites, and partial substitution of Portland cement with pozzolanic materials to reduce calcium hydroxide in the matrix. They produced composites for this investigation using two matrices, one with 50% partial cement replacement by metakaolin (PC-MK) and the other composed of ordinary Portland cement (PC). The two composites were subject to 25 wet/dry aging cycles and tested under a 4-point bending load configuration at ages ranging from 28 days to 5 years.

Additional microstructural investigation was performed using a scanning electron microscope to observe fiber degradation after being exposed to wet/dry cycles (Filho, Silva, and Filho 2013).They tested the samples to bending loads after 25 wet/dry cycles. They observed a ductile behaviour with multiple cracking formation in the Portland cement-metakaolin (PC-MK) system for both reference and aged samples.

Conversely the Portland cement (PC) composites presented a progressive degradation process with increasing wet/dry cycles. Additionally, they observe that both ductility and bending strength is reduced to the same level as an unreinforced matrix after 25 wet/dry cycles (Filho, Silva, and Filho 2013).

They report that aging cycles does not affect fracture behaviour of the PC-MK composites, whereas the cycles affect the fracture process of the PC composite changing its behaviour from multiple to single cracking formation, with a threshold level of 10 wet/dry cycles for the PC composite (Filho, Silva, and Filho 2013).

They conducted a microstructural investigation with fibers extracted from the PC-MK and PC aged composites to investigate the degradation process. The fiber structure of the sisal extracted from the PC-MK composite remained intact with no signs of degradation, and sisal extracted from the PC composite showed signs of degradation with the fiber-cells being mineralized due to high calcium hydroxide concentration. The authors show a decomposition of hemicellulose and lignin sisal fibers in the two matrices following the wet/dry cycles. They highlight the role of lignin and hemicellulose for linking the microfibril structure. Additionally, their degradation can possibly lead to a reduction in the macro-mechanical properties of the sisal fiber (Filho, Silva, and Filho 2013).

Wei and Meyer (Wei and Meyer 2015) in their work discuss the degradation mechanisms of natural fiber in the alkaline and mineral rich environment of the cement matrices. They studied the durability of sisal fiber reinforced cement composites by exposing them to wet/dry cycles, as well as studying the compositional changes, mechanical, and physical properties of the embedded sisal fiber.

The samples were subject to wetting/drying cycle after a 28-day curing period, with the alkalinity of pore solution investigated as a critical actor leading to the alkaline hydrolysis of amorphous components in the natural fiber. The authors highlight the role of lignin, pectin, and hemicellulose in the overall degradation of natural fibers.

The paper highlights the degradation process by which fibers in the composite absorb water accompanied by volume expansion from the cement composite during mixing and curing. During the hardening process, the cement captures some of the water from the fibers to form a high alkali pore solution in the space between matrix and fiber caused by drying shrinkage, accelerating the deterioration process.

They propose improvements in durability of the sisal fiber by replacing 30% by mass of cement with metakaolin, controlling the pH value of the pore solution. They report that the tensile strength of fiber immersed in Portland cement (PC) suffers severe reduction as evidenced by the degradation of lignin and hemicellulose and their increased crystallinity (Wei and Meyer 2015). Lignin and hemicellulose functions as a protective barrier arresting the precipitation of portlandite in cell walls (Wei and Meyer 2015).

The authors highlight four interactional steps for natural fiber degradation:

1. Degradation of lignin and hemicellulose exposing holocellulose.
2. Degradation of hemicellulose leading to loss of integrity and cell wall stability.

3. Degradation of intra-molecular hydrogen bonding leading to cellulose microfibril dispersion.

4. Alkaline hydrolysis of amorphous regions leading to complete degradation of cellulose micro-fibrils. Additionally, hydration products infiltrate the cell wall leading to mineralization and embrittlement of natural fiber. This leads to loss of strength and strain capacity of the composite (Wei and Meyer 2015).

Filho et al. (Tolêdo Filho et al. 2003) addressed the issues of fiber durability in an alkaline environment for vegetable fiber reinforced mortar composites (VFRMC). The modified VRMC were exposed to wet/dry cycles and open-air weathering. They were then studied for their influence on the microstructure and flexural behaviour of composites.

The authors utilized a range of modified VFRM composites based on the following specifications and were then exposed to the wet/dry cycle (Tolêdo Filho et al. 2003).

1. A Control mix \ OPC mortar mix, reinforced with randomly distributed short (25 mm) untreated sisal or coconut fibers, and aligned long (375 mm) untreated sisal fibers both cured for 28 days.

2. Carbonation of matrix in a co2 incubator, post curing, for 109 days.

3. Fibers immersed in silica fume prior to their incorporation into the matrix. \ long sisal fibers were immersed in slurried silica fume for 10 min and air dried for 15 min.

4. 10% by weight of OPC matrix replaced with undensified silica fume.

5. 40% by weight of OPC matrix replaced with blast furnace slag.

6. 40% by weight of OPC matrix replaced with blast furnace slag, aligned long sisal fibers immersed in slurried silica fume.

Based on these modifications the authors studied the following mixes (Tolêdo Filho et al. 2003)

1. M1—mortar mix (1:1:0.4—cement: sand: water by weight)
2. M1ms—mortar mix M1 with 10% by weight of cement replaced with silica fume;
3. M1slag—mortar mix M1 with 40% by weight of cement replaced with slag
4. S2S1—2% of randomly distributed short sisal fiber (25 mm) plus 1% of aligned continuous sisal fiber (375 mm)
5. C2S1—2% of randomly distributed short coconut fiber (25 mm) plus 1% of aligned continuous sisal fiber (375 mm)

The durability of untreated VFRMC samples were evaluated based on the flexural properties of the specimens before and after exposure to various environments. The samples were obtained from untreated control specimens cured for 28 days. The reference specimens were carbonated for 109 days and subjected to various ageing regimes with bending load-deflection tests carried out. A post cracking ductility behaviour is observed both for control and reference specimens (Tolêdo Filho et al. 2003).

The durability of aged and unaged VFRMCs incorporating silica treated fibers were subject to load-deflection tests. A comparison of final cracking strength, flexural strength, and toughness of the treated and untreated sisal-fiber mortar at 28 days show that the treatments resulted in strength reductions of 30-40%, with the decrease in values attributed to the reduced bonding between fibers and matrix. After 180 days of ageing the treated specimens presented higher FCS, flexural strength and toughness than the untreated specimens at the age of 28 days (Tolêdo Filho et al. 2003).

The authors also studied the immersion of the aligned long sisal fibers in a silica fume slurry prior to their addition to a matrix in which 40% by weight of the OPC was replaced with

blast furnace slag. Load-deflection curves were measured 28 days after ageing. The specimens were then weathered outdoor for 322 days with the results showing a retention of composite flexural toughness and strength with age (Tolêdo Filho et al. 2003).

Filho et al. (Toledo Filho et al. 2009) studied the durability of compression moulded sisal fiber-cement mortar laminates (SFRML) . They created two mixes using Portland cement (PC)-M1 and a calcium hydroxide (CH)-free PC-calcined clay matrix embedded with sisal fibers-M2 and subjected to accelerated wet/dry cycles while studying its microstructure and flexural behaviour. They assembled the composite in moulds layering the modified Portland cement and unidirectional aligned sisal fibers alternatively, up to a total of 5 layers. SFMRL were created using PC and a CH-free PC-calcined clay matrix and subjected to accelerated wet/dry cycles, with the microstructures and flexural behaviour being studied.

The experiment involved the partial reinforcement of PC by metakaolin (MK) and crushed waste calcined clay bricks (CWCCB) ranging from 10% to 55% creating multiple pastes with final matrix composed of 20% of CWCCB and 30% of MK. Creating the compression moulded laminates, the mortar mix was placed in a steel mould, one layer at a time, followed by one layer of long unidirectional aligned fibers(up to five layers) and vibration resulting in a sisal fiber volume fraction of 10%. They were unmoulded after 24 hours and fog cured for 28 days.

The authors studied durability based on the four-point bending test after controlled cycles of wetting and drying. The authors highlight a drop in CH content from 14.92% (reference matrix) to 1.41% in composites using 10%, 30%, and 40% of PC substitution by MK

The authors studied durability of the two composites based on toughness and flexural strength obtained before and after 25, 50, 75 and 100 cycles of aging. For M1 they observed that first crack strength increased up to 45% with aged specimens subject to the wet/dry cycle presenting multiple-cracking behaviour. The un-aged reference specimen presenting ductile behaviour drastically decreased by the aging process.

For M2, ductile behaviour is observed for both reference and aged specimens. They observed that first crack strength increased up to 65% after 100 cycles, with a higher increase for specimens containing pozzolans. The authors attribute this behaviour to a combination of sisal fiber degradation in the OPC mixtures with the aging process and the late pozzolanic reaction in the CH-free mixtures.

The contribution of sisal fiber mineralization in strength reduction and strain capacity leads the authors to posit the reduction in the homogenized session of the OPC composites occurs after exposing specimens to the wetting and drying cycles. Additionally, they highlight the role of Pozzolanic reactions in higher FCS values once hydration reactions of OPC progress at late ages and CH produced is consumed by the pozzolan along with the evolution of these reactions (Toledo Filho et al. 2009). Additionally, it is the author's opinion that increase in FCS observed in both composites cannot exclusively be attributed to thermos-activated hydration process and requires further understanding.

Ferreira et al (Ferreira et al. 2014) investigated the hornification on the sisal fiber-matrix bond adhesion as well as dimensional stability and mechanical behaviour of sisal fibers under direct tension. Additionally, they analysed the characteristics of sisal fiber reinforced cement composite using bending load tests.

The authors prepared the fibers by immersing them in water until saturated and dried and mixed with the matrix composed of 30% Portland cement, 30% metakaolin, and 40% fly ash. They present results in which the fibers exposed to 10 wet/dry cycle displayed a decrease in water retention capacity by 50%. The authors attribute it to the stiffening of the polymeric structure of the fiber-cells (Ferreira et al. 2014).

For fibers 255mm in length, the fiber treatment improved maximum adhesional stress by 40% and a 50% increase in frictional stress. The fibers with a length of 50mm showed breakage within the matrix, and a 34.4% increase in maximum tension due to fiber treatment. From the values of pull-out loads, an increase in embedment length from 25mm to 50mm increased the maximum pull out loads of untreated fibers from 3.73 to 6.35 N. The maximum load for the treated fibers increased from 4.53 to 8.46 N. The stiffness value displayed and increase in stiffness ranging from 40-120%. The Composites reinforced with treated sisal fiber showed a better mechanical behaviour under bending loads. Their samples showing an increase in tensile strength and strain at failure for the hornified sisal fibers by 5% and 39% respectively (Ferreira et al. 2014).

Cellulose at Building Scale.

Cellulose in the form of paper tubes.

In addition to the traditional uses of cellulose in the form of wood, there are numerous ways cellulose has been used in novel ways most recently by Japanese architect Shigeru Ban. There is a unique tradition of utilizing cellulose or paper in Japan as barriers, partitions, skins in traditional Japanese architecture, colloquially referred to as “shoji”. Since the 80s Shigeru ban has been pushing the boundaries of sustainable materials and construction methodologies through research and pioneering recycled paper tubes, initially used in small scale pavilions

and experimental disaster relief structures, eventually used in large scale structures such as civic spaces and exhibition pavilions (Ban 2009). Ban took paper tubes conventionally used as molds in construction and brought it to the fore crafting a unique identity for the material.

Ban has been pivotal in developing and creating a formal structural logic around cellulose in the form of recycled paper tubes. The paper tubes are made from re-constituted post-consumer recycled paper and treated with, waterproofing and adhesive, for stability and their hydrophilic property (Ban 2009). Initially utilized as a minor component in the larger structural framework Ban, refined it and utilized It as a structural material underpinning several of his major large and small-scale work.

Ban's first free standing structure to utilize paper tubes was, paper tube structure 01 for the 1989 world design expo in Nagoya. It was designed as a contemplative space, to provide respite from an urban setting. The structure uses 48 paper tubes, 4 meters high, capped by a compression ring and tent fabric to enclose the space. The tubes are waterproofed using paraffin and additional strength is provided by adhering them together with a glue compound. (Ban 2009).

In addition to creating a structural logic out of paper tubes for residences and pavilions, he utilized them as the basis for temporary shelters, one of them being the paper log house which has been fabricated and built in Japan, Turkey, and India following severe earthquakes. The homes share a similar typology with walls constructed out of 4 mm paper tubes and 106 mm diameter and filled with shredded waste paper for extra insulation, with a spongy adhesive tape used in the interstitial spaces between the paper tubes, along with fiberglass roofing in some of the units. The houses were elevated using locally available beer crates stuffed with sand bags (Ban 2009).

Thin shell concrete structures

Shells are spatially curved surface structures which support external loads. The American Concrete Association defines shells as: “A three-dimensional spatial structure made up of one or more curved slabs or folded plates whose thicknesses are minor compared to their other dimensions” They are characterized by their three-dimensional load carrying behaviours which is determined by the geometry of their forms, support conditions, and nature of applied load. The behaviour of shell structures can also be also referred to as ‘form resistant structures’ (Committee). They afford tremendous opportunity in carrying external loads perpendicular to the surface by in plane membrane action.

In the 20th century concrete shell structures were pioneered by individuals such as Hans Isler, Felix Candela, and Eero Saarinen pushing the boundaries through efficient form finding and load distribution. Some of the prominent examples of thin shell concrete structures are, the Church of San José Obrero by Félix Candela in Monterey built 1959, Alster-Schwimmhalle in Hamburg built 1967, and Kresge auditorium by Eero Saarinen built 1955 (Figure 2-1) (Adriaenssens et al. 2014). Thin shell concrete structures are classified according to their curvatures, single curvature for cylindrical and conical, synclastic for dome-like, anticlastic for saddle-like or experimental. A concrete shell transfers load to its supports mainly though forces acting in the plane of the shell surface, otherwise known as membrane stress. Membrane stress that is formed in the shell can be predominantly compression or a combination of compression and tension.

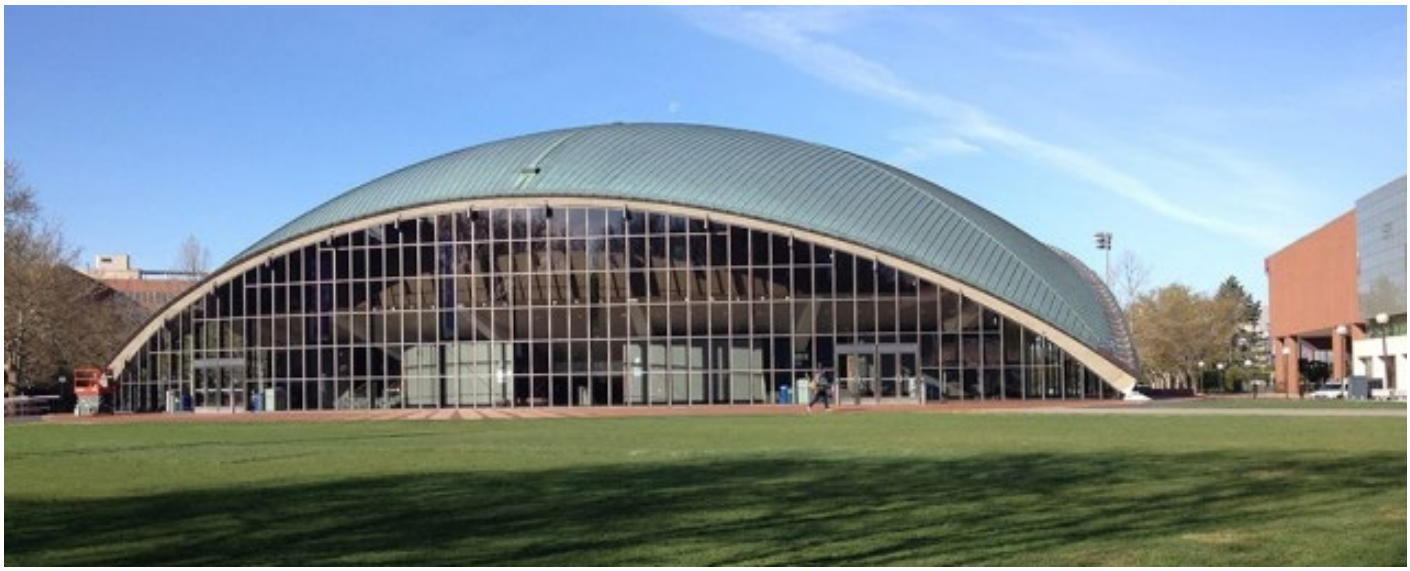

Figure 2-1 Kresge auditorium by Eero Saarinen on the MIT campus built 1955. MIT Library.

CHAPTER 3. CONTEMPORARY APPLICATIONS

This section details the investigations that were pursued utilizing existing literature and research on cellulose, leading applications in design and construction.

1. The first investigation utilized cellulose nanocrystals to create thin shell concrete structures. The aim of creating a thin shell concrete structure was to provide a framework for cellulose based spatial applications. A shell could be utilized as community gathering space in rural regions. Additionally, they could be utilized in disaster hit areas where rapid and safe construction of shelters is integral.

2. The second investigation utilized microclimate data sourced from the mobile diagnostics lab and an adjacent weather station to obtain baseline data of a composite concrete assembly. The baseline data of the composite concrete panel was compared to the composite concrete panel seeded with biofibers to determine thermal effectiveness.

3. The third investigation utilized sisal fiber to improve the mechanical properties of engineered cement composites. The primary aim of this investigation was to analyse the improvements ¼'' resin coated fibers can display on the tensile strength of the composite.

Scale Concrete Shells with Cellulose Nanocrystals

The aim of this investigation was to create scale concrete shells as a means of testing cellulose-based applications utilizing cellulose nanocrystals. This study would be the primary step for testing cellulose-based applications with region specific fibers. This would provide alternatives to the spatial conditions that define the standardized wall assembly. Additionally, this would provide a framework for incorporating region specific fibers reducing reliance on contemporary modes of construction that contribute to higher energy consumption and community-based equity.

The CNC is chemically modified product where the cellulose fibers are aligned in single direction when dispersed in water, imparting higher mechanical properties (CelluForce 2016). The spindle shape of the fibers allow them to form liquid crystals in a fluid medium. Concentration of the fluid results in the spindles self-orienting and forming layers where each layer is oriented in the same direction. The high crystallinity imparts the CNC with its high strength. Each crystal has a stiffness of 150 GPa and a tensile strength in the order of 10 GPA.

Concrete shells are designed through form finding methods where an optimum form, which can resist the various loads through its curvature in both directions, is generated. The concrete matrix resists compressive loads through membrane action to the supports with reinforcement to tackle tensile forces that develop in the shell.

A well-formed concrete shell has almost no bending apart from membrane stresses, axial compression and tension, allowing a thickness of 80mm for reinforced or prestressed concrete.

Therefore, the objectives of this study were to create scale concrete shells by mixing the cellulose nanocrystals (CNC) with concrete investigating application strategies through digital design and physical mock-ups. Sample test cylinders were created to test and study the role of CNC in improving its mechanical properties. The structural strength demonstrated through the addition of cellulose nanocrystals is currently attributed to close packing of the crystals allowing for reduced inter-fiber spacing in the cement matrix. This leads to greater interaction between the cellulose and the cement system during the curing process, thereby demonstrating greater potential to alter micro-cracking leading to increased overall strength (Cao et al. 2015).

Previous experiments involving the blending of cellulose with concrete aimed at studying chemical interactions between the cellulose nanocrystals and the cement system leading to improvements its physical properties (Cao et al. 2015). Their investigations studied the make-up of the cement matrix at the cellular level and CNC-cement structure through x-ray diffraction, additionally they studied the influence of the CNCs on the degree of hydration during the curing process which influenced the micro-cracking, influencing the final strength of the concrete system.

Yet, previous studies did not investigate the possibilities of utilizing this strengthened concrete mix as part of a built structure which this paper aims to study by casting scale thin shell concrete structures.

The thin shells could be utilized in humanitarian crises areas or in rural communities instead of a contemporary assembly which relies on standard materials. The shells could be set up rapidly with a modular formwork. The reusability of the formwork combined with region

specific fibers to create the shells can help in the construction of a greater number of thin shell concrete structures in comparison to traditional thin shell concrete structures.

The concrete cylinders were first cast to test structural strength and thermal properties in a laboratory setting creating a baseline and recording improvements in mechanical strength of the concrete system with a consistent mix and varying CNCs. A total of 4 cylinders will were cast, with the first one acting as a control mix. Commercially available quikcrete® was selected as the basis of creating the concrete mix with ratios outlined in (Table 3-1). The remaining 3 cylinders were cast with increasing levels of the CNCs by weight of water (1%-4%), with the final test cylinder consisting of the highest percentage of CNC (4% by weight of water) as specified by the manufacture.

Therefore, this thesis will investigate the possibility of utilizing the CNC strengthened mix in creating shells as a framework for future applications. By casting the strengthened concrete in the formal structural system of a shell, the intent is to vary the thickness of the CNC cast shell while achieving structural stability, incorporating region specific fibers.

Materials

To create the concrete prototypes, mechanically strengthened cellulose fibers in the form of cellulose nanocrystals or Nanocrystalline Cellulose (NCC™), were obtained from CelluForce Inc. The CNCs through their interaction with the cement matrix improves the mechanical properties and final strength of the concrete mix (Hospodarova, Stevulova, and Sicakova 2015). The CNCs are in the form of a white powder that disperse in water creating a colloidal solution which can be used in the concrete mix.

Experimental Set-Up

For the first stage of the experiment cylindrical prototypes were cast utilizing the cellulose Nano crystals in an increased ratio (Table 3-1), combined with concrete. The cast prototypes were then studying for their mechanical properties.

Table 3-1 Experimental matrix for the CNC reinforced concrete mix. RM - reference mix, CM - concrete mix.

Mix	Cement wt.(oz)	Aggregate wt.(oz)	Water wt.(oz)	Cellulose Nano crystals wt.(oz)	Percentage
RM	19.2	14.7	12.5	0	0
CM-1	19.2	14.7	12.5	0.25	2
CM-2	19.2	14.7	12.5	0.3	3
CM-3	19.2	14.7	12.5	0.6	6

For the cylindrical moulds 4 paper tubes measuring 3'' by 4'' were used for casting the concrete samples. The first mold (RM) was cast without the cellulose nanocrystals to act as control cylinder to which the other cylinders (CM) would be compared. The remaining three moulds were cast with increasing percentages of Cellulose Nano crystals (0 %, 1%, 2%, and 4% by weight of water).

First, the crystals were dispersed in de-ionized water in a beaker using a magnetic stirrer. The magnetic stirrer was used to create a vortex. Once a vortex formed the crystals were added and agitated till, they formed a colloidal solution. Agitation continued for an hour to ensure uniform distribution of the cellulose nanocrystals and prevent clumping. Once adequate dispersion had been achieved, the solution was used to create a concrete mix with the ratios specified in table 3.

The cylinders were cast at room temperature (72ºF) and left to cure in the same environment for two days. After the second day the paper tube moulds were peeled off and the cylinders were left to cure to full strength in the space at 72ºF.

Testing

Concrete testing will be carried out to determine various properties of a formulated mix, with compressive strength being the most common test parameter, with durability being the other during the structure's lifespan. The test results are used for quality control, and estimating the strength of concrete that forms the structure (NRMCA 2003). The cylinders will be tested according to ASTM C 39 (International 2017). Compressive strength is measured by testing concrete samples in a compression testing machine. The samples are loaded onto the machine and an increasing load is applied onto the cylinders till failure. To ensure accuracy two samples are created and tested to obtain the cross-section on both cylinder's axis. The compressive strength is then calculated by dividing the failure load by the cross-sectional area of the sample resisting the load, and output as pound-force per square inch (PSI).

Concrete Shell Models

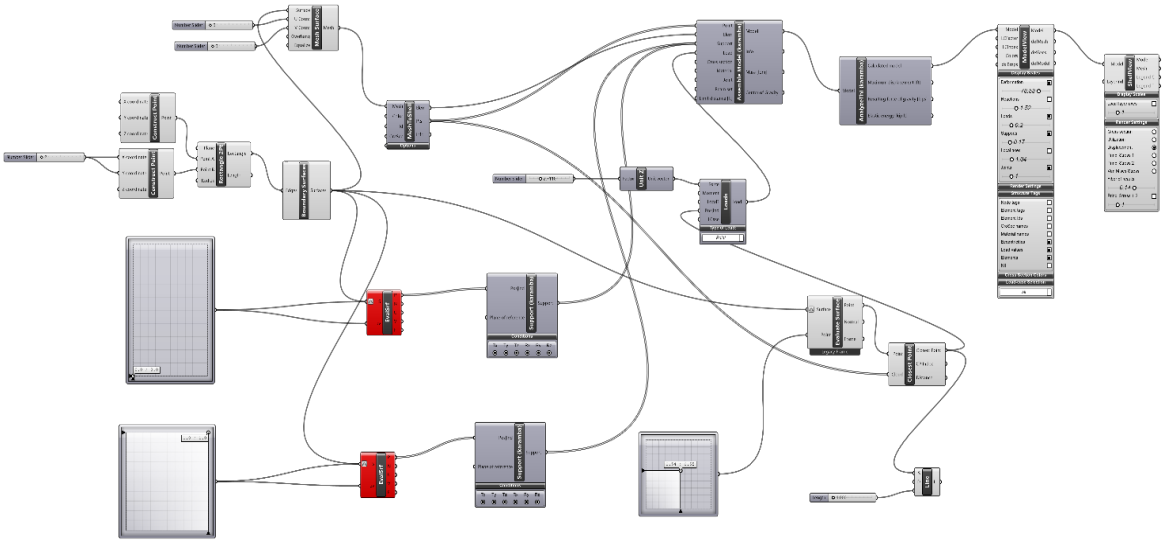

Figure 3-1 Karamba script in grasshopper highlighting the workflow for creating 3d shell model, which was used to build the framework.

The next stage of the casting process involved creating two concrete shells, one with a standard concrete mix and the second shell embedded with 2% CNC crystals by mass of water, as recommended by the CNC supplier. The concrete shell was digitally modelled in rhino and grasshopper using the karamba plugin (Veenendaal and Block 2014) (Figure 3-1). Karamba is a parametric structural engineering tool which provides analysis of structural systems, in this case shells. The script specifies the base co-ordinates and generates a 3-dimensional curved mesh. The deformation of the mesh is based on support conditions and point load acting upon the surface.

Figure 3-2 Scale wood frame model constructed with reference rhino model, grasshopper and karamba, using ½’’x ½’’ basswood members.

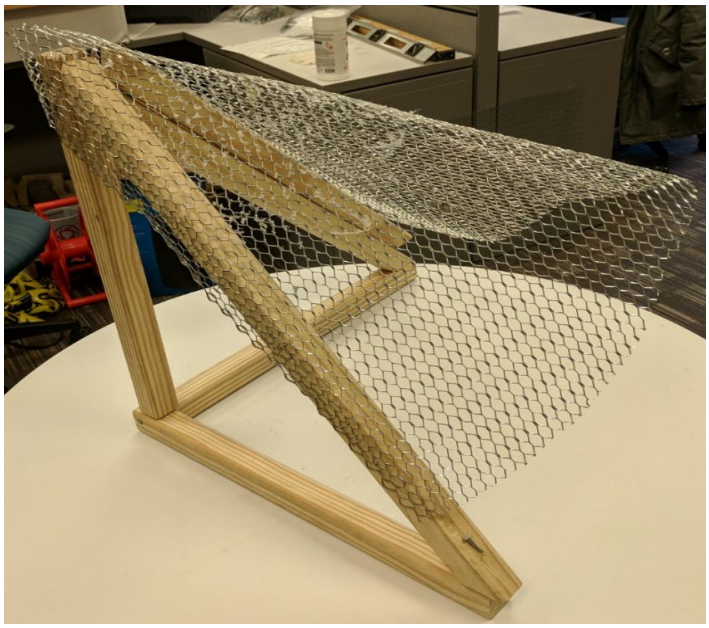

Figure 3-3 Scale wood frame model with larger 1’’ X 1’’ lumber to account for lateral stress exerted by the metal mesh.

A pyramidal framework (Figure 3-1) was then constructed based on the dimensions modelled in Rhino and Karamba. Initially bass wood measuring ½'' x ½'' was used due to workability and to cast half a shell measuring 1'X1'X1', with the aim of scaling future casts by utilizing two frames, to cast a complete shell. The framework was based on the point load of 1kN, fixed two point supports and deflection required based on the load specified in Karamba.

A steel mesh was spanned between the wood frame to align it as close as possible to the target shape and deflection as specified in Karamba. Connecting the mesh formwork to the basswood members proved insufficient in creating a rigid formwork due to the strong lateral stress imposed by the mesh. Therefore, the framework was reconstructed with thicker pieces of wood measuring 1'' x 1'' (Figure 3-2). The aim was to create two shells and compare them in terms of structural stability.

The first shell (Figure 3-3) was cast with regular concrete without coarse aggregates to reduce the weight of the shell. 12.5 ounces of water was added to a 10lb bag of quikcrete® and mixed

Figure 3-4 Cast concrete shell without CNC measuring 1' X 6'' X 11½'' and ½'' thick.

Figure 3-5 Cast concrete shells with CNC measuring 1’ X 6’’ X 11½’’ and 1/4’’ thick.

with a hand trowel. The prepared mix was spread on to the mesh frame (Figure 3-2) and formed by hand to conform to the contour of the mesh curve to obtain desired structural stability. The shell measured 1’ X 6’’ X 11½’’ with the thickness of the shell coming to ½’’. The shell was left to cure at room temperature (73ºF) for 2 days after which it was un-molded from the formwork (Figure 3-4).

The second shell (Figure 3-5) was cast with 2% cellulose nanocrystals by weight of water. 0.43 ounces of CNCs were added to 12.5 ounces of water and agitated for an hour to ensure uniform dispersal. After an hour of agitation, the colloidal solution was added to the dry concrete mix and hand mixed to ensure uniform dispersal.

The CNC-concrete mix was again hand formed on the same mesh wood frame curve and the thickness of the shell was reduced to ¼'' to account for the improvement in physical strength attributed to the addition of the cellulose nanocrystals. The shell was cured in the same environment as the control shell at room temperature (73ºF) for 2 days after which it was unmoulded from the formwork (Figure 3-4).

Results and Discussion

The shells were monitored for cracking and/or buckling over the next few weeks to document the influence of the cellulose nanocrystals on the shell's structural stability. Following the long-term study of the shells and utilizing this data a CNC-concrete mix will be formulated, with the ratio of CNC to cement optimized for a stable shell structure. This will form the basis of future studies utilizing region specific fibers that could replace the CNC.

The goal of this study was creating a rapid deployment framework for humanitarian crises regions and rural communities. The framework would be deployed with local fibers being used as a reinforcement replacement for varying spatial conditions. Further work is needed for the support structure used to cast the shells especially with region specific fibers that would change the nature of the shell. Additionally, the support structure could be moulded by these local fibers, selected based on their source and their technical properties.

CHAPTER 4. TESTING CONCRETE ASSEMBLIES IN THE MOBILE DIAGNOSTICS LAB

Expressing the properties of cellulose, through orientation or layering, yields composites that can resist thermal fluctuation. Based on the inherent thermal properties of cellulose (Gibson 2012), this study dealt with embedding bio-fibers in concrete, creating a thermally efficient composite assembly. Additionally, the goal is to utilize region specific bio-fibers when creating wall panels as it holds implications for the energy economy, and material vernacular.

In addition to using cellulose as a reinforcement replacement in concrete for non-integral uses. Using cellulose in an assembly and as a hybrid composite can lead to thinner composite panels with desired thermal resistance. This material composite with optimized mix proportions can lead to reduced concrete and material consumption.

The first goal was to test the performance of a standard concrete panel assembly, with thermal data compared to the performance of future cellulose-based composite panels. This data would be used to create a framework where various composites could be measured against baseline data for cellulose based concrete assemblies.

The mobile diagnostics lab was utilized for the duration of the experiment. Data was generated from custom concrete panels inserted into the removable wall assembly to create a baseline with which to compare the cellulose concrete panels. The results are presented under (Figure 4-5, Figure 4-6, Figure 4-7, Figure 4-8, Figure 4-9, and Figure 4-10)

Figure 4-1 Profile of the Mobile Diagnostics Lab with removable wall panel in the rear wall.

.

Mobile Diagnostics Lab

The mobile research and diagnostics lab (MDL), is a mobile structure designed and constructed by an interdisciplinary team of researchers at the Centre for Building Energy Research (CBER) at Iowa State University (Jeanblanc 2017) (Figure 4-1). The lab is designed to be flexible, so it can be moved to various locations collecting performance data. The trailer is embedded with a suite of thermistors and humidity sensors within the wall assembly.

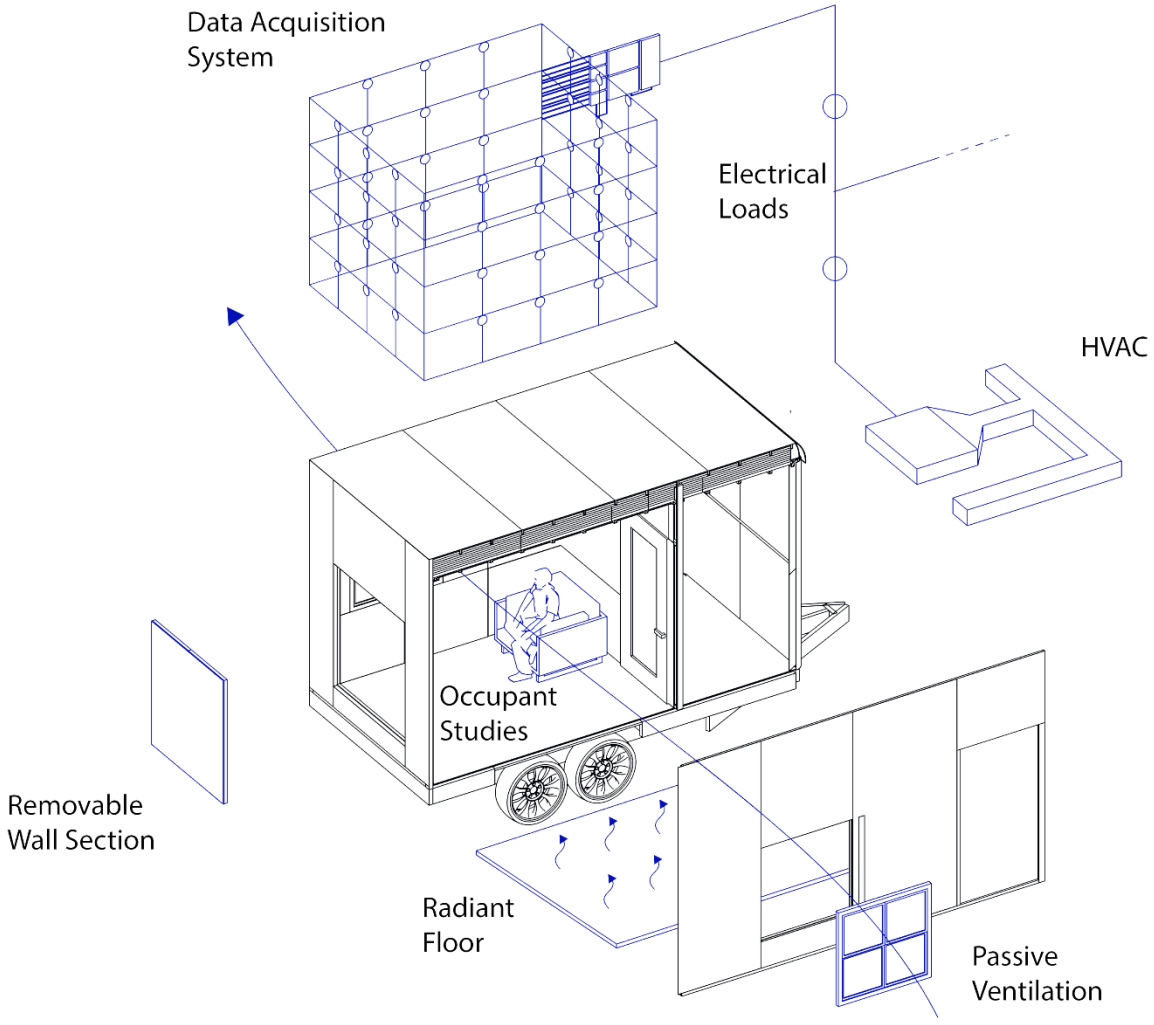

Figure 4-2 Exploded diagram of the MDL displaying options for, passive ventilation studies, temperature, and humidity monitoring, energy consumption, and custom material studies (Jeanblanc 2017).

The trailer can be towed to various locations collecting temperature and humidity data to create site specific micro-climate studies that can better inform building design. Temperature and humidity sensors are evenly distributed through the wall gradient, with one thermistor per layer. This enables the collection of multiple data points specific to the material assembly as heat flows through the assembly. The assembly consists of two layers of insulation, one polystyrene, the second a foam faced insulation, wood framing, interior polycarbonate sheathing that can be removed for easy access to the wall assembly, and an exterior metal sheathing that protects the entire assembly (Figure 4-2).

The trailer is split into two sections, the data collection and HVAC space, and the measurement space where experiments such as, heat flow through the thermal assembly, passive ventilation, comfort analysis, material analysis can be conducted. The MDL has removable interior wall panels allowing access to the wall assembly, insulation, and thermistors.

Additionally, the rear wall of the trailer has a segment that can be removed and replaced with a custom wall assembly. This allows for testing of different material assemblies within the conditioned space, comparing assembly performance to established high performance assemblies.

The custom assemblies can be tested for water resistance, humidity resistance, and thermal gradient through the custom assembly. The assembly can also be used to test changes in energy consumption with microclimatic variation (Jeanblanc 2017).

Experiment

For the duration of the experiment, the MDL was parked in Des Moines adjacent to the birth and wellness centre at the intersection of 19th and Leyner Street in Sherman Hill. An onsite weather station continuously monitors and logs weather data at regular intervals. Additionally, the centre has a collection of sensors distributed throughout the interior collecting data at regular intervals. The data collected from the weather station and interior sensors allows us to compare and analyse the data collected from the MDL both with the standard assembly and the concrete assembly.

The goal was to create a data set based on two conditions. The first was to collect the baseline data based on a concrete wall assembly. This would serve as a control set for future experiments to compare collected data to existing onsite data collected from the weather station and internal sensors.

The second condition was to obtain a data set after switching the existing rear wall assembly (RWA) with a custom concrete wall assembly and measuring the changes in the data set and comparing it to baseline measurements conducted initially and the existing onsite weather station.

For the first portion of the experiment, the sensors collected data with the standard assembly with the RWA. The RWA starting from the exterior consists of exterior metal finish, polystyrene, wood framing, foil facing insulation, and finished with white interior polycarbonate (Figure 4-3)

For the second portion of the experiment, 4 wall panels measuring 55'' x 12'' layered with 1½ ''thick concrete slab, and 1½'' thick foil faced insulation, were inserted in lieu of the RWS, with metal sheathing on the exterior face of the MDL. The concrete mix and foil facing insulation was commercially obtained (Figure 4-3).

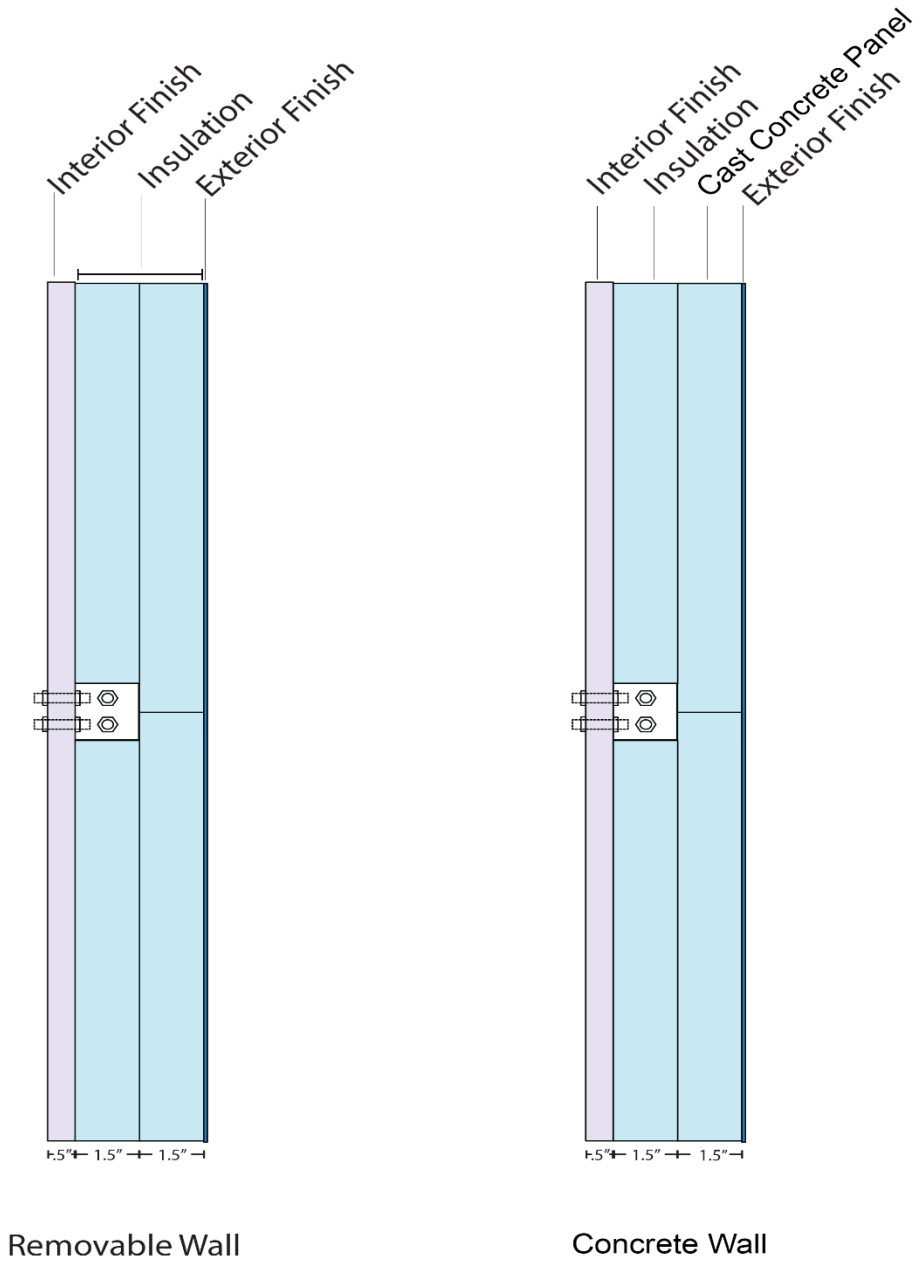

Figure 4-3 Detailed wall section for the Removable Wall Section (RWS), and custom concrete wall assembly.

Experimental Set Up

For the first part of the experiment, the trailer was parked adjacent to the health and wellness centre in Sherman Hill while the sensors collected data from the passively conditioned space. The trailer was oriented in the NW-SE orientation. The space was not conditioned as for the duration of the experiment. Additionally, passive ventilation was constrained by keeping the windows shut.

The panels were switched out after the data for the first section of the experiment was downloaded. The second set of panels consisted of a 11/2'' concrete slab followed by an 11/2''foam faced insulation towards the interior side, followed by sheathing on either side.

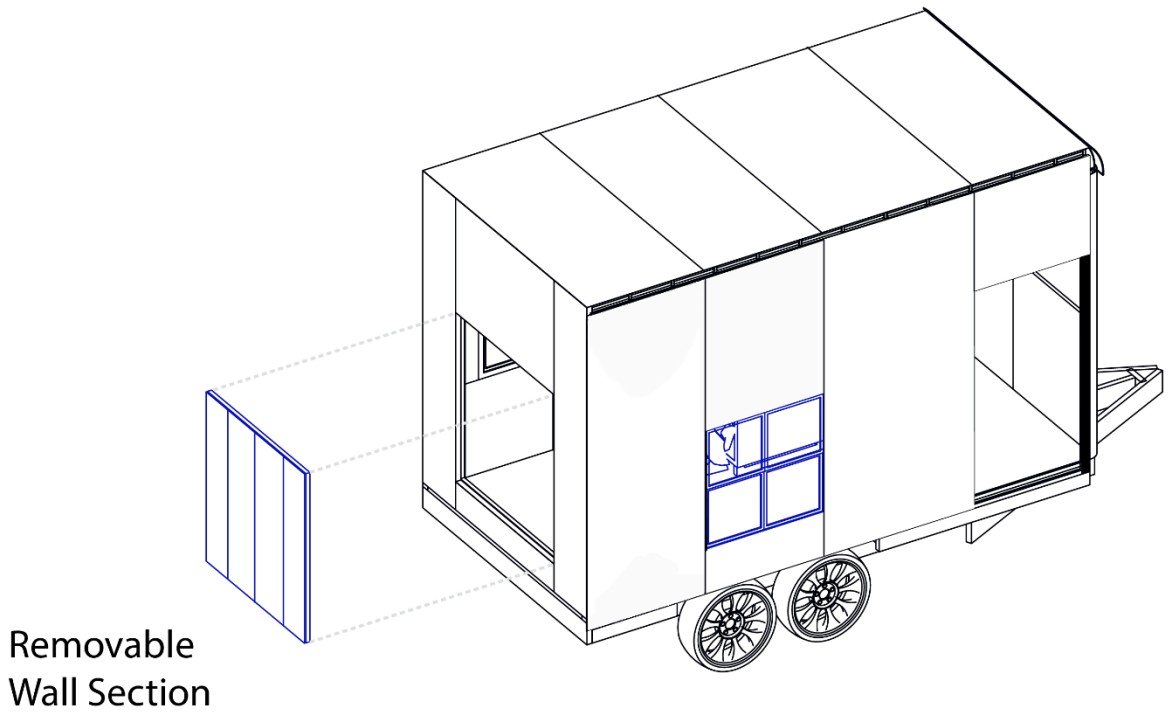

Figure 4-4 RWS being switched from the standard panel to the hybrid concrete panel.

Data Comparison

Two days of data were collected from the MDL while it was parked adjacent to the weather station. The first day was May 02, 2018 (Figure 4-5 and Figure 4-6), with the standard RWS being used. The standard RWS consists of the same material assembly as the rest of the trailer. The second day was May 06, 2018 (Figure 4-7 and Figure 4-8), with the standard RWS switched out in lieu of the composite concrete assembly.

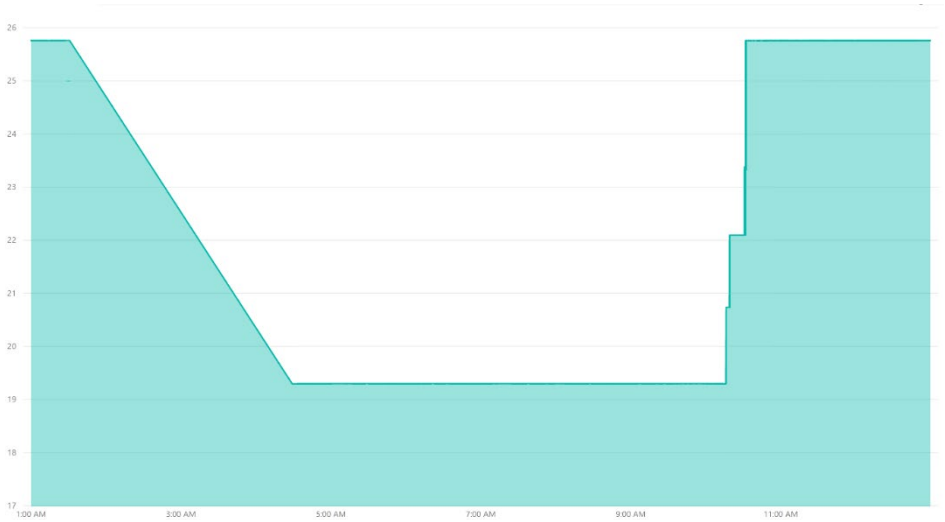

Figure 4-5 Average temperature vs time graph taken from an average of thermistors in the unconditioned space May 02, 2018.

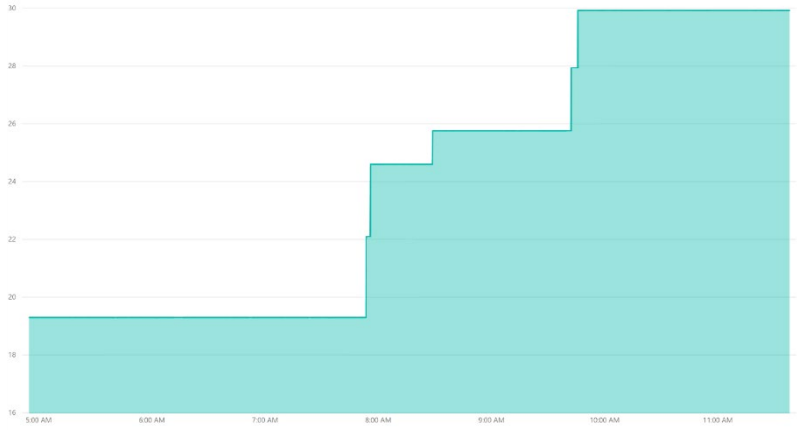

Figure 4-6 Average temperature vs time Graph taken from an average of thermistors in the unconditioned space on May 06, 2018.

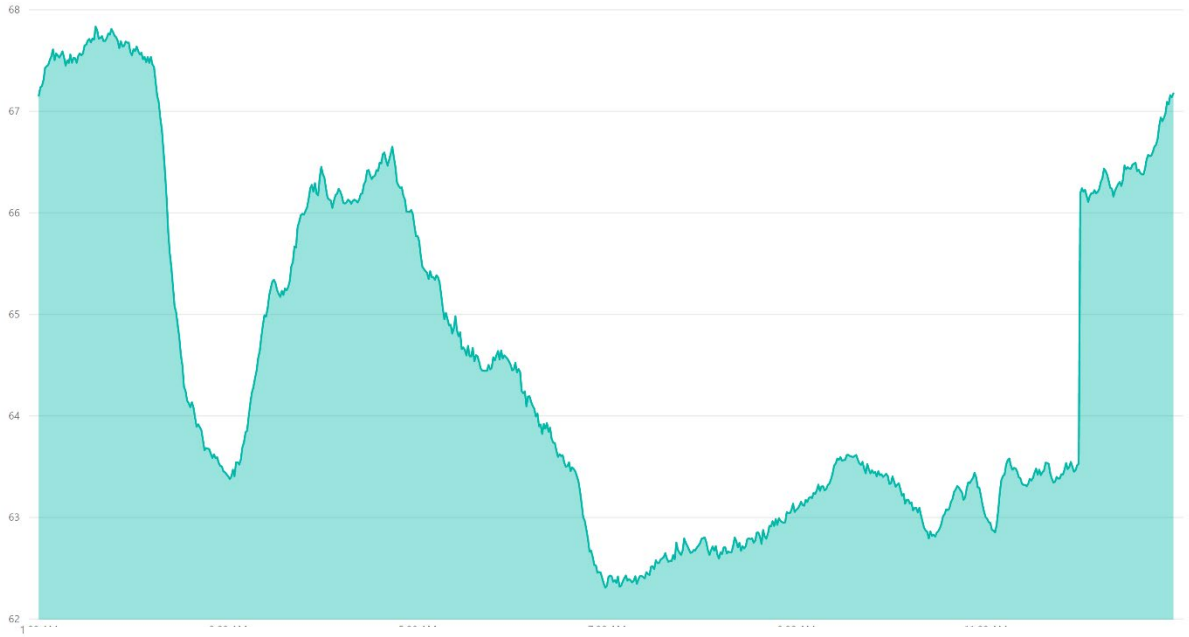

Figure 4-8 Average temperature vs time taken from the onsite weather station for the on May 06, 2018.

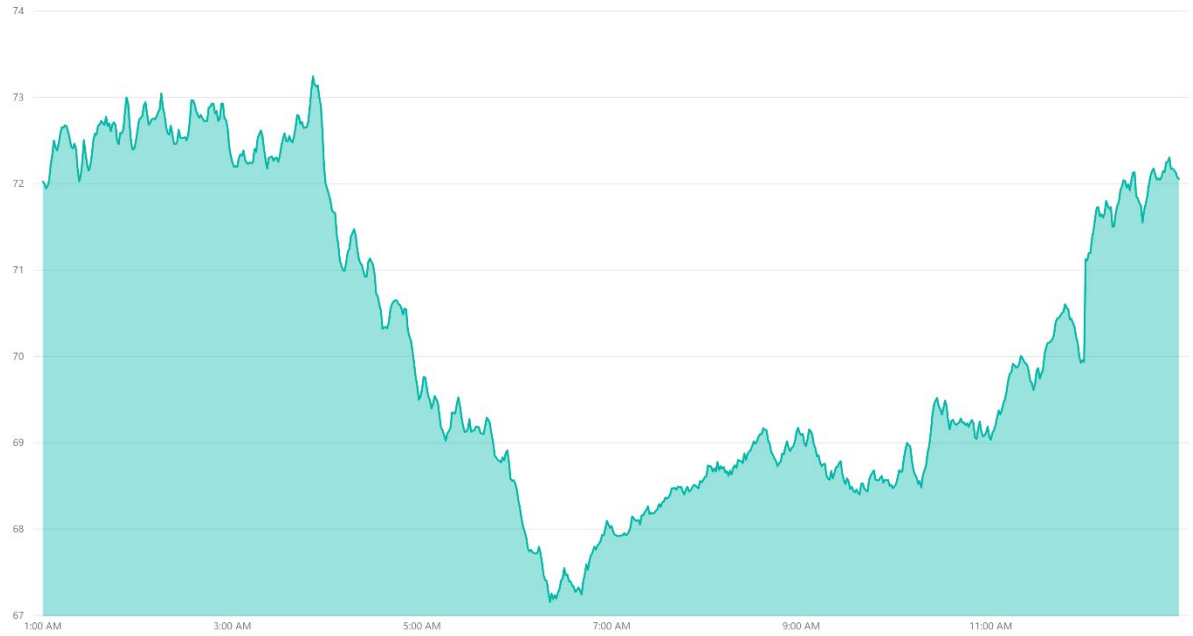

Figure 4-7 Average temperature vs time taken from the onsite weather station for May 06, 2018.

(Figure 4-5 and Figure 4-7) highlight the temperature changes for the two days, with two different wall assemblies being utilized. For the first data set collected on May 2nd, the standard RWS was utilized (Figure 4-5). When we compare it to the average temperature measured at the weather station (Figure 4-7), we see that average temperature inside the MDL for a sizable portion of the day is higher than the average ambient temperature measured at the station. The temperature measured at the weather station reached highs of 68ºF whereas in the MDL, apart from a few hours between 3:00 Am and 5:00 AM where the MDL and Average temperature coincide, we see that it constantly a couple degrees higher, reaching highs of 71ºF.

A probable reason for the higher than average ambient temperature in the MDL could be how the MDL is oriented on site, where the NW-SE axis of orientation exposes a sizable portion of the assembly to solar exposure. Additionally, with the windows tightly closed, built up heat could not be easily dissipated via passive ventilation.

Another factor that could affect the temperature readings in the MDL could be local cloud cover and precipitation. The cloud cover based on the station at the Des Moines airport on May 2nd was 52%, with the chance of precipitation in the range of 3.5% to 5.6% between the hours of 8:00 AM and 2:00 PM.

For the second data set collected on May 6th, the composite concrete assembly was utilized (Figure 4-5). The data collected in the MDL was compared to the average temperature measured at the weather station (Figure 4-7 and Figure 4-8). The average temperature collected in the MDL was marginally higher in the morning and exhibited higher average temperatures when compared to the average temperature logged by the weather station.

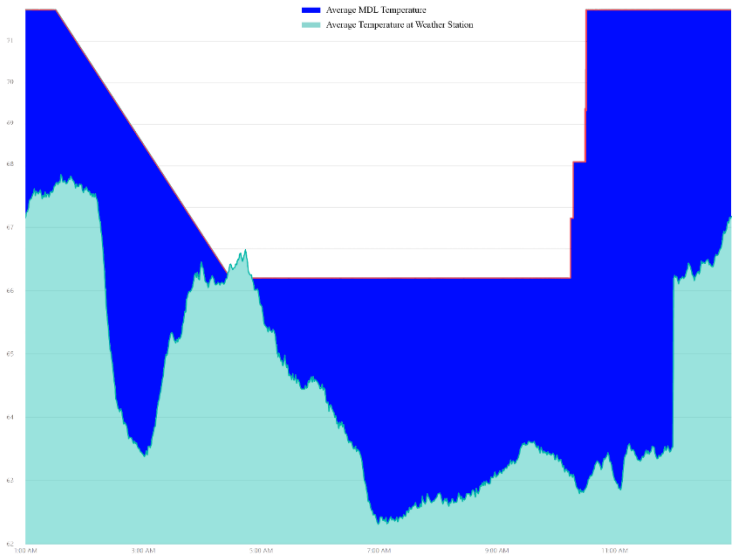

Figure 4-9 Average temperature comparison between MDL and onsite weather station on May 2nd.

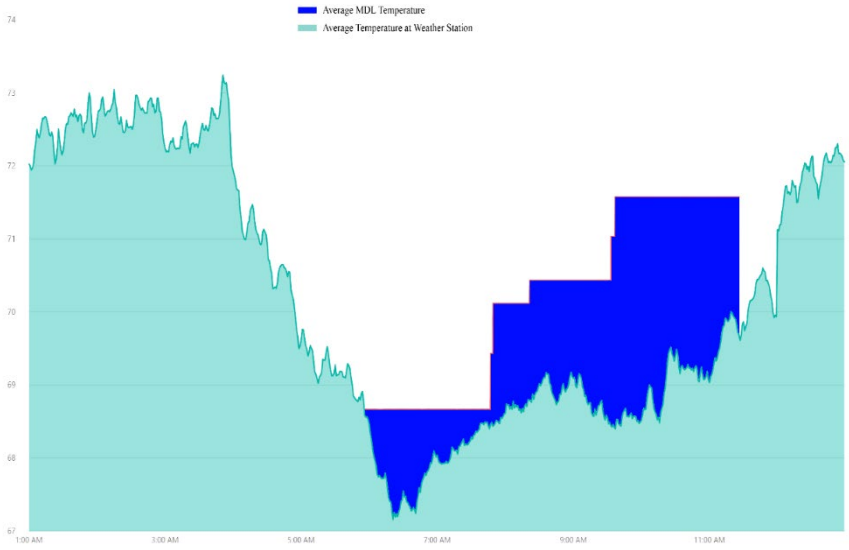

Figure 4-10 Average temperature comparison between MDL and onsite weather station on May 6th.

Discussion- MDL Composites

The mobile diagnostics lab was utilized for the duration of the experiment. Data was generated from custom concrete panels inserted into the removable wall assembly to create a baseline with which to compare the cellulose concrete panels.

With a baseline established for a standard concrete wall assembly the next goal, will be to incorporate conclusions from the material study utilizing sisal fibers. An optimized mix based on the proportions outlined in (Table 5-3) is necessary to reduce concrete consumption in creating composite wall assemblies. Currently initial studies with the sisal fiber mix utilizes a higher proportion of cement in the mix ratio.

The study is geared toward optimizing fiber proportion for effective mechanical properties of the composite. Additional work needs to be carried out where the fiber and mix proportion are optimized toward creating a thermally efficient composite panel. Thus, the quantity of both fiber and concrete can be explored to achieve a thermally effective panel.

In addition, the choice of cellulosic material can be varied depending on location, fiber sourcing, properties, and program requirements based on microclimate. Apart from sisal there are a host of other natural and waste fibers (Table 5-1) from various sources that can be used in varying proportions.

For example, kraft pulp fiber, generated from wastepaper, could be the preferred fiber in regions where natural fibers are difficult to source. This is relevant in regions where large quantities of paper waste are generated and sent to landfills. In Iowa, corn Stover left over from harvesting could be the preferred fiber. This also has implications for carbon sequestration as a significant portion of carbon present in the Stover is absorbed back by the environment rather than the soil.

CHAPTER 5. RESIN COATED SISAL FIBER REINFORCED COMPOSITES FOR ENHANCED DUCTILITY AND DURABILITY.

Engineered cement composites (ECC) are a group of fiber reinforced composites exhibiting high ductility (Li 2003, 1998). This improvement in composite ductility is due to microstructure tailoring with synthetic polyvinyl alcohol (PVA) fibers achieving significant improvements in tension (Li, Wang, and Wu 2001). This material optimization is achieved with low fiber volume fractions ranging from 2-3%. Due to the nature of ECC applications for large volume usage, the cost of synthetic fibers in addition to higher proportion of cement can be significant (Wang and Li 2007, Li 2003). Additionally, synthetic fibers are produced from petroleum-based products. Therefore, an opportunity exists for developing an ECC mix with cheaper class of fibers that are abundant.

Natural fibers are versatile, abundant, and can be sourced from a variety of bio-matter including plants, trees, crops, and waste fibers (Wambua, Ivens, and Verpoest 2003). Natural fibers exhibit low-density, have low-cost, are renewable, consume lesser energy, and are biodegradable. These properties give it certain benefits over synthetic fibers with cost, abundance, and carbon neutrality being significant features. Natural fibers come in a variety of forms with varying diameter, aspect ratio, length, surface structure, and form (Ardanuy, Claramunt, and Toledo Filho 2015).

Sisal fibers are a type of natural fiber which display physical properties such as low density, stiffness, and strength (Wambua, Ivens, and Verpoest 2003). Sisal fiber embedded cementitious composites exhibit improved toughness, ductility, flexural capacity, and crack resistance compared with non-reinforced cementitious composites (Silva, Mobasher, and Filho 2009). One of the advantages of sisal reinforced cementitious composites is the fiber-bridging mechanism during and after cracking helping transfer the loads.

Additionally, the fibers enhance flexural strength, toughness, and impact resistance (Savastano, Warden, and Coutts 2003, Tolêdo Filho et al. 2003) (Ardanuy, Claramunt, and Toledo Filho 2015).

Sisal Fiber

(Table 5-1) compares the properties of a few natural fibers, highlighting tensile strength and percentage incorporated into concrete by previous researchers. The sisal fiber was selected for its flexural strength, crack bridging abilities (Silva, Mobasher, and Filho 2009), sourcing, and its bio-degradability.

Although the bio-degradability of the sisal fiber creates challenges, where the sisal fiber is susceptible to alkaline attack in a cementitious matrix (Filho, Silva, and Filho 2013). Due to this vulnerability the tensile properties of the sisal fiber, which impart composite concrete its ductility and flexural strength, is compromised. Thus, various resin-based coatings provide avenues for protection improving the longevity of the fiber in the cementitious composite.

The fibers were obtained from a commercial supplier who procured them from the sisal plant grown in Kenya. The sisal fiber microstructure is made up of individual fiber cells which are about 6-30µm in diameter. The morphology of a typical sisal fiber can classified into 55-66% cellulose, 12-17% hemicellulose, 7-14%lignin, 1% pectin and 1-7% ash (Filho, Silva, and Filho 2013). The sisal fibers were cut to ¼'' length (Table 5-1) (Institute 1986).

Although the addition of sisal fibers to cementitious matrices afford numerous advantages, the durability of the fiber is a primary source of concern. The fibers demonstrate an increase in fracture over time and decrease in fiber pull out. Additionally, the fibers are weekend due to a combination of alkali attack, migration of hydration products to the lumen

of the fiber resulting in fiber mineralization, and variation in space and volume due to high water absorption (Figure 5 1) (Ardanuy, Claramunt, and Toledo Filho 2015).

Table 5-1 Comparison of cellulose fibers from different plant species.

Fiber	**Tensile Strength**	**Fiber Length**	**Incorporated into mortar vs concrete**	**% incorporated into composite**	**Young modulus**	**Coating**
Hemp	400 - 800 N/mm^2	20 - 50 mm long	As chopped fiber for use in plastering, flooring, and non-load bearing wall applications.	14-16%	14.4 GPa, and 19.6 ±14.8 GPa to 70 GPa	
Sisal Fibers	350- 600 N/mm^2	0.5 - 1.0M long	Incorporated as raw fiber into mortar creating products such as roof tiles and building blocks.	3%	8-9 - 19 GPa	Epoxy, Polyester, Polyurethane Vinylester
Coconut/Coir Fibers	90±35 MPa or 192 ±3 37 - 162 ± 32 MPa (White Coir) and 343 ± 36 - 186 ± 55 Mpa (Brown Coir)	2.5 - 4.5 mm and from 50 - 120 mm	Early incorporation in cement-based matrices saw corrugated slabs, and cement-bonded boards. Additionally, work has been carried out into improving fiber durability in alkaline environment, such as utilizing pozzolanic cement, or enveloping fibers in silica fume slurry.	1-5%	2.6 ±0.7 GPa, 3.44(white) and 4.94(brown)	-
Kraft Pulp Fiber	1000 MPa	Varies	As bleached/unbleached in composites, with occasional coating.	4-8%		Molten Asphalt, Molten Plasticized Sulphur
Pineapple Leaf Fibers	170 - 1600 N/mm^2	Individual fiber from 2.5 to4.5 mm, and technical fiber from 50 to 120 mm	Predominantly utilized in the textile industry, used in hybrid combinations with other natural fibers such as epoxy, polyethylene, among others. Used to reinforce thermoset, thermoplastic, bioplastics and natural rubber.	-	From 4.49 to 82.5 Gpa	-
Kenaf Fibers	170 - 600 /900 N/mm^2	25-38mm long (1/4th inch Día)	Fibers were chemically pretreated by dipping them in Urethane solution.	2.40%	12.8 to 34.2 G Pa	Urethane

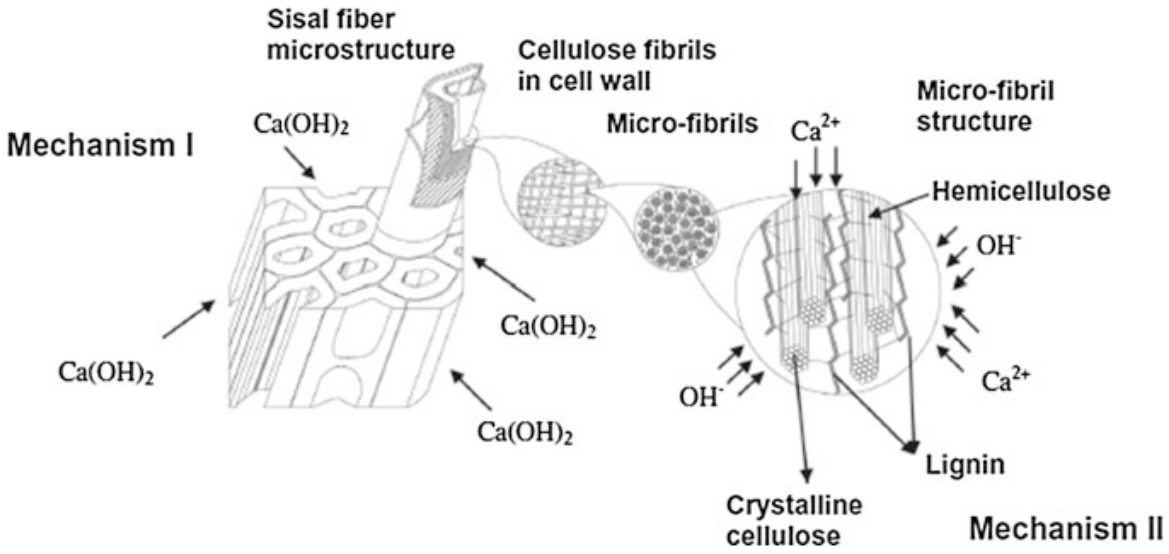

Figure 5-1Mechanisms of natural fiber degradation in a Portland cement matrix (de Melo Filho et al 2013). Reprinted from Cement and Concrete Composites, Volume 40, João de Almeida Melo Filho, Flávio de Andrade Silva, Romildo Dias Toledo Filho, Degradation kinetics and aging mechanisms on sisal fiber cement composite systems, Pages 30-39., July 2013, with permission from Elsevier.

Therefore, this study presents research conducted on the interfacial bond between the fiber and the cement matrix by coating fiber surface in polyester resin prior to dispersion in the cementitious matrix. The goal of this study is to discern the reinforcement capabilities of the coated fibers for ductility and flexural strength. The type of fiber, resins, modes of mixing, and strength test are all presented.

Coatings

The polyester resin was commercially obtained from Michaels, an art store in Des Moines. The natural coating, shellac was commercially obtained from Lowe's home improvement store.

Resins.

Two resins were utilized to coat the sisal fiber and protect it in the ECC composite. The first was a synthetic polyester resin, and the second was a naturally occurring resin called shellac. Polyester resins are synthetic resins created by mixing dibasic organic acids and polyhydric alcohols. They're commonly utilized as sealers for furniture protecting them from moisture.

Shellac is a naturally occurring resin obtained from the lac beetle found on tree species native to the forests of India and South East Asia. Shellac is bio-adhesive polymer chemically similar in composition to synthetic polymers and can be an alternative to synthetic polymers. They have numerous uses, from coatings for pharmaceutical pills to furniture sealers and as a varnish.

For the ECC-Sisal-Resin composites varying amounts of resin fiber proportions were mixed together to determine effective coating percentage and curing time. Based on visual observation, the sisal fibers utilized for the preliminary and main study were coated with the polyester resin. The amount of resin used was 85% by mass of the total fiber, to ensure adequate fiber to resin ratio. This was to ensure the uniform resin curing time across all samples and easy dispersion during mixing, and to avoid clump formation. Consistent amounts of resin catalyst were used to ensure consistent curing time which was two hours and fifteen minutes. This allowed adequate time for fiber dispersal during mixing.

For the sisal-Shellac composites, an aerosol-based spray was utilized to uniformly coat the fiber and mixed with a hand mixer and sprayed again followed by hand mixing to ensure uniform coating. Due to the method of shellac dispersion, curing time was between forty-five minutes to an hour and half.

Matrix design.

The mix percentage used for formulating the various composite mix is listed underTable 5-2.

Table 5-2Reference ECC mix for cube, cylinder, and beam samples.

Cement	27.95%
SCM 1 (F Ash)	33.54%
Fine Aggregate	22.35%
Water	16.15%

The Concrete mix was designed using an Engineered Cementitious Composite (ECC) mix as the base mix based on compositions refined by Victor Li (Li 2003). Multiple sisal mixes of fiber proportions ranging from 2%-7% by weight and treated with polyester resin and shellac were created using ECC mix proportions as the base matrix.

Li et al. engineered ECC as a fiber reinforced cement composite to achieve high ductility under tensile and shear loading (Li 1998, 2003, Li, Wang, and Wu 2001, Lin, Kanda, and Li 1999). They employed micromechanics-based material design, improving maximum ductility exceeding 3% under axial loading with 2% fiber content by volume.

The fibers utilized in ECC are polyvinyl alcohol (PVA) fibers with fiber volume fraction no greater than 2%, demonstrating tensile strain capacity at a range of 3MPa to 5MPa. Additionally, the ECC matrix has been incorporated with higher proportion of fly ash resulting in tensile strain capacity at 3% to 4% and tensile strength above 4.5 Mpa (Wang and Li 2007). The micromechanical-based design process of modifying the individual fiber, matrix and interface for performance makes this an ideal base matrix to test and compare coated natural fiber ECC composite.

Testing Methodology

Flow

Flow testing was done on a flow table with samples being used from fresh mixes cast for the preliminary study and conforming to ASTM C1437-15. The flow results are presented under the preliminary study section.

Compressive strength

Compressive testing was carried out on a Humboldt compression machine and conforming to ASTM C109 standards. Three 2'' x 2'' cubes were cast in plastic molds, per mix, for the preliminary study and cured for 7 days in the moisture curing chamber. They were tested until failure in the machine with the results presented under the preliminary study section. Three 4'' x 8'' cylinders were cast in plastic molds, per mix, for the main study and cured for 7, 14, and 28 days in the moisture curing chamber. They were tested in machine until failure with results presented under the main study section.

Split tensile strength

Split tensile testing was carried out on a universal testing machine (UTM), part of the Instron industrial series model and conforming to ASTM C496. Three 4'' x 8'' test cylinders were cast in plastic mold, per mix, for the main study, cured for 28 days, and tested in the UTM until failure with results presented under the main study section.

Flexural strength

Flexural testing was carried out on a UTM conforming to ASTM D6272. Three rectangular beams measuring 14’’x 4’’x 3’’were cast, per mix, in plastic molds and cured for 28 days in the moisture curing chamber. The cured beams were then placed on two supports, 1 inch from the edge of the specimen, with loading span 1/3 of the support span and tested in the UTM until ultimate failure. The results are presented under the main study section.

Durability testing

To test the durability of the coated and uncoated fibers, an accelerated degradation test setup was devised to simulate the effects of wetting and drying cycles. two beams, an ECC composite and 2.0% uncoated sisal composite, were used to determine the minimum duration for the wetting and drying cycle. For the wetting cycle each beam was immersed in a water bath at ambient temperature and weighed every 24 hours until complete absorption. The beam was then placed in a oven kept at 50 C and weighed every 24 hours until all the moisture had evaporated. The rate of moisture absorption, and desorption was used as the wet/dry cycle time for the accelerated aging tests. 8 beams, per mix, were cast in plastic molds and cured in moisture curing room for 28 days.

Composite Casting.

Based on (Table 5-3) multiple mixes of varying natural fiber proportions were cast for the preliminary and main study. (Table 5-4) presents the mix proportion for the uncoated and coated composites separated by fiber proportions, and coatings. The first mix was a plain ECC composite with 0% fibers. The Second mix was an ECC composite with 2% PVA fibers, the

other 7 mixes were embedded with varying proportions of sisal fiber from 2% to 5.0%. The fibers were either uncoated or coated with polyester resin or shellac (Table 5-3).

Table 5-3-Mix proportions of the various coated and uncoated fiber mixes with a base control (lbs.).

0% control		• 2% PVA (ECC) • 2% Uncoated-Sisal		• 2% Shellac-Sisal • 2% Resin-Sisal		• 3.5% Shellac-Sisal • 3.5% Resin-Sisal		• 5.0% Shellac-Sisal • 5.0% Resin-sisal	
Fiber	0	Fiber	0.89	Fiber	0.89	Fiber	1.56	Fiber	2.23
Fly Ash	53.43	Fly Ash	53.43	Fly Ash	53.43	Fly Ash	53.43	Fly Ash	53.43
fine agg.	35.60	fine agg.	35.60	fine agg.	35.60	fine agg.	35.60	fine agg.	35.60
water	25.73	water	25.73	water	25.73	water	25.73	water	25.73
cement	44.52	cement	44.52	cement	44.52	cement	44.52	cement	44.52

For the preliminary study, the matrices with various concentrations of sisal, PVA fibers, and their coatings were cast using a Hobart mixer for the 2 x 2-inch cube samples. To create the cube samples, the dry materials (fine aggregate, cement, fly ash) were mixed for 5 minutes, followed by the addition of water, and mixed for an additional 5 minutes. Once the mix had attained a good flow and dispersion, the PVA fibers, or sisal fibers with or without the polyester or shellac coating were dispersed into the mixture by hand ensuring no clumps are formed and mixed for 5 minutes. Miniscule amounts of the superplasticizer Glenium 700 was added to mix to ensure sufficient flow. The mix was then poured into cube molds, which were demoulded after 24 hours and placed in a curing chamber for 7 days and tested.

Table 5-4 Flow for various mix proportions for the preliminary study.

Flow		
Control	2.0% ECC-PVA fiber sample	2
	0% ECC Composite	2.7
Uncoated	2.0% Uncoated Sisal-WM	2
	3.0% Uncoated Sisal-WM	2.5
	5.0% Uncoated Sisal-WM	4
Shellac	2.0% Shellac-Sisal-WM	2.5
	2.0% Shellac-Sisal-WM	2.2
Resin	2.0% Resin Sisal-WM	2
	3.5% Resin-Sisal-DM1	1.2
	3.5% Resin Sisal-DM2	1.1
	3.5% Resin Sisal-WM	1.2
	7.0% Resin-Sisal-WM	5

For the main study, a pan mixer was used for the 14 x 4 x 4-inch beam, and 4 x 8-inch cylinder samples. The methodology followed was similar to the cube casting, with the dry materials being added to the drum followed by the water at 10 minute intervals, with the sisal fibers dispersed by hand in the mix once it had attained a good flow and dispersion, ensuring no clumps are formed. The mix was poured into 4 X 8 cylinders demoulded after a day and tested at 14, and 28 days

Preliminary Study - Cube Samples

A set of preliminary mixes were made to optimize mixing process, order of introducing materials into the composites, mixing time, natural fiber proportion, and tested for flow and compressive strength. (Table 5-4) shows flow values for the various mixes. (Table 5-5) shows 7-day average compressive strength for 2’’x2’’ cubes. The samples were mixed together with

varying dispersion methods, material addition order, mixing time, and amount of high-range water reducer to achieve a mix in which the fibers are dispersed efficiently, while obtaining good flow. Natural fibers were used as uncoated, resin coated, and shellac coated.

Three 2''x2'' cubes, per mix, were cast using variable mixing order to optimize fiber percentage, resin coating, and curing time to ensure effective dispersion in the cementitious matrix. The mix order was classified as Dry Method (DM1, DM2) and Wet Method (WM). The coated fibers were added to the mix 15 minutes before they were completely hardened to avoid clumping. For DM1, the semi-cured resin and shellac fiber were added during the mixing of fine aggregates. For DM 2, the semi-cured resin and shellac fiber were added during the mixing of all the dry ingredients-cement, fine aggregate, and fly ash, and Glenium. For the WM, the semi-cured resin and shellac fiber were added during the mixing of the dry and wet materials-cement, fine aggregate, fly ash, water, and Glenium. The cubes were then cured in a moisture curing room for 7 days and tested, with the results presented under (Table 5-5, Figure 5-2, Figure 5-3, Figure 5-4, and Figure 5-5).

Table 5-5 -7 day average compressive strength of 2’’x 2’’ preliminary cubes embedded with various proportions of natural fiber, ordered by mixing method.

7 Day Average Compressive Strength (Psi)		
Control	ECC Composite	4,583
	2.0% ECC-PVA fiber sample	5,001
Wet Method	2.0% Uncoated Sisal-WM	4,272
	2.0% Resin-Sisal-WM	3,829
	2.0% Shellac-Sisal-WM	2,998
	2.0% Shellac-Sisal-WM	4,285
	3.0% Uncoated Sisal-WM	4,834
	3.5% Resin-Sisal-WM	4,705
	5.0% Uncoated Sisal WM	4,553
	7.0% Resin-Sisal WM	2,188
Dry Method	3.5% Resin-Sisal-DM2	3,166
	3.5% Resin-Sisal-DM1	2,707

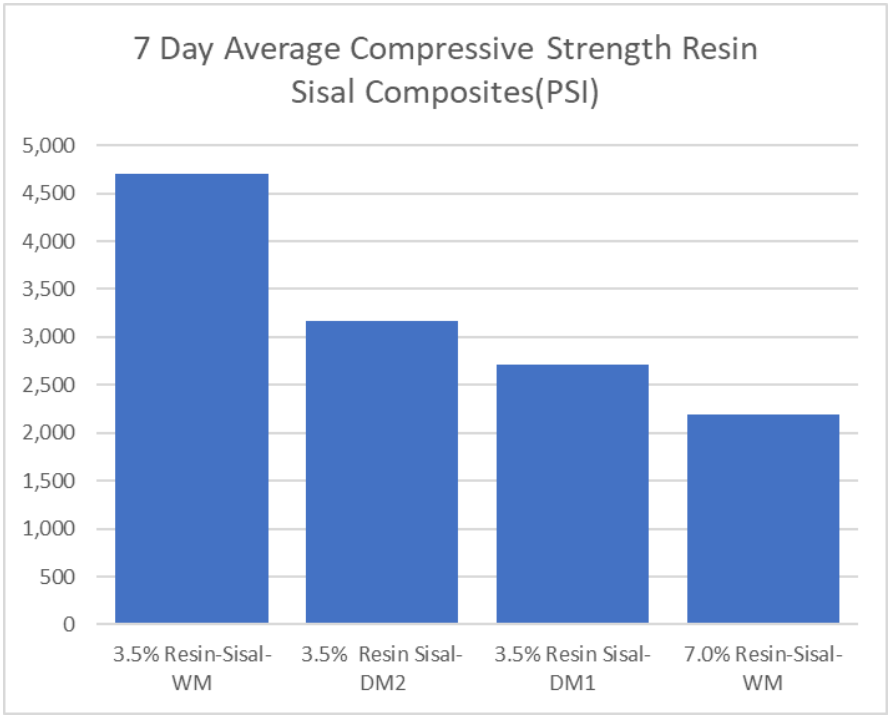

Figure 5-2 -7 day average compressive strength of the resin-coated sisal fiber embedded in concrete.

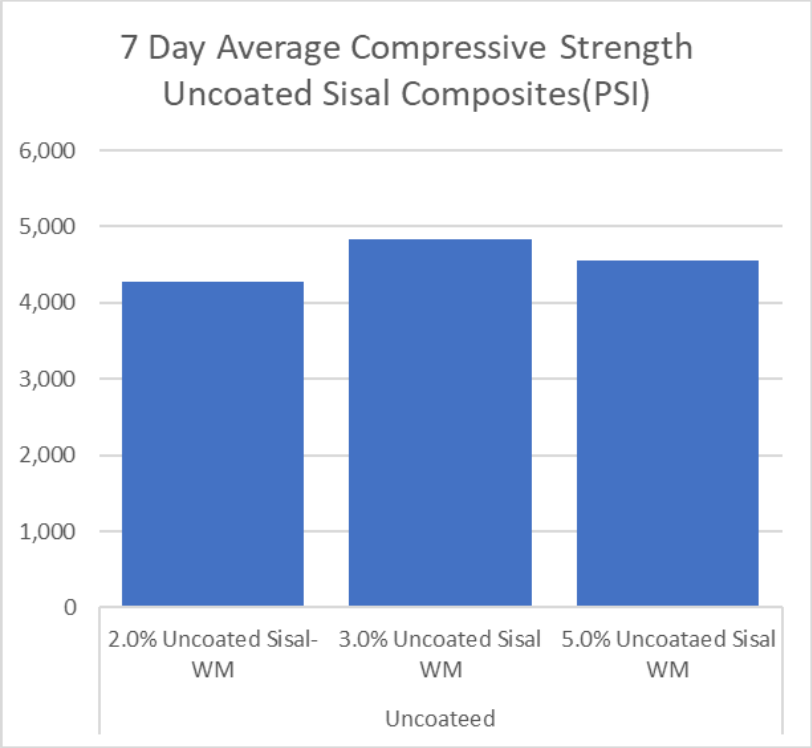

Figure 5-3 -7 day average compressive strength of uncoated sisal fiber embedded in concrete.

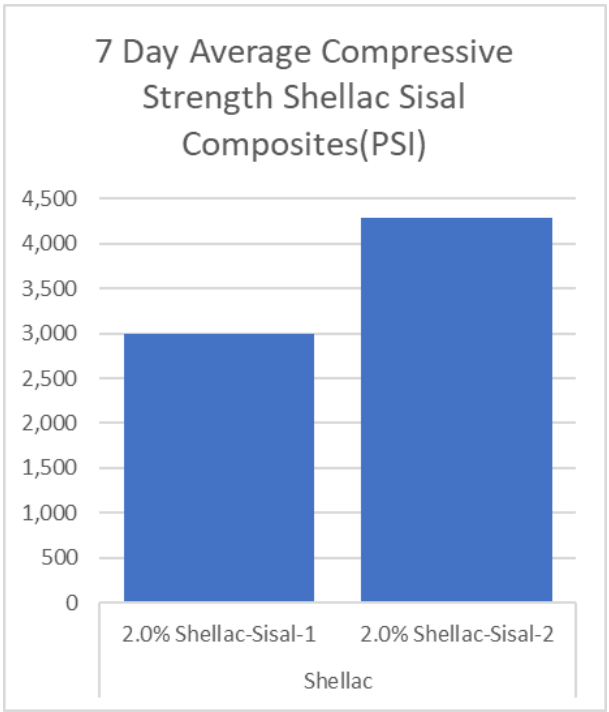

Figure 5-4 -7 day average compressive strength of shellac coated sisal fiber embedded in concrete.

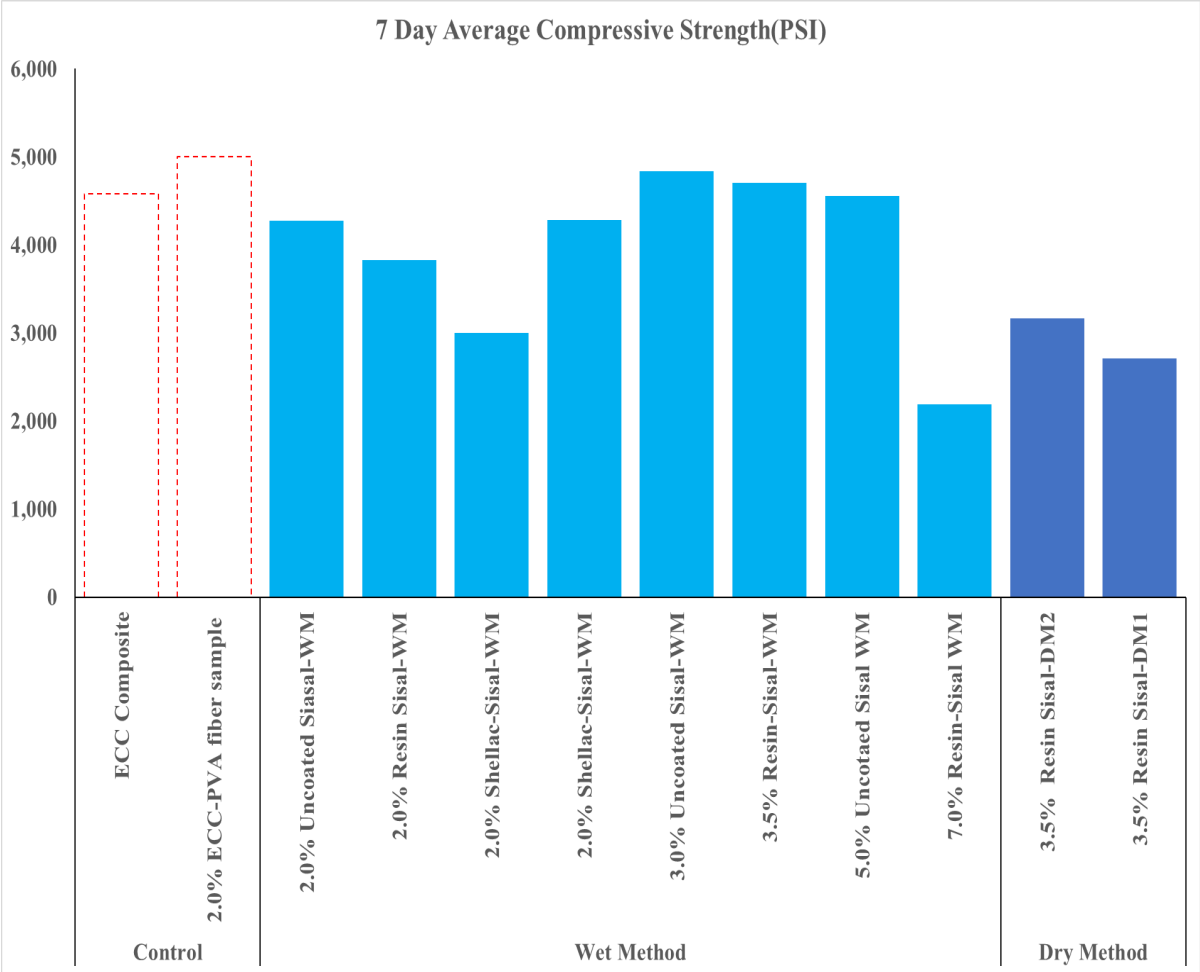

Figure 5-5 -7 day average compressive strength of all preliminary cube samples organized by mixing method.

Preliminary mechanical properties

Various dispersion methods were tested to determine the optimum sisal fiber proportion after being coated with resin. For the first dispersion method, the resin coated fibers, 3.5% Resin-Sisal-DM2 (Figure 5-5), were mixed using DM2. For the second dispersion method the coated resin fibers, 3.5% Resin Sisal-DM1 (Figure 5-5), were mixed using DM1. For the third mix the coated sisal Fibers, 3.5% Resin-Sisal-WM (Figure 5-5)were mixed using WM.

The first method DM1 lowered compressive strength when compared to the WM (Figure 5-2) due to the semi-cured resin being absorbed by the aggregate during the initial period of mixing. The second method DM2 also displays lowered compressive strength due to the semi-cured resin being absorbed by the dry materials during mixing. The third mix 3.5% Resin-Sisal utilizing WM (Figure 5-5) displayed an improvement in compressive strength when compared to the former two methods of dispersing the sisal fiber. Therefore, the third method was selected for its effective dispersion and subsequent mechanical properties.

After selecting an effective dispersion methodology, additional samples were then cast focusing on the dosage of sisal fiber in the mix ranging from 2.0%, 3.5%, 5.0% to 7.0% by mass to determine an optimum ratio beyond which any additional fiber would be detrimental to the mechanical properties and behavior of the composite (Figure 5-2, Figure 5-3, Figure 5-4, and Figure 5-5).

The 2.0% samples were the first to be cast as previous researchers work highlight it as an optimum ratio amongst a range of values. The 2.0% ECC PVA fiber sample display the highest mechanical properties when compared to the other Coated/uncoated sisal composites.

The 3.0% uncoated, and 3.5% Resin-Sisal-WM composites display better compressive strength when compared to the other mixes. The 7.0% resin sisal displayed significantly lowered compressive strength, highlighting a reduction in mechanical strength for an increase in fiber percentage over 5.0%.

In addition to the resin coating, the natural coating shellac was utilized to compare it as an alternative to polyester resin coating (Figure 5-4). The first lightly coated 2.0% Shellac-Sisal fibers display similar mechanical properties as the 2.0% Resin-Sisal fibers. Conversely

the generously coated 2.0% Shellac-Sisal fiber display lower compressive properties when compared to the 2.0% Resin-Sisal-WM.

With an increase in fiber percentages flow is reduced and becomes difficult to efficiently agitate the mix and requires the addition of superplasticizer. Therefore, a mix percentage of 2.0%, 3.5%, 5.0% by mass, with resin and shellac coating was selected as the focus of the main study.

Surface Microstructure (SEM)

Un-coated and coated sisal fiber

The ¼'' natural fibers were studied under a scanning electron microscope (SEM) to understand their surface properties, and the resin and shellac coating mechanism. Several images were captured using a FEI Quanta-250 scanning electron microscope (SEM) with a resolution of 1.0 nm to understand the interaction between the surface of the sisal fiber, resin and shellac coating and concrete matrix.

Additionally, standard secondary and backscattered electron detectors were utilized to characterize the chemical composition of the coated fiber samples in concrete. The first three samples utilized in the SEM were a small clump of sisal fibers, the first one uncoated, the second resin coated, the third shellac coated. The images obtained are presented under (Figure 5-6, Figure 5-7, Figure 5-8, Figure 5-9, Figure 5-10, Figure 5-11, Figure 5-12, Figure 5-13, and Figure 5-14).

Uncoated sisal fiber

At 50x magnification the surface of the ¼ ‘’ uncoated fibers display a striated surface pattern, possibly indicative of the processing (Figure 5-6). Additionally, the surface of fiber shows signs of abrasion due to processing or the way fiber was harvested. At 500x magnification the striation pattern is highlighted in better detail, and additional deposits such as calcium can be identified (Figure 5-7). The Calcium crystal deposit can be clearly identified in (Figure 5-8). In (Figure 5-9), comparing multiple areas of the uncoated sisal fiber, we can see that the amount of carbon oxygen is lower in uncoated organic sample of sisal fiber. There is also the possibility of hydrogen lowering the C-O bond.

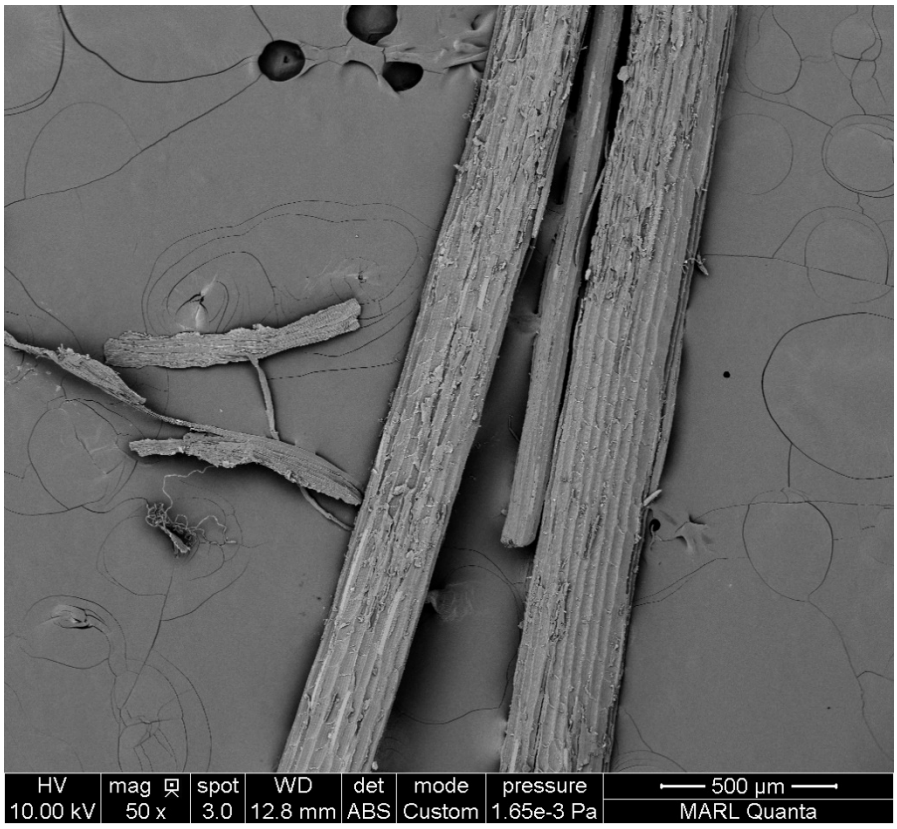

Figure 5-6-SEM image of uncoated sisal fiber highlighting surface morphology at 50x utilizing back scatter electron.

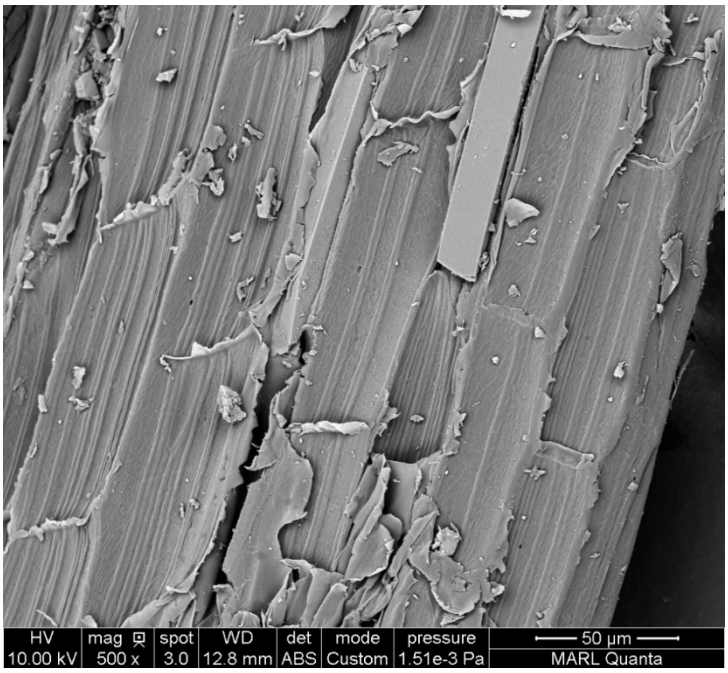

Figure 5-7-SEM image of sisal fiber highlighting surface morphology at 500x utilizing back scatter electrons.

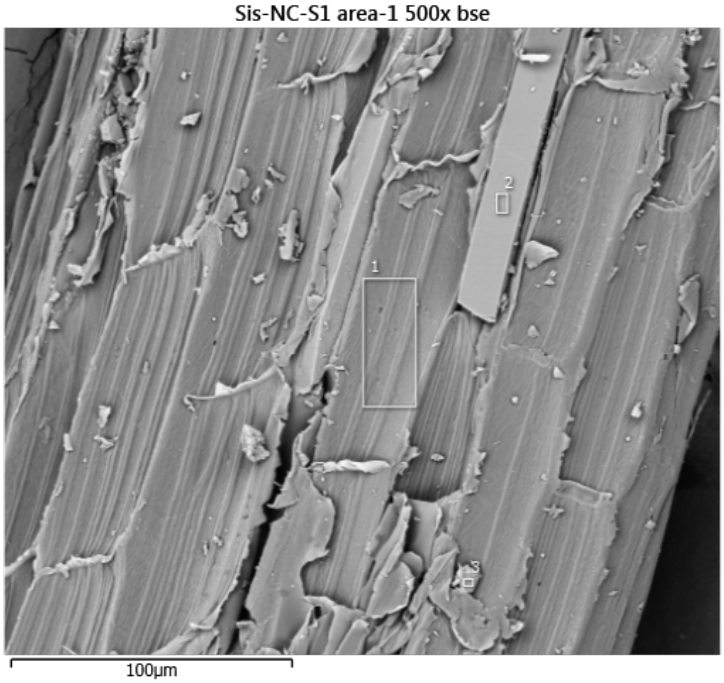

Figure 5-8 - SEM image of sisal Fiber highlighting surface morphology at 500x utilizing back scatter electrons. Area-1 highlights base fiber with EDS highlighting its chemical characteristics. Area-1 is the base fiber. Area 2 contains Ca, C, and O.

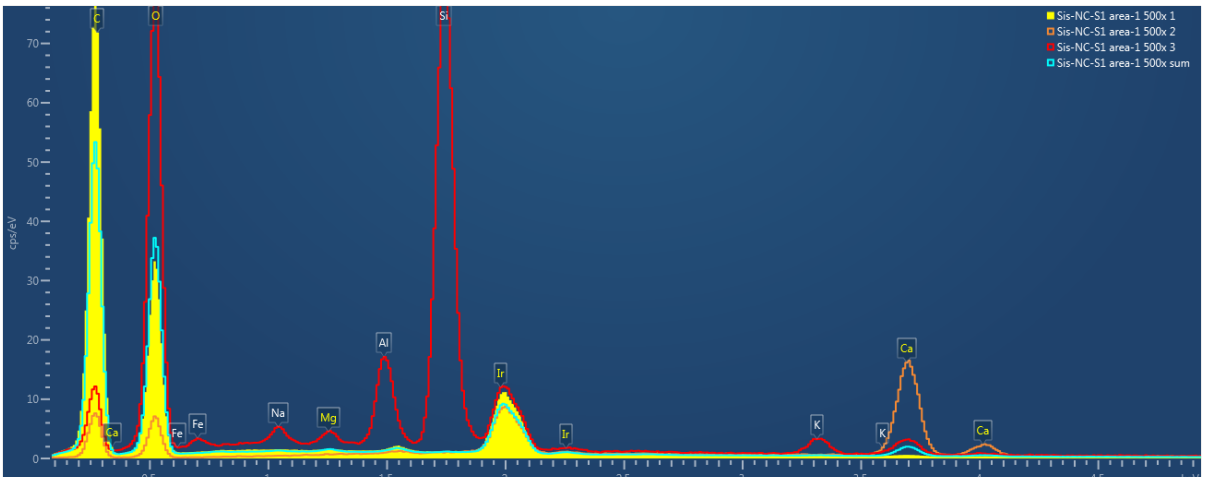

Figure 5-9-Comparative chemical analysis of various regions of the uncoated sisal fiber. Area-1 is the base fiber. Area 2 contains Ca, C, and O and calcium carbonate.

Resin coated fiber

1/4 ‘’ resin coated sisal fibers which were completely cured was used to study its surface property. At 50x magnification we can see the polyester resin has uniformly coated the surface of the ¼ ‘’ sisal fibers, displaying a membrane like surface (Figure 5-10). The resin during the curing process flows into the irregularities present on the sisal fiber surface. Additionally in (Figure 5-11), there are segments of sisal fiber poking through the membrane due the irregular surface which can be observed in image- at 150x magnification. In (Figure 5-11) there’s evidence of tearing left behind in the resin due to the fiber being ripped out possibly during the resin curing, and agitation process. The resin forms a membrane over the surface of the fiber with few segments of the fiber poking out.

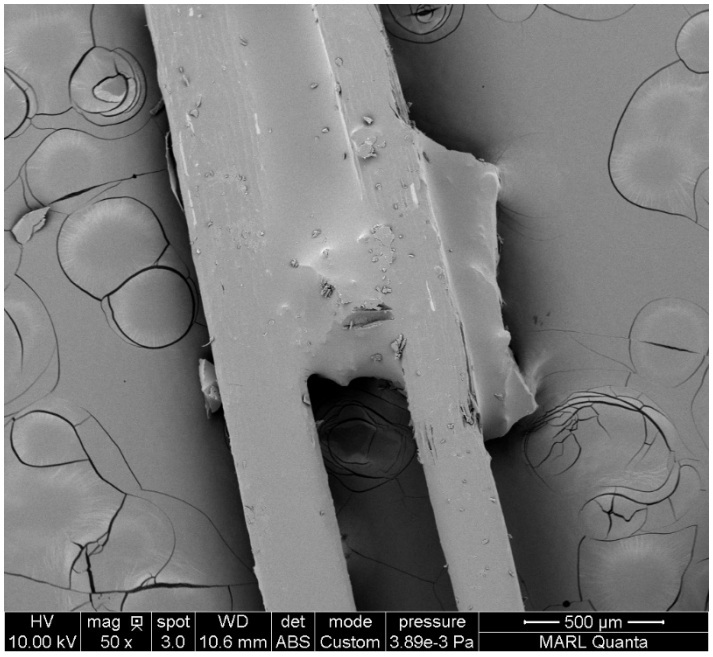

Figure 5-10-SEM image of resin coated sisal fiber highlighting surface morphology at 50x utilizing back scatter electrons. Hardened resin membrane over fiber surface is observable.

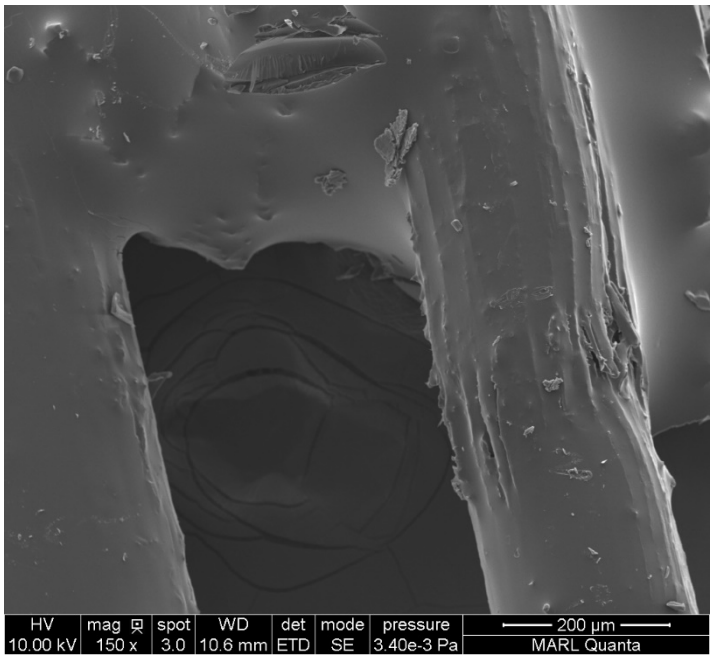

Figure 5-11-SEM image of resin coated sisal fiber highlighting surface morphology at 150x. Hardened viscous resin flowing over surface irregularities can be clearly identified.

Shellac coated

1/4 ‘’ shellac coated sisal fiber which were completely cured was used to study its surface property (Figure 5-12 & Figure 5-13). At 50x magnification we can see the shellac has uniformly coated the surface of the ¼ ‘’ sisal fibers, displaying a membrane like surface like the resin coated sisal fibers (Figure 5-12). Conchoidal fractures, possibly due to ripping of fibers during sample preparation, can be observed. At 150x magnification we can see the membrane surface with surface irregularities, highlighting the effectiveness of the coating on the fiber surface(Figure 5-13). The shellac coating has traces of sodium and chlorine (Figure 5-14).

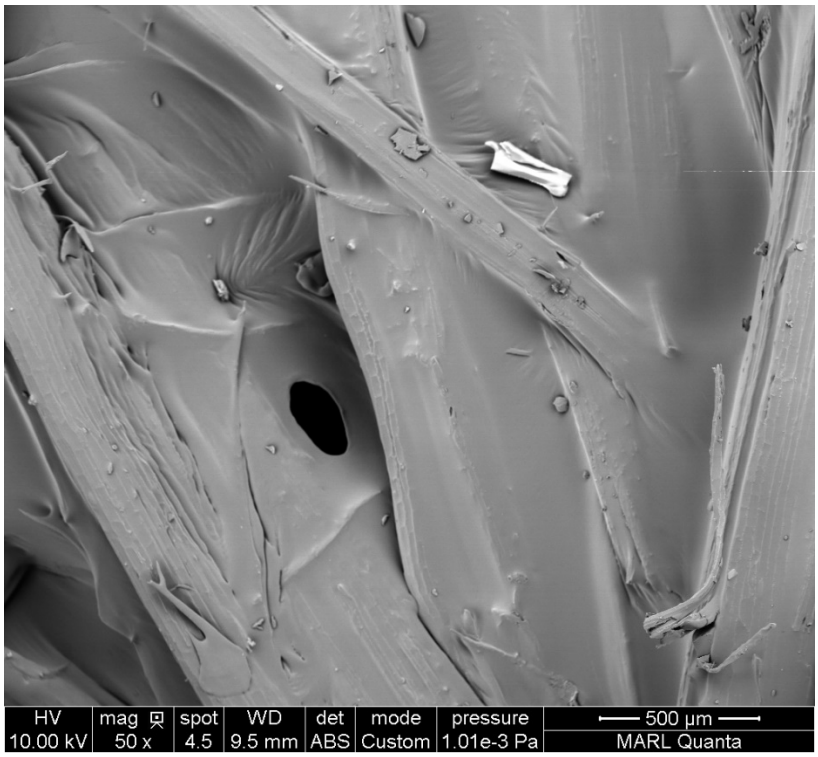

Figure 5-12-SEM image of shellac coated sisal fiber highlighting surface morphology at 50x magnification.

.

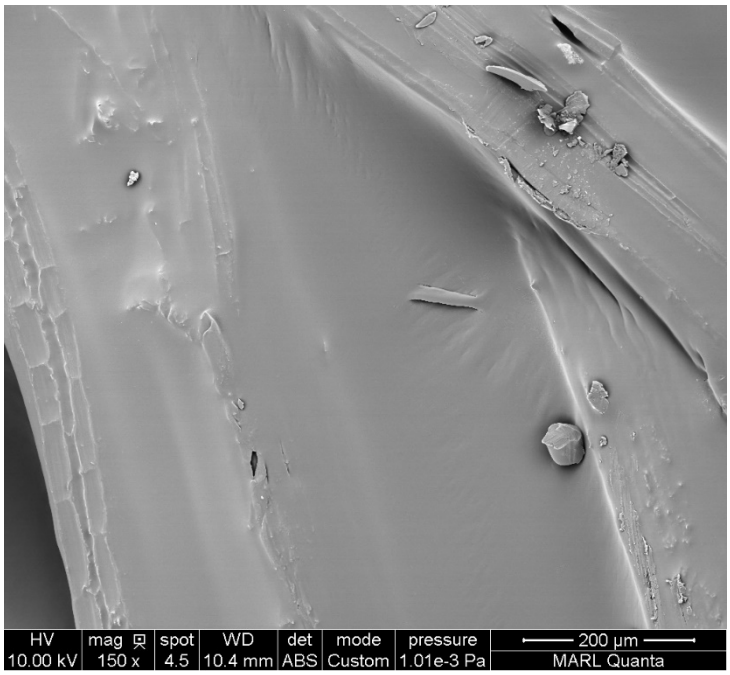

Figure 5-13-SEM image of shellac coated sisal fiber highlighting surface morphology at 150 times magnification.

Chemical composition.

(Figure 5-14) highlights the chemical composition of the uncoated, resin coated, and shellac coated fibers, we can compare the chemical compositions of the three fibers to highlight the changes in composition from uncoated to coated fibers. The combined graph highlights the changes in the carbon and oxygen content from the uncoated to the coated fibers. The changes in chemical composition, specifically the reduction in the oxygen molecules in the coated samples (Figure 5-14) highlight how the resin and shellac coating form OH bonds with the hydrogen in the water.

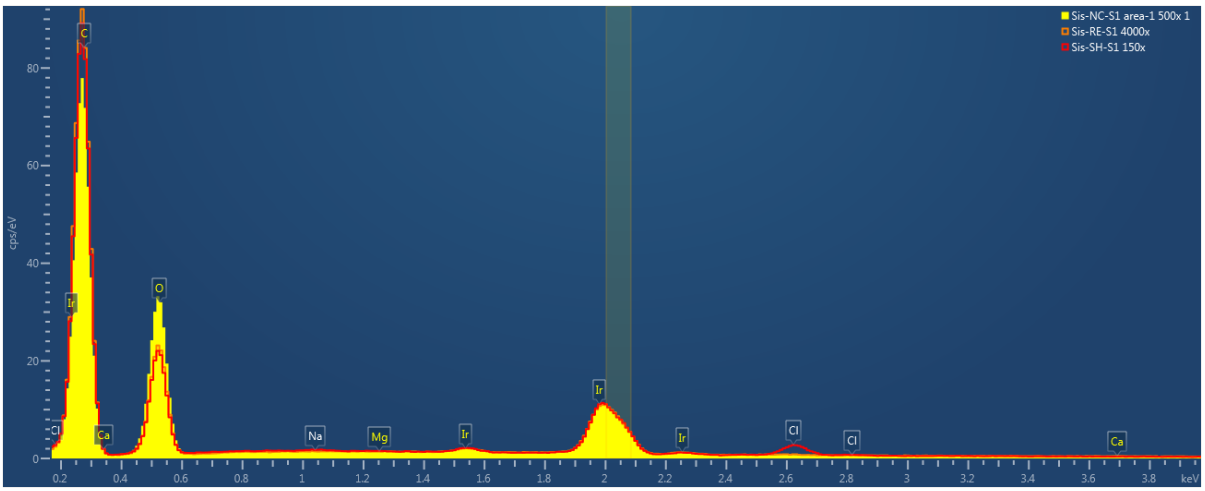

Figure 5-14-Comparative spectrographic analysis of the three specimens, uncoated, resin coated, and shellac coated, highlighting the major and minor elements. Sis-NC- uncoated sisal composite, Sis-Re- resin coated sisal composite, Sis-SH-shellac coated sisal Composite.

Un-coated and coated sisal fiber cementitious composites

For this section, the un-coated and coated fibers were embedded in a cementitious matrix based on the proportion outlined in (Table 5-3). The mix was then poured into plastic cube molds, cured for 7 days in a moisture curing room and then imaged. The images are presented in this section (Figure 5-15, Figure 5-16, Figure 5-17, Figure 5-18, Figure 5-19, and Figure 5-20).

Un-coated fiber composite

We can see from (Figure 5-15) magnified 150x that the surface of the ¼ ‘’ uncoated fibers host various hydration products on the fiber surface. This occurs during the curing process where a variety of products migrate from the matrix to the fiber surface (Figure 5-15 and Figure 5-16). One of the products observed on the fiber being calcium hydroxide. The various hydration products can be clearly seen when we look at (Figure 5-16) magnified 500x. Additionally we can see some of the fly ash that hasn’t been hydrated completely.

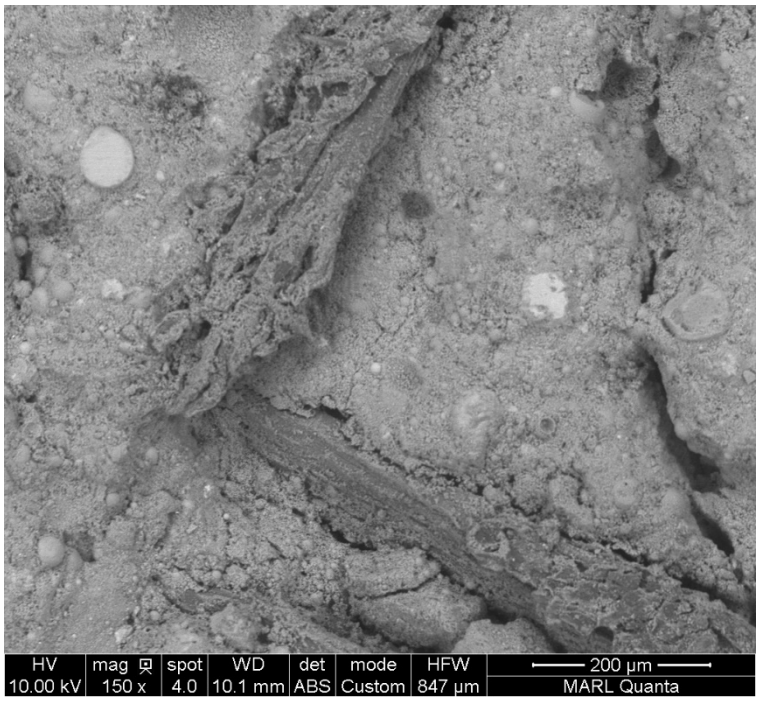

Figure 5-15-SEM image magnified 150x highlighting surface detail of the un-coated sisal fiber in a cementitious matrix cured for 7 days.

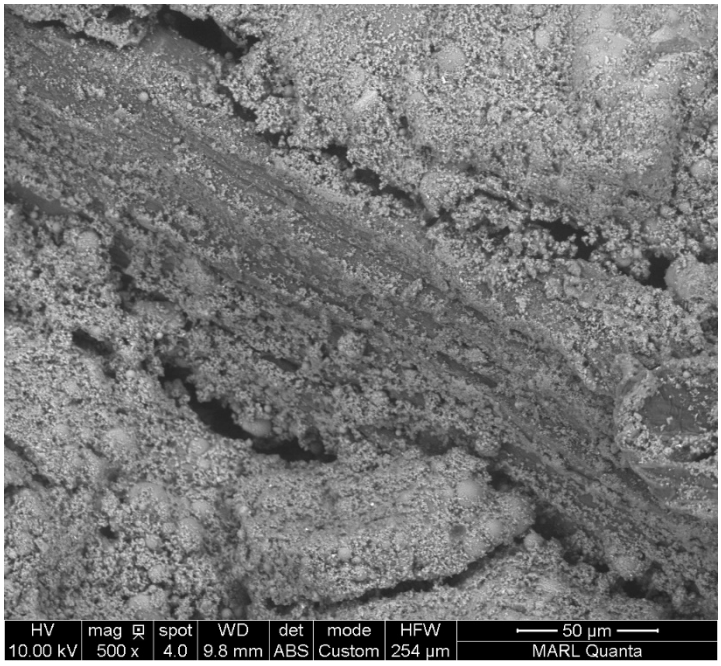

Figure 5-16-SEM image magnified 500x highlighting surface detail of the un-coated sisal fiber in a cementitious matrix cured for 7 days.

Resin coated fiber composite

When we look at (Figure 5-17), the shellac coated composite magnified 150x we can clearly make out the cross-section of the coated fiber embedded in the matrix. Additionally, a tiny void can be identified at the top of the fiber. When we magnify by 500x we can clearly identify a small distinct void space possibly due to the coating absorbing water from the surrounding matrix (Figure 5-18). This could be due to the coating absorbing moisture from the matrix at the matrix fiber interface.

Shellac coated fiber composite

When we observe the shellac coated composite magnified 150x we can clearly make out the diagonal cross-section due to fiber pull out (Figure 5-19). Additionally, we can identify an irregular void at the bottom of the fiber like the one found in the resin coated composite (Figure 5-19). In (Figure 5-20) we can clearly make out the void and a few hydration products on the surface of the fiber.

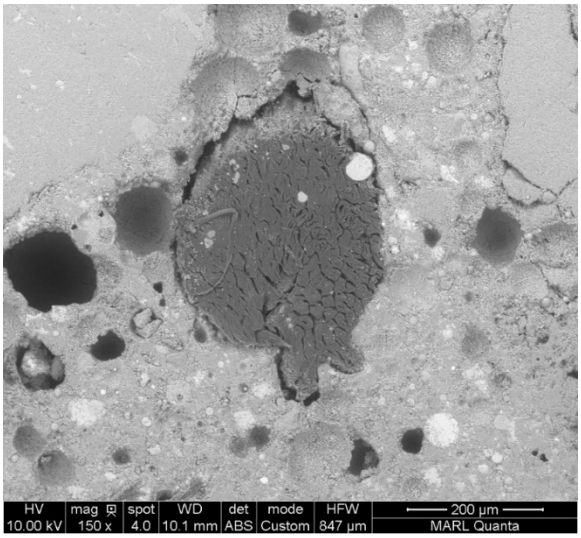

Figure 5-17-SEM image magnified 150 highlighting the cross-section of the resin-coated sisal fiber in a cementitious matrix cured for 7 days.

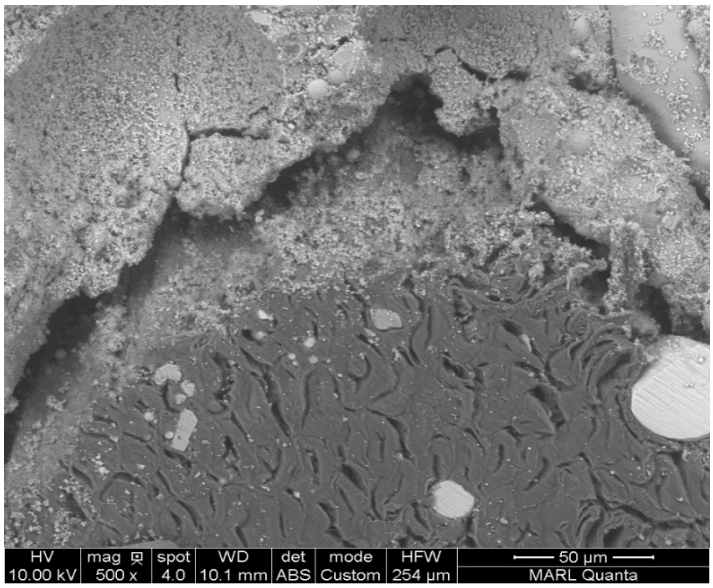

Figure 5-18-SEM image magnified 500 highlighting interface detail of the resin-coated sisal fiber cross-section in a cementitious matrix cured for 7 days.

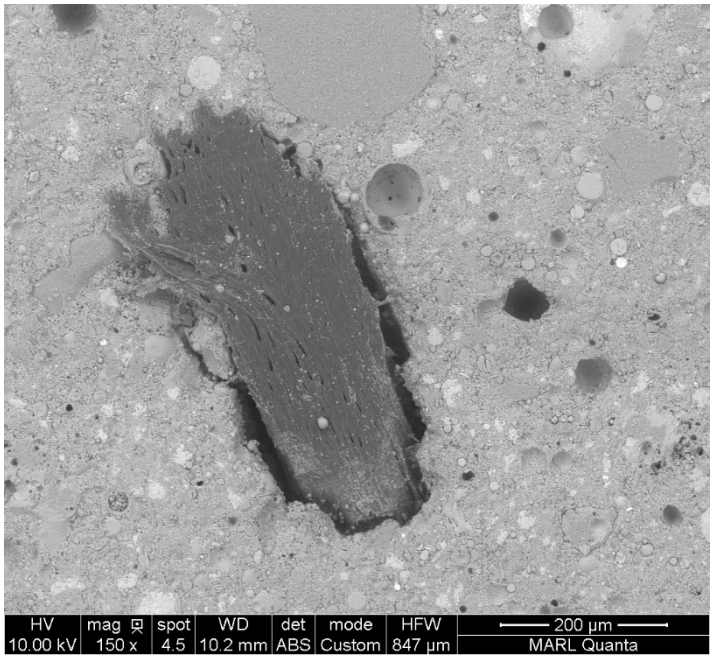

Figure 5-19-SEM image magnified 150 highlighting the cross-section of a shellac-coated sisal fiber in a cementitious matrix cured for 7 days.

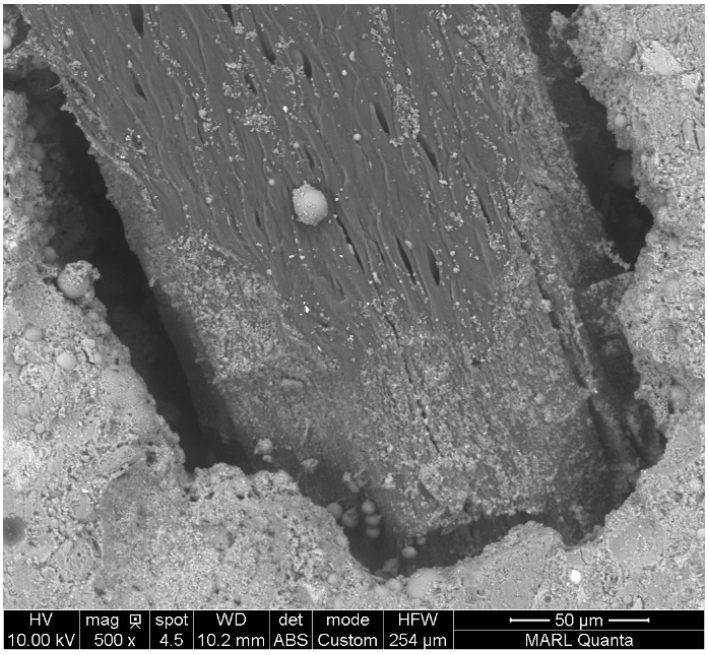

Figure 5-20-SEM image magnified 500 highlighting interface detail of the shellac-coated sisal fiber cross-section in a cementitious matrix cured for 7 days.

Results and Discussion

For the main study, three 4’’x 8’’ cylinders, and three 14’’x4’’x3’’ beams were cast for each mix in plastic molds. The samples were demolded and placed in the moisture curing room for 7, 14, 28 days depending on the study and tested at the end of the curing period. Compressive, split tensile, flexural testing was then carried out on the samples with the results being presented under (Table 5-6, Figure 5-21, and Figure 5-22)for compressive (Table 5-7 and Figure 5-23) for split tensile, and (Table 5-8 and Figure 5-24) for flexural strength. The goals for the main study are outlined below.

1. Investigating the effects of natural fiber on the mechanical properties of cementitious composites.
2. Optimum fiber coating to obtain effective composite properties.
3. Effective fiber proportion to obtain optimum mechanical properties.

Table 5-6 - Average compressive strength values of coated and uncoated sisal fiber composites.

Average Compressive Strength (PSI)				
Mix		7-day	14 Day	28 Day
Control	ECC Composite	3351.0		7844.7
	2% PVA-Control	4926.7		5536.0
Uncoated	2% Uncoated-Sisal		4806	7850.0
	3.5% -Sisal - Uncoated	3812.0		6189.3
	5.0% -Uncoated-Sisal	3506.7		5532.7
Resin-Coated	2% Resin-Sisal		4134	7779.0
	3.5% Resin-Sisal	4252.0		4961.3
	5.0% Resin-Sisal	4120.3		4929.3
Shellac-Coated	2% Shellac-Sisal		3499	6056.0
	3.5% -Shellac-Sisal	3429.0		5531.7
	5.0% -Shellac-Sisal	3162.7		4686.7

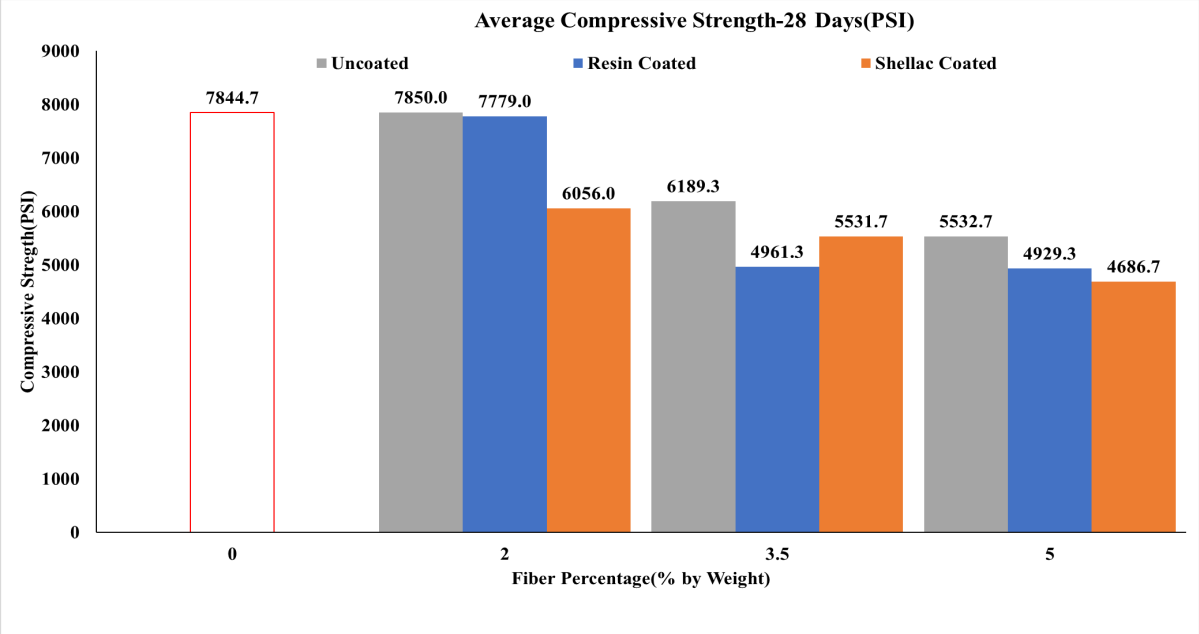

Figure 5-21 - Comparisons of average compressive strength of coated and uncoated sisal fiber composites at 28 days

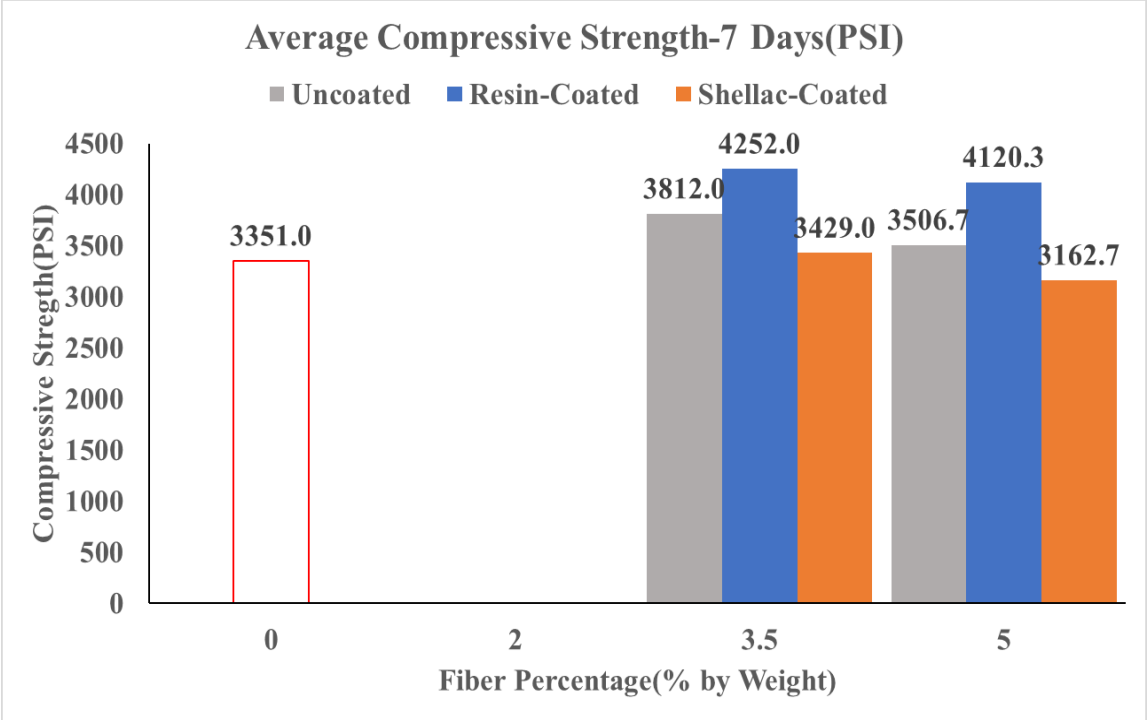

Figure 5-22 - Comparisons of average compressive strength of coated and uncoated sisal fiber composites at 7 days.

Table 5-7 - Average split tensile strength values of coated and uncoated sisal fiber composites.

28 Day Average Split Tensile (PSI)		
Control	ECC Composite	2266.3
	2% PVA-Control	3391.0
Uncoated	2% Uncoated-Sisal	2276.3
	3.5% -Sisal - Uncoated	2304.0
	5.0% -Uncoated-Sisal	2302.7
Resin-Coated	2% Resin-Sisal	2074.7
	3.5% Resin-Sisal	2647.0
	5.0% Resin-Sisal	2508.0
Shellac-Coated	2% Shellac-Sisal	2292.3
	3.5% -Shellac-Sisal	2394.0
	5.0% -Shellac-Sisal	2020.7

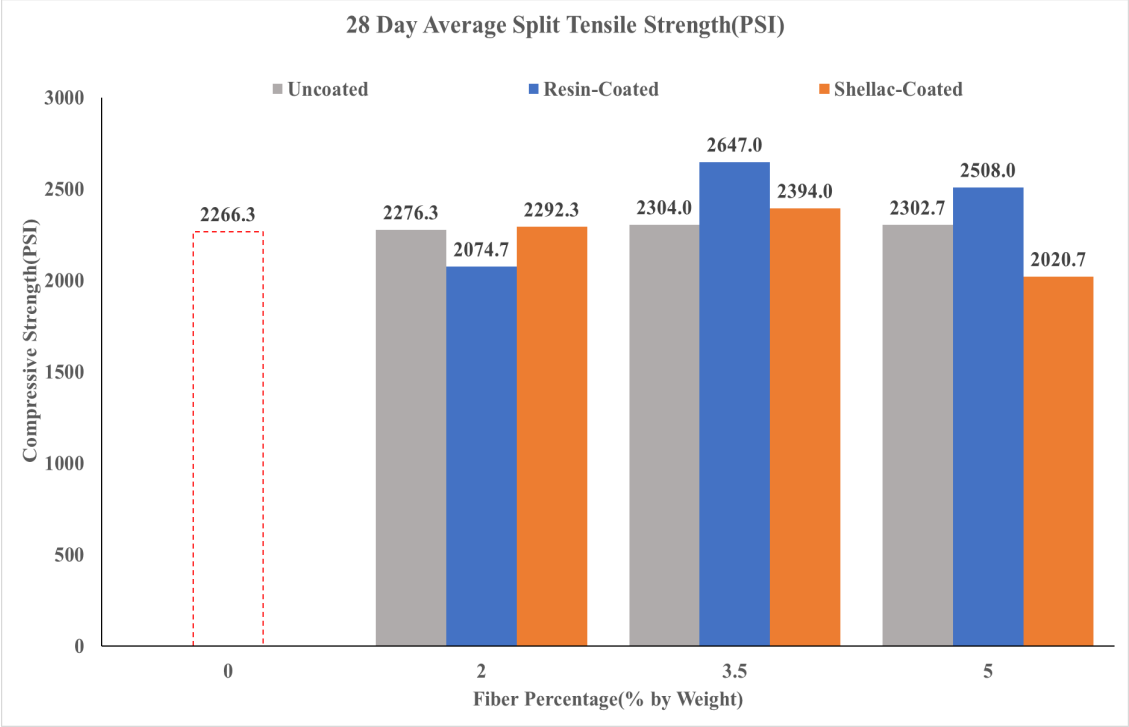

Figure 5-23 - Comparisons of average split tensile strength of coated and uncoated sisal fiber composites.

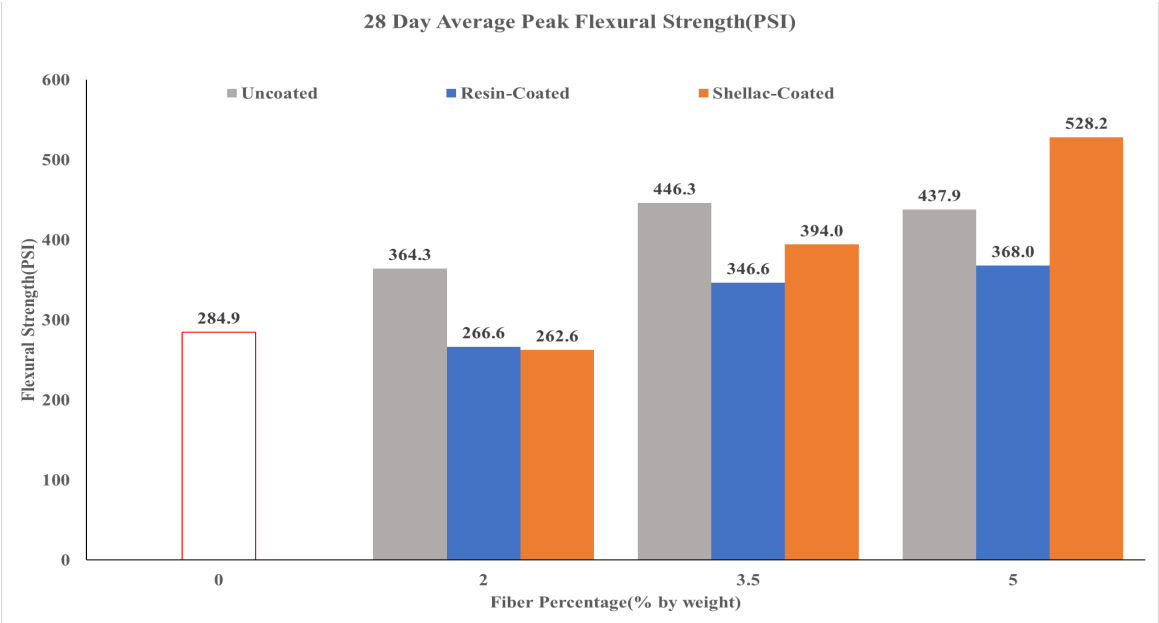

Figure 5-24-Comparisons of average flexural strength of coated and uncoated sisal fiber composites, to plain ECC composite.

Table 5-8 - Average values of ultimate flexural strength of coated and uncoated sisal fiber composites.

28 Day Average Peak Flexural Strength (PSI)		
Control	ECC Composite	284.9
	2% PVA-Control	723.5
Uncoated	2% Uncoated-Sisal	364.3
	3.5% -Sisal - Uncoated	446.3
	5.0% -Uncoated-Sisal	437.9
Resin-Coated	2% Resin-Sisal	266.6
	3.5% Resin-Sisal	346.6
	5.0% Resin-Sisal	368.0
Shellac-Coated	2% Shellac-Sisal	262.6
	3.5% -Shellac-Sisal	394.0
	5.0% -Shellac-Sisal	528.2

Mechanical properties- sisal fiber composites

Several 4 x 8 cylinders, and 14 x 4 x 3 beams were cast to study the comprehensive properties of the resin coated fibers in a concrete matrix, including compressive, split tensile, flexure, and durability of fibers in the cementitious matrix. Three fiber proportions with different applications were utilized in the casting process (Table 5-6).

The proportions of the sisal in concrete varied from 2.0% by mass to 5.0% with resin and shellac used as the coating for the coated fiber concrete mixes based on the preliminary study. A plain ECC mix, and 2.0% PVA fiber embedded in a concrete matrix were used as control to compare the effect of the three fiber percentages and coatings. This provided a set of properties highlighting the abilities of natural fibers in a cementitious matrix.

Compressive strength

The mean values for compressive strength of the various mixes are reported in (Table 5-6). A relationship can be established between fiber percentages and coatings on the compressive strength of the composite (Figure 5-21 and Figure 5-22). Increasing fiber percentage after a threshold negatively affects the compressive strength of the composite. Additionally, resin coated composites display better compressive strength than uncoated fiber composites, which display better performance than the shellac coated composites. This indicates the influence of polyester resin, and shellac during composite curing on the compressive strength of the composite.

The compressive strength of the various mixes was tested at 7 and 28 days. For the 7-day compressive strength the 2% PVA control mix displays the greatest strength at4926 PSI followed by the 3.5%, and 5.0% resin coated sisal fiber mixes at 4252 PSI and 4120 PSI.

The 3.5% Sisal uncoated, 5.0% Sisal uncoated, and 3.5% Sisal shellac display the next highest strength at 3812 PSI, 3506 PSI, and 3429 PSI, respectively. The 5.0% Sisal shellac and plain concrete mix displays lowered compressive strength at 3162 PSI and 3351PSI compared to the other mixes at 7 days(Figure 5-22).

When comparing the compressive strength at 7 days for the various fiber percentages we see a decrease of 8.02% when the fiber proportion changes from 3.5% to 5.0%. This indicates a decrease in performance for uncoated fiber composites with increasing fiber percentages as observed in the preliminary studies (Table 5-6 & Figure 5-21).

Comparing the resin coated composites at increasing fiber percentages for 7-day strength we see that, the compressive strength decreases by 3.10% specifically when the fiber proportion changes from 3.5% to 5.0%.

Comparing the shellac coated composites, we see that at increasing fiber percentages, compressive strength drops by 7.78%, and is lower when compared to the uncoated and resin coated sisal composites. When compared to the resin coated composites, the compressive strength of the shellac coated composites is 19.35% and 9.6% lower for the 3.5% and 5.0% fiber composites (Table 5-6 & Figure 5-21).

For the 28-day compressive strength, the ECC composite 7844 PSI, 2% uncoated 7850 PSI, and Resin-Sisal mix 7779 PSI displays the highest strength, followed by 2% Shellac-Sisal mix 6056 PSI, and 3.5% sisal uncoated 6189 PSI. The 3.5% Resin-Sisal mix 4961 PSI, and 5.0% Resin-Sisal 4120 PSI displays the lowest strength compared to the other mixes but not significantly different than the highest mixes apart from the plain ECC composite 7844 PSI (Table 5-6 and Figure 5-22).

Comparing the mechanical properties of the uncoated composites at 28 days for increasing fiber percentages we see that compressive strength is lowered by 21.15% for the 2.0% and 3.5% composites and further decreases by 10.61% for the 5.0% composites.

Comparing the resin coated composites for increasing fiber percentage from 2.0% to 3.5% we see compressive strength drop significantly by 36.22%. The compressive strength is similar when the fiber proportion is increased to 5.0%.

For the Shellac-Sisal composites, we see similar behavior where the compressive strength slightly drops by 8.66% when the fiber percentage increases from 2.0% to 3.5%. The compressive strength drops further by 15.27% when the fiber proportion increases from 3.5% to 5.0% (Table 5-6 and Figure 5-22).Therefore at 28 days, the uncoated and coated fiber composites see a significant reduction in compressive strength when compared to the control plain ECC composite.

The 5.0% sisal fiber composites display the highest loss in mechanical strength. Additionally, due to the hydrophilic nature of polyester resin, the oxygen atoms form hydrogen bonds with the water molecules in fresh mortar, resulting in a greater absorption by the coated composite. This results in void formation at the fiber-matrix interface ultimately reducing compressive strength for higher proportions of coated fibers (Ahmad and Fan 2018). (Figure 5-7 and Figure 5-8) highlights these voids for the coated samples.

Split tensile

The split tensile tests were carried out on a universal testing machine on 4 x 8 cylinders placed on bearing plates. The mean values for the split tensile tests was conducted at 28 days and are presented in (Table 5-7 and Figure 5-23). As with the values for compressive strength a relationship can be established between fiber percentages and coatings on tensile strength. Increasing fiber percentages doesn't affect the mechanical properties of the uncoated composites. Resin fiber composites display better values for split tensile compared to uncoated fiber, and shellac fiber composites at specific fiber compositions.

The cylinders were tested at 28 days for their split tensile strength. The 2.0% PVA control 3391 PSI displays the highest mechanical strength. The 3.5%, 5.0% Resin-Sisal 2647 and 2508 PSI display the next highest values for split tensile strength. The uncoated sisal 2276, 2304, and 2303 PSI, shellac 2292, 2394, and 2021 PSI, and plain ECC mix 2266 PSI displays the next lowest values for split tensile with all of them within range of each other.

Comparing the split tensile values for the increasing fiber percentages we see that mechanical properties of the uncoated sisal composites remain similar from 2.0% sisal composites to 5.0% sisal composites indicating minor difference in split tensile values for increasing fiber percentages.

Comparing the values for the resin coated fiber composites we see a distinct variation in values based on the fiber percentages. Tensile strength increases by 27.26% with increasing fiber percentage from 2.0 to 3.5%. Tensile strength decreases by 5.25% with an increase in fiber percentage from 3.5 to 5.0%.

Comparing split tensile values for the shellac coated composites we see an increase of 4.45% with increasing fiber percentage from 2.0% to 3.5%. The tensile strength decreases 15.62% with fiber percentage increasing from 3.5% to 5.0%.

Therefore at 28 days, the performance of the 3.5% resin, and shellac coated, and 5.0% resin coated composites display a significant increase in tensile strength when compared to the plain ECC composite, indicating the role the coated sisal fibers play in resisting tensile stress. This is due to the ability of the sisal fibers bridge matrix cracks, transferring applied loads. Filho et al (Silva, Mobasher, and Filho 2009) in their work highlight the ability of longitudinal fibers in enhancing strength, ductility, and the crack bridging mechanism allowing a distributed microcrack system to develop in the reinforced composites.

Flexural strength

A 4-point bending test was conducted on the 14'' x 4'' x 3'' composite beams to determine flexural strength. The test was conducted on a UTM. Stress vs strain graphs, ultimate load, and final crack strength (FCS) to calculate toughness were obtained. The mean values for flexural strength are presented in (Table 5-7). (Figure 5-26, Figure 5-25, and Figure 5-27) presents typical values for stress vs strain relationship for the composite beams.

Stress vs strain

The composite beams, both coated and uncoated, display complex behavior in their stress vs strain relationship but significantly higher ductility compared to the brittle plain ECC composite. When comparing the stress vs strain graphs for the coated and coated graphs we see a characteristic dip in the linear elastic range before climbing towards ultimate tensile strength before tapering out, indicating the role of the resin and shellac in the coated fiber composites.

Additionally, there is observable difference in the size of initial dips between the resin coated, and shellac coated composites possibly due to the interfacial interaction between the coatings and cementitious matrix. The plain ECC composite highlights the largest initial dip when compared to the coated samples. The uncoated fiber composites apart from the 2.0% fiber composite display no dips further highlight the role of the coatings on flexural properties.

When comparing the 2.0% sisal fiber composites (Figure 5-25), we see there is observable difference between the resin, shellac coated composites, and uncoated composites. The 2.0 % resin, and shellac composites past the characteristic initial dip reaches its ultimate flexural strength earlier when compared to the 2.0% uncoated, and plain ECC composite (Figure 5-25).

When comparing the 3.5% sisal fiber composites (Figure 5-26), we can separate the performance of the resin sisal composite from the uncoated and shellac coated composite. The resin sisal composite exhibits the characteristic first dip highlighting the role of the fiber, but also sees another dip before achieving its ultimate flexural strength far earlier when compared to the shellac coated, and uncoated composite. The shellac coated composites exhibit the first

dip later in the graph, achieving its peak flexural strength sooner than the uncoated samples, 13.70% lower than the uncoated sample.

When comparing the 5.0% sisal fiber composites (Figure 5-27), we can see that the resin, and shellac coated display higher values of stress and ultimate stress but display lower ductility when compared to the uncoated fiber composite. All the 5.0% fiber composites display better values for peak stress and ductility when compared to the plain ECC composite.

Ultimate flexural strength

The average ultimate values of tensile strength were obtained from the 4-point bending tests conducted on the UTM. The results are presented in (Table 5-8 and Figure 5-24).

The 5.0% Shellac coated composite displays the highest flexural strength 528 PSI, followed by the 2.0%, 3.5 %, and 5.0% uncoated fibers 364.3 PSI, 446.3PSI, 437.9PS. The 3.5% resin and shellac coated, and 5.0% resin coated display the next highest values for tensile strength 346.6 PSI, 394 PSI, 368 PSI. The 2.0% resin coated, and shellac coated composites display the lowest tensile strength and slightly lower than the plain ECC composite.

When comparing the uncoated composites at higher fiber percentages we see that the 3.5% composite displays a 22.52% increase in peak flexural strength over the 2.0%. The 5.0% fiber composite displays similar values for peak flexural strength as the 3.5% composite.

For the resin coated composites, we see a similar behavior as the uncoated composites where the 3.5% composite displays a 30.00% increase in peak flexural strength over the 2.0% composite. The 5.0% composite displays a 6.35% increase in peak flexural strength over the 3.5% composite. When comparing the shellac coated composites, the 3.5% composites display a 50.38% increase in peak strength over the 2.0% composite. The 5.0% composite displays a 34.06% increase in strength over the 3.5% composite. The 28-day values for peak flexural

strength for the 3.5%, 5.0% uncoated and coated composites display better ultimate tensile strength than the plain ECC composite relationship between fiber proportion and peak strength.

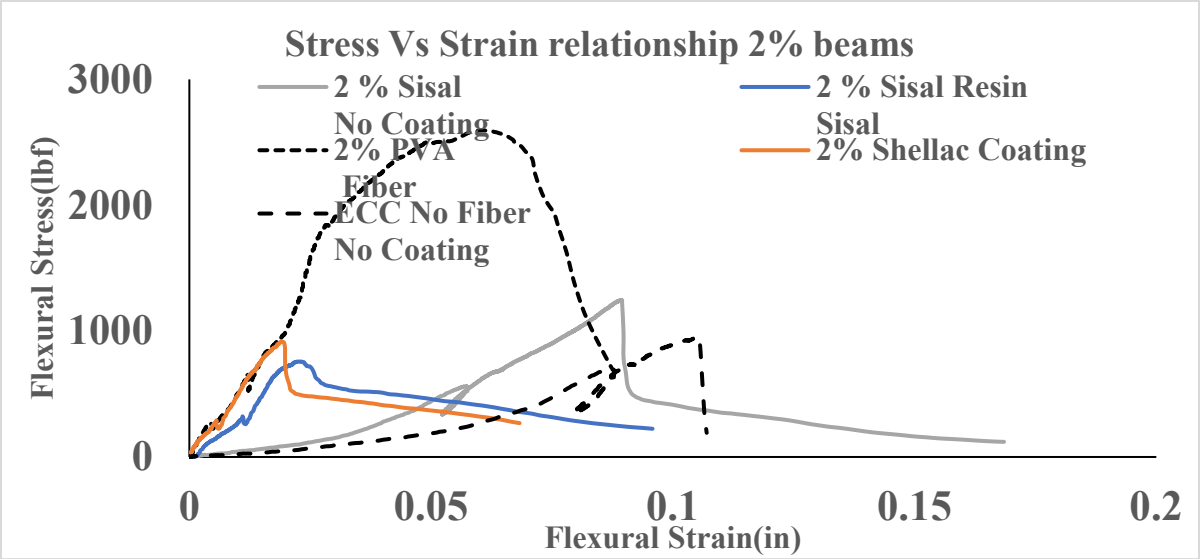

Figure 5-26 - Stress vs Strain relationship, 2% fiber composites compared to plain ECC composite.

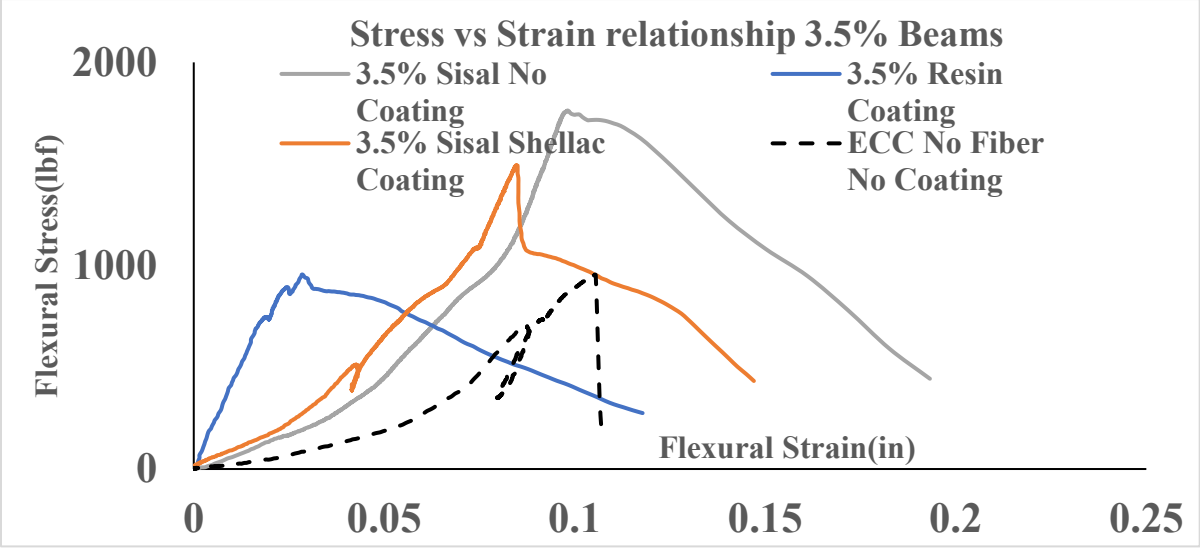

Figure 5-25 - Stress vs Strain relationship, 3.5% fiber composites compared to plain ECC composite.

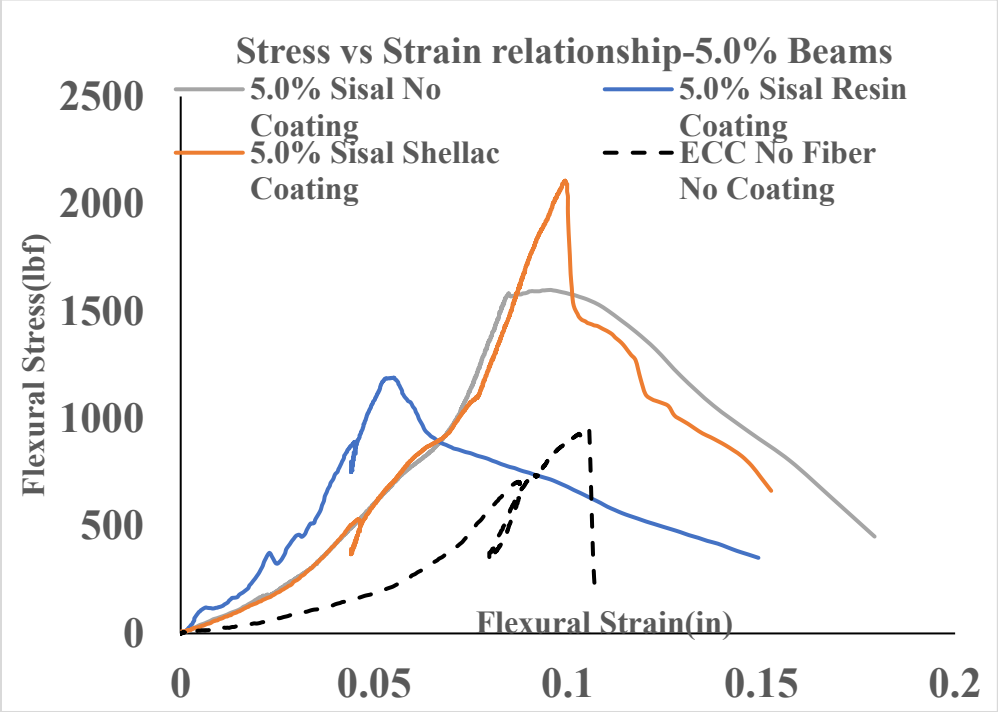

Figure 5-27 - Stress vs Strain relationship, 5.0% fiber composites compared to plain ECC composite.

Toughness

Toughness was calculated from area under load vs deflection graphs obtained from the 4-point bending test. The values for toughness for each of the tested beams are presented under (Table 5-9 and Figure 5-28).The various values are compared in order of increasing fiber percentage and coating condition. A plain ECC composite is used as a control beam to compare the average toughness for the coated fiber samples. From (Figure 5-28) we see that 3.5 % and 5.0% uncoated, and 5.0% shellac coated display the highest values of toughness. The 3.5% and 5.0% resin coated, the 3.5% shellac coated, and 2.0% uncoated display the next highest values of toughness.The 2.0% resin and shellac coated composites display the lowest values and is closer the plain ECC composite.

Table 5-9 - Average toughness values for coated and uncoated sisal fiber composites.

Average Toughness(lb/in)		
Control	ECC Composite	33.61
	2% PVA-Control	139.53
Uncoated	2% Uncoated-Sisal	66.30
	3.5% -Sisal - Uncoated	133.29
	5.0% -Uncoated-Sisal	132.95
Resin-Coated	2% Resin-Sisal	35.01
	3.5% Resin-Sisal	73.69
	5.0% Resin-Sisal	97.83
Shellac-Coated	2% Shellac-Sisal	34.92
	3.5% -Shellac-Sisal	85.80
	5.0% -Shellac-Sisal	142.25

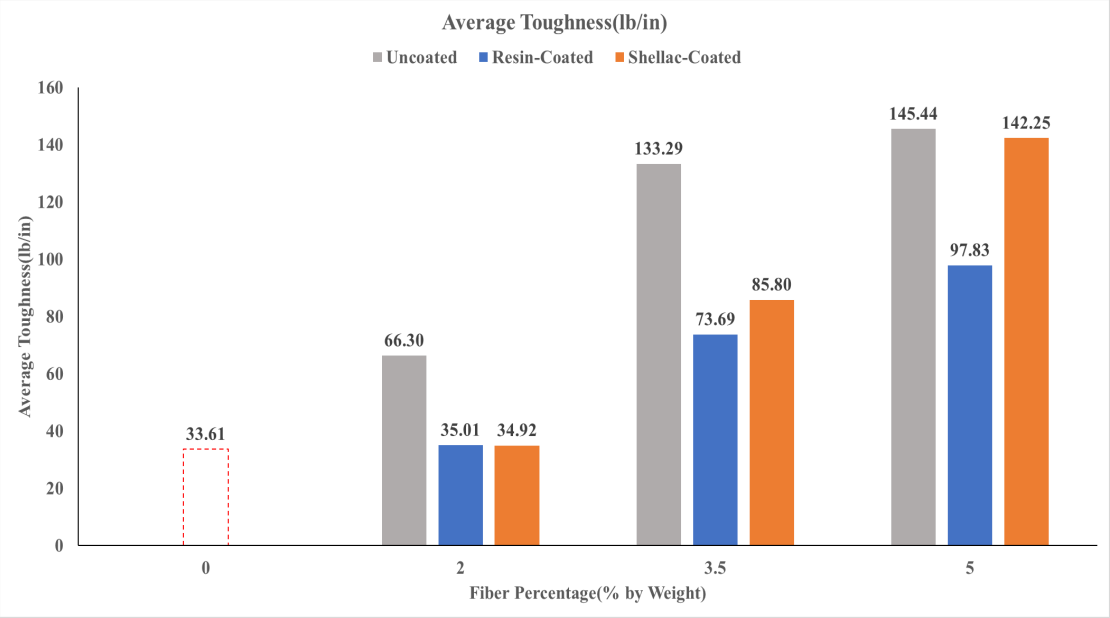

Figure 5-28 - Comparisons of average Toughness for coated and uncoated sisal fiber composites

When comparing the values for toughness in order of increasing fiber percentage from2.0% to 5.0% for the uncoated composites we see that an increase in fiber percentage results in higher values of toughness. This is possibly due to the sisal fibers providing greater ductility and increased fiber bridging mechanism in the Cementitious matrix.

When comparing the values for increasing fiber percentage for the resin-coated composites we see a similar behavior as that of the uncoated composites where increasing resin coated fiber results in increased toughness. Although the toughness values are lower when compared to the equivalent uncoated values. There could be many reasons for this, possibly due to the resin fibers curing faster than intended and clumping together.

The shellac coated composites at increasing fiber percentages see higher toughness similar the uncoated and resin coated composites. The 5.0% Shellac-Sisal coated composite specifically displays the highest toughness compared to the rest of the composites. This could possibly be due to the effective dispersion of the shellac coated fibers in the cementitious matrix when compared to the resin coated fibers.

Durability studies

Preliminary studies, informed by work done by previous authors , were carried out to determine an effective time period for accelerated aging tests. (Tolêdo Filho et al. 2000) observed the saturation of the sample which occurred in the first 24 h and the loss of about 72% of the gained mass in six days, after which they picked a 7-day cycle. In this cycle, they left a sample for a day under water at 18°C and six days drying in the conditioned laboratory room. Following a set number of cycles, the beams were tested for their flexural strength.

(Toledo Filho et al. 2009) created a forced air flow chamber (FAFC) to simulate the drying cycles. They designed the FAFC to control wind velocity, and air temperature simulating environmental conditions which their custom molded laminates were tested. The chamber was set to a temperature of 36 ± 1 °C with wind velocity of 0.5 m/s. They defined the wet/dry cycle as a sample completely saturated in water at 30 °C and left to dry in the FAFC. After 24 h in water the sample absorbed about 90% of its total saturation capacity and, after 48 h it lost about 70% of gained mass.

For the durability study, a plain concrete beam, and 2.0% sisal fiber beam was used to determine effective cycling time. One cycle was defined as the total time spent in a water bath or oven before being moved to the next cycle. To determine an effective cycle the beams were first weighed and then placed in a water bath kept at ambient temperature. The beams were then constantly weighed for 24 hours until the composite had absorbed all the moisture.

Conclusion - Sisal Fiber Composites

The following conclusions can be drawn based on the results obtained from the study.

1. The uncoated and coated fiber composites see a significant reduction in compressive strength at 28 days when compared to the control plain ECC composite. The 5.0% sisal fiber composites display the highest loss in compressive strength highlighting the role of fiber proportion in the cementitious matrix. Additionally, Due to the hydrophilic nature of resins, the oxygen atoms form hydrogen bonds with the water molecules in fresh mortar, resulting in a greater absorption by the coated composite, ultimately reducing compressive strength for higher proportions of coated fibers.

2. At 28 days, the performance of the 3.5% resin, and shellac coated, and 5.0% resin coated composites display a significant increase in tensile strength when compared to the plain ECC composite, indicating the role of coated sisal fibers play bridging matrix cracks, and transferring applied loads.
3. The composite beams, both coated and uncoated, display higher ductility compared to the plain ECC composite which is brittle. The coated and uncoated composites see a characteristic dip in the linear elastic range, indicating the role, resin and shellac play in resisting flexural stress.
4. The 28-day values for peak flexural strength for the 3.5%, 5.0% uncoated and coated composites display better ultimate tensile strength than the plain ECC composite indicating a relationship between fiber proportion and peak strength.
5. The shellac-coated composites at increasing fiber percentages in higher toughness. The 5.0% shellac sisal coated composite specifically displays the highest toughness due to the effective dispersion of the shellac coated fibers in the cementitious matrix when compared to the resin coated fibers.

Therefore, this study investigated the interfacial bond between the fiber and cement matrix by coating the fiber surface in polyester resin prior to dispersion. The goal of this study was to discern the reinforcement capabilities of the coated fibers for non-essential structural uses. The cellulose fiber chosen for this project was the sisal fiber. The fiber was chosen from a group of fibers, (Table 5-1), that reflect higher tensile properties relevant for creating tensile

composites. Two resins, polyester resin and shellac, were chosen to protect the sisal fiber in the cementitious matrix helping achieve effective properties.

The sisal fiber embedded cementitious composites exhibited improved toughness, ductility, and flexural capacity, compared with non-reinforced cementitious composites,(Table 5-5, Table 5-6, Table 5-7, Table 5-8, Table 5-9, Figure 5-2, Figure 5-3, Figure 5-4, Figure 5-5, Figure 5-21, Figure 5-22, Figure 5-23, Figure 5-24, Figure 5-26, Figure 5-25, Figure 5-27, and Figure 5-28). The coated fiber composites exhibited lowered compressive strength (Figure 5-21 and Figure 5-22) due to void formation. They displayed better flexural strength, higher tensile strength, and higher toughness than the unreinforced ECC composite. One of the advantages of cellulose reinforced cementitious composites is the fiber-bridging mechanism during and after cracking helping transfer the loads reflected in the flexural tests.

The sisal fiber chosen for this investigation was cultivated in Kenya and holds implications for future work. As the premise is focused on material locality, and cellulose manifesting in various forms, additional investigation is required.

These investigations could focus on the different types of fibers that are region specific and display high tensile properties in creating a fiber reinforced composites (Table 5-1). For example, coconut fibers native to tropical climates display higher values of tensile strength when compared to sisal fibers Table 4. Due to this widespread availability, coconut fibers would make a better alternative for tensile composites in regions such as South India.

CHAPTER 6. CONCLUSION – CELLULOSE BASED COMPOSITES

The three investigations explored utilizing cellulose, in two forms, as an alternative to non-renewable materials making up the standardized wall assembly. This would reduce the reliance on energy intensive transformation of non-renewable raw materials into standardized construction products. Additionally, focusing on a widely available, renewable, and bio-degradable material such as cellulose allows for a versatile building envelope while achieving reduced energy use and overall sustainability. Therefore, the primary goals were:

1. Reducing the percentage of non-renewable materials utilized in the contemporary wall assembly.
2. Utilizing a widely available, biodegradable, and renewable material such as cellulose as an alternative to traditional building materials.
3. Transforming cellulose, manifesting as various fibers, into a structural or thermal component based on location, availability, and programmatic requirements

Cellulose Based Tensile Composites

This study investigated the interfacial bond between the fiber and cement matrix by coating the fiber surface in polyester resin and shellac prior to dispersion in the composite mix. The goal of this study was to discern the capabilities of the coated fibers as a partial reinforcement for engineered cementitious composites. The cellulose fiber chosen for this project was the sisal fiber. The fiber was chosen from a group of fibers (Table 5-1) that reflect higher tensile properties relevant for creating tensile composites.

Two resins, a polyester resin and shellac, were chosen to protect the sisal fiber in the cementitious matrix to achieve effective properties.The sisal fiber embedded cementitious composites exhibited improved toughness, ductility, and flexural capacity, compared with unreinforced ECC composites.

The sisal fiber chosen for this investigation was native to Kenya and holds implications for future work. As the premise is focused on material locality, and cellulose manifesting in various forms, additional investigation is required. This investigation could focus on the different types of fibers that are region specific and display high tensile properties in creating a tensile composite (Table 5-1). For example, coconut fibers native to tropical climates display higher values of tensile strength when compared to sisal fibers (Table 5-1). Due to this widespread availability, coconut fibers would make a better alternative for tensile composites in regions such as South India.

Cellulose Based Thermal Composites

The mobile diagnostics lab was utilized to generate Data from custom concrete panels inserted into the removable wall assembly creating a baseline to compare future cellulose concrete panels.

With a baseline established for a standard concrete wall assembly the next goal, will be to incorporate conclusions from the material. An optimized mix based on the proportions outlined in (Table 5-3) is necessary to reduce concrete consumption in creating composite thermal assemblies. Currently initial studies with the sisal fiber mix utilizes a higher proportion of cement in the mix ratio. A higher proportion of cement was utilized to achieve demonstratable properties.

The fiber composite study primarily optimized fiber proportion for effective mechanical properties. Therefore, additional work needs to be carried out into fiber and mix proportion optimization to create a thermally efficient composite panel. This means that the quantity of both fiber and concrete can be explored to achieve a thermally effective panel.

In addition, the choice of cellulosic material can be varied depending on location, fiber sourcing, properties, and program requirements based on microclimate. Apart from sisal there are a host of other natural and waste fibers Table 4 from various sources that can be used in varying proportions.

For example, kraft pulp fiber, generated from wastepaper, could be the preferred fiber in regions where natural fibers are difficult to source. This is relevant in regions where large quantities of paper waste are generated and sent to landfills. In agricultural areas, Stover left over from harvesting could be the preferred fiber. This also has implications for carbon sequestration as a significant portion of carbon present in the Stover is absorbed back by the environment rather than the soil.

Cellulose Based Thin Shell Structures

Thin shell structures were cast as a framework for future applications utilizing cellulose available in various forms around the world (Table 5-1). The shell structures were seeded with cellulose nanocrystals to create stronger composites. The modelling and mock-ups create a framework with which to integrate region specific fibers and programmatic uses in framing spatial conditions. The shells were envisioned as enclosures for community gathering spaces in regions where access to construction products would be difficult. Additionally, they could form as a blueprint for crafting spaces in regions facing humanitarian crises and shortage of traditional building materials such as lumber, Glass, steel, and brick.

These three investigations provide a framework for building enclosures with cellulose based materials. The framework can be optimized based on cellulose properties, morphologies, economy, and life-cycle cost. Additionally, their interaction with thermal, structural, regional, and programmatic conditions can lead to an efficient and versatile space. Spatial enclosures defined by these interactions can then provide an alternative to the standardized building materials that define the contemporary wall assembly.

References

Adriaenssens, Sigrid, Philippe Block, Diederik Veenendaal, and Chris Williams. 2014. *Shell structures for architecture : form finding and optimization / edited by Sigrid Adriaenssens, Philippe Block, Diederik Veenendaal, and Chris Williams*: London ; New York : Routledge/ Taylor & Francis Group.

Ahmad, Hassan, and Mizi Fan. 2018. "Interfacial properties and structural performance of resin-coated natural fibre rebars within cementitious matrices." *Cement and Concrete Composites* 87:44-52. doi: 10.1016/j.cemconcomp.2017.12.002.

Ardanuy, Mònica, Josep Claramunt, and Romildo Dias Toledo Filho. 2015. "Cellulosic fiber reinforced cement-based composites: A review of recent research." *Construction and Building Materials* 79 (C):115-128. doi: 10.1016/j.conbuildmat.2015.01.035.

Ban, Shigeru. 2009. *Shigeru Ban : paper in architecture / essays by Riichi Miyake ; edited by Ian Luna & Lauren A. Gould*. Edited by Riichi Miyake, Ian Luna and Lauren A. Gould. New York: New York : Rizzoli International Publications.

Board, California Integrated Waste Management. 2000. Designing With Vision: A Technical Manual for Material Choices in Sustainable Construction. California: California Environmental Protection Agency.

Burgert, I., J. Keckes, K. Frühmann, P. Fratzl, and S. E. Tschegg. 2002. "A Comparison of Two Techniques for Wood Fibre Isolation - Evaluation by Tensile Tests on Single Fibres with Different Microfibril Angle." *Plant Biology* 4 (1):9-12. doi: 10.1055/s-2002-20430.

California, Integrated, Waste, Management, and Board. 2000. Designing With Vision: A Technical Manual for Material Choices in Sustainable Construction. California: California Environmental Protection Agency.

Cao, Yizheng, Pablo Zavaterri, Jeff Youngblood, Robert Moon, and Jason Weiss. 2015. "The influence of cellulose nanocrystal additions on the performance of cement paste." *Cement and Concrete Composites* 56:73-83. doi: 10.1016/j.cemconcomp.2014.11.008.

CelluForce. 2016. "Core Properties of Cellulose Nanocrystals." CelluForce inc, accessed August 20. https://www.celluforce.com/en/products/core-properties/.

Committee, A. C. I. "Concrete Shell Structures Practice and Commentary." *Journal Proceedings* 61 (9). doi: 10.14359/7822.

Dixit, Manish K., Charles H. Culp, and Jose L. Fernandez-Solis. 2015. "Embodied energy of construction materials: integrating human and capital energy into an IO-based hybrid model." *Environmental science & technology* 49 (3):1936. doi: 10.1021/es503896v.

Eder, Michaela, Olivier Arnould, John Dunlop, Joanna Hornatowska, and Lennart Salmén. 2013. "Experimental micromechanical characterisation of wood cell walls." *Wood Sci Technol* 47 (1):163-182. doi: 10.1007/s00226-012-0515-6.

Eichhorn, S., C. Baillie, N. Zafeiropoulos, L. Mwaikambo, M. Ansell, A. Dufresne, K. Entwistle, P. Herrera-Franco, G. Escamilla, L. Groom, M. Hughes, C. Hill, T. Rials, and P. Wild. 2001. "Review: Current international research into cellulosic fibres and composites." *Journal of Materials Science* 36 (9):2107-2131. doi: 10.1023/A:1017512029696.

El-Hosseing, F., and D. H. Page. 1975. "The mechanical properties of single wood pulp fibres: Theories of strength: El-Hosseing, F. and Page, D. H. Fibre Science and Technology, Vol 8 No 1 (Jan 1975) p 21." 6:278-278. doi: 10.1016/0010-4361(75)90024-5.

Fall, Andreas B., Stefan B. Lindstrm, Joris Sprakel, and Lars Wgberg. 2013. "A physical cross- linking process of cellulose nanofibril gels with shear- controlled fibril orientation." *Soft Matter* 9 (6):1852-1863. doi: 10.1039/c2sm27223g.

Fall, Andreas B., Stefan B. Lindström, Ola Sundman, Lars Ödberg, and Lars Wågberg. 2011. "Colloidal stability of aqueous nanofibrillated cellulose dispersions." *Langmuir : the ACS journal of surfaces and colloids* 27 (18):11332. doi: 10.1021/la201947x.

Ferreira, Saulo Rocha, Paulo Roberto Lopes Lima, Flávio Andrade Silva, and Romildo Dias Toledo Filho. 2014. "Effect of Sisal Fiber Hornification on the Fiber-Matrix Bonding Characteristics and Bending Behavior of Cement Based Composites." *Key Engineering Materials* 600-600 (6):421-432. doi: 10.4028/www.scientific.net/KEM.600.421.

Filho, JoaO De Almeida Melo, FlaVio De Andrade Silva, and Romildo Dias Toledo Filho. 2013. "Degradation kinetics and aging mechanisms on sisal fiber cement composite systems." *Cement and Concrete Composites* 40:30.

Fuchs, Matthias. 2008. *Energy manual : sustainable architecture / Hegger [and three others]*. Edited by Manfred Hegger, Gerd H. Ṡöffker, Philip Thrift, Pamela Seidel and Architektur-Dokumentation Institut für Internationale: Basel ; Boston : Birkhäuser ; Munich : Edition Detail.

Gassan, Jochen, and Andrzej K. Bledzki. 1999. "Possibilities for improving the mechanical properties of jute/epoxy composites by alkali treatment of fibres." *Composites Science and Technology* 59 (9):1303-1309. doi: 10.1016/S0266-3538(98)00169-9.

Gibson, Lorna J. 2012. "The hierarchical structure and mechanics of plant materials." *Journal of the Royal Society, Interface* 9 (76):2749.

Gillian, F. Menzies, Khasreen Mohamad Monkiz, and F. G. Banfill Phillip. 2009. "Life-Cycle Assessment and the Environmental Impact of Buildings: A Review." *Sustainability* 1 (3):674-701. doi: 10.3390/su1030674.

Hospodarova, V., N. Stevulova, and A. Sicakova. 2015. "Possibilities of using cellulose fibres in building materials." *Possibilities of Using Cellulose Fibres in Building Materials* 96 (1):012025. doi: 10.1088/1757-899X/96/1/012025.

Håkansson, Karl M. O., Andreas B. Fall, Fredrik Lundell, Shun Yu, Christina Krywka, Stephan V. Roth, Gonzalo Santoro, Mathias Kvick, Lisa Prahl Wittberg, Lars Wågberg, and L. Daniel Söderberg. 2014. "Hydrodynamic alignment and assembly of nanofibrils resulting in strong cellulose filaments." *Nature communications* 5:4018. doi: 10.1038/ncomms5018.

Institute, American Concrete. 1986. "State-of-the art report on fiber reinforced concrete: reported by ACI Committee 544. ACI 544.1 R-82."

International, ASTM. 2017. ASTM C39 / C39M-17b,Standard Test Method for Compressive Strength of Cylindrical Concrete Specimens. West Conshohocken, PA.

Iwamoto, Shinichiro, Akira Isogai, and Tadahisa Iwata. 2011. "Structure and mechanical properties of wet- spun fibers made from natural cellulose nanofibers." *Biomacromolecules* 12 (3):831. doi: 10.1021/bm101510r.

Jeanblanc, Evan Michael. 2017. Exploring the complex development of a mobile research lab for the design of built environments. Iowa State University Digital Repository.

Jeffery, G. B. 1922. "The Motion of Ellipsoidal Particles Immersed in a Viscous Fluid." *Proceedings of the Royal Society of London. Series A, Containing Papers of a Mathematical and Physical Character* 102 (715):161-179.

Jencks, Charles. 2016. Notopia: The Singapore paradox and the style of Generic Individualism. *The Architectural Review*.

Johnson, Richard K., Audrey Zink-Sharp, Scott H. Renneckar, and Wolfgang G. Glasser. 2008. "Mechanical properties of wetlaid lyocell and hybrid fiber-reinforced composites with polypropylene." *Composites Part A* 39 (3):470-477. doi: 10.1016/j.compositesa.2007.12.007.

Kaplan, David. 1998. *Biopolymers from renewable resources / D.L. Kaplan (ed.)*. Berlin ; New York: Berlin ; New York : Springer.

Kiriya, Daisuke, Ryuji Kawano, Hiroaki Onoe, and Shoji Takeuchi. 2012. "Microfluidic Control of the Internal Morphology in Nanofiber- Based Macroscopic Cables." *Angew. Chem.* 124 (32):8066-8071. doi: 10.1002/ange.201202078.

Klemm, Dieter, Brigitte Heublein, Hans-Peter Fink, and Andreas Bohn. 2005. "Cellulose: fascinating biopolymer and sustainable raw material." *Angewandte Chemie (International ed. in English)* 44 (22):3358.

Kumar, P. Mehta. 2001. "Reducing the Environmental Impact of Concrete." *Concrete International* 23 (10).

Köster, Sarah, Heather M. Evans, Joyce Y. Wong, and Thomas Pfohl. 2008. "An in situ study of collagen self- assembly processes." *Biomacromolecules* 9 (1):199. doi: 10.1021/bm700973t.

Le, Corbusier. 1970. *Towards a new architecture, by Le Corbusier. Translated from the French by Frederick Etchells*. Edited by Corbusier Le. New York: New York, Praeger.

Li, Victor C. 1998. "Engineered cementitious composites-tailored composites through micromechanical modeling."

Li, Victor C. 2003. "On engineered cementitious composites (ECC)." *Journal of advanced concrete technology* 1 (3):215-230.

Li, Victor C, Shuxin Wang, and Cynthia Wu. 2001. "Tensile strain-hardening behavior of polyvinyl alcohol engineered cementitious composite (PVA-ECC)." *ACI Materials Journal-American Concrete Institute* 98 (6):483-492.

Lin, Z, T Kanda, and Victor C Li. 1999. "On interface property characterization and performance of fiber reinforced cementitious composites."

Matos, Grecia, and Lorie Wagner. 1998. "CONSUMPTION OF MATERIALS IN THE UNITED STATES, 1900– 1995 1." *Annual Review of Energy and the Environment* 23 (1):107-122. doi: 10.1146/annurev.energy.23.1.107.

Mitchell, William J. 2004. "Constructing complexity in the digital age.(Essay: beyond the ivory tower)." *Science* 303 (5663):1472. doi: 10.1126/science.1091973.

Mori, Toshiko. 2002. *Immaterial/ultramaterial : architecture, design, and materials / edited by Toshiko Mori*. Cambridge, Mass.: Cambridge, Mass. : Harvard Design School in association with George Braziller.

Nishino, Takashi, Kiyofumi Takano, and Katsuhiko Nakamae. 1995. "Elastic modulus of the crystalline regions of cellulose polymorphs." *Journal of Polymer Science Part B: Polymer Physics* 33 (11):1647-1651.

NRMCA. 2003. "CIP 35 - Testing Compressive Strength of Concrete." NRMCA. https://www.nrmca.org/aboutconcrete/cips/35p.pdf.

Reiterer, A., H. Lichtenegger, S. Tschegg, and P. Fratzl. 1999. "Experimental evidence for a mechanical function of the cellulose microfibril angle in wood cell walls." *Philosophical Magazine A* 79 (9):2173-2184. doi: 10.1080/01418619908210415.

Sauer, Christiane. 2010. *Made of -- : new materials sourcebook for architecture and design / Christiane Sauer*. Berlin: Berlin : Gestalten.

Savastano, H., P. G. Warden, and R. S. P. Coutts. 2003. "Mechanically pulped sisal as reinforcement in cementitious matrices." *Cement and Concrete Composites* 25 (3):311-319. doi: 10.1016/S0958-9465(02)00055-0.

Silva, Flávio de Andrade, Barzin Mobasher, and Romildo Dias Toledo Filho. 2009. "Cracking mechanisms in durable sisal fiber reinforced cement composites." *Cement and Concrete Composites* 31 (10):721-730. doi: 10.1016/j.cemconcomp.2009.07.004.

Siró, István, and David Plackett. 2010. "Microfibrillated cellulose and new nanocomposite materials: a review." *Cellulose* 17 (3):459-494. doi: 10.1007/s10570-010-9405-y.

Toledo Filho, Romildo Dias, Flávio de Andrade Silva, E. M. R. Fairbairn, and João de Almeida Melo Filho. 2009. "Durability of compression molded sisal fiber reinforced mortar laminates." *Construction and Building Materials* 23 (6):2409-2420. doi: 10.1016/j.conbuildmat.2008.10.012.

Tolêdo Filho, Romildo D., Khosrow Ghavami, George L. England, and Karen Scrivener. 2003. "Development of vegetable fibre–mortar composites of improved durability." *Cement and Concrete Composites* 25 (2):185-196. doi: 10.1016/S0958-9465(02)00018-5.

Tolêdo Filho, Romildo D., Karen Scrivener, George L. England, and Khosrow Ghavami. 2000. "Durability of alkali-sensitive sisal and coconut fibres in cement mortar composites." *Cement and Concrete Composites* 22 (2):127-143. doi: 10.1016/S0958-9465(99)00039-6.

Trebbin, Martin, Dagmar Steinhauser, Jan Perlich, Adeline Buffet, Stephan V. Roth, Walter Zimmermann, Julian Thiele, and Stephan Förster. 2013. "Anisotropic particles align perpendicular to the flow direction in narrow microchannels." *Proceedings of the National Academy of Sciences of the United States of America* 110 (17):6706. doi: 10.1073/pnas.1219340110.

Veenendaal, Diederik, and Philippe Block. 2014. "Design process for prototype concrete shells using a hybrid cable-net and fabric formwork." *Engineering Structures* 75 (C):39-50. doi: 10.1016/j.engstruct.2014.05.036.

Wambua, Paul, Jan Ivens, and Ignaas Verpoest. 2003. "Natural fibres: can they replace glass in fibre reinforced plastics?" *Composites Science and Technology* 63 (9):1259-1264. doi: 10.1016/S0266-3538(03)00096-4.

Wang, Shuxin, and Victor C Li. 2007. "Engineered cementitious composites with high-volume fly ash." *ACI Materials journal* 104 (3):233.

Wei, Jianqiang, and Christian Meyer. 2015. "Degradation mechanisms of natural fiber in the matrix of cement composites." *Cement and Concrete Research* 73:1-16. doi: 10.1016/j.cemconres.2015.02.019.

Zabalza Bribián, Ignacio, Antonio Valero Capilla, and Alfonso Aranda Usón. 2011. "Life cycle assessment of building materials: Comparative analysis of energy and environmental impacts and evaluation of the eco-efficiency improvement potential." *Building and Environment* 46 (5):1133-1140. doi: 10.1016/j.buildenv.2010.12.002.